AFOSR-TR-97 0410

REPORT DOCUMENTATION PAGE

Form Approved
OMB No. 0704-0188

1. AGENCY USE ONLY (Leave blank)	2. REPORT DATE	3. REPORT TYPE AND DATES COVERED
	14 July 1997	FINAL TECHNICAL 14Feb94-13FEB97

4. TITLE AND SUBTITLE

SPECTROSCOPY AND THERMAL DECOMPOSITION MECHANISM OF NTO

5. FUNDING NUMBERS

(G) F49620-94-1-0125
61102F
2303/ES

6. AUTHOR(S)

Charles A. Wight

7. PERFORMING ORGANIZATION NAME(S) AND ADDRESS(ES)

University of Utah
Office of Sponsored Projects
1471 Federal Way
Salt Lake City, UT 84102

8. PERFORMING ORGANIZATION REPORT NUMBER

9. SPONSORING/MONITORING AGENCY NAME(S) AND ADDRESS(ES)

Dr. Michael R. Berman
Air Force Office of Scientific Research
AFOSR/NL
110 Duncan Avenue, Suite B115
Bolling AFB, DC 20332-0001

10. SPONSORING/MONITORING AGENCY REPORT NUMBER

11. SUPPLEMENTARY NOTES

12a. DISTRIBUTION/AVAILABILITY STATEMENT

Unclassified. Distribution Unlimited.

12b. DISTRIBUTION CODE

DISTRIBUTION STATEMENT A
Approved for public release
Distribution Unlimited

13. ABSTRACT *(Maximum 200 words)*

The physical and chemical propoerties of the high explosive NTO have been investigated by infrared spectroscopy and thin film infrared laser pyrolysis in order to determine the initial chemical steps in the decomposition mechanism. It was found that the initial steps form carbon dioxide by a bimolecular reaction mechanism involving reaction of two NTO molecules in the crystal. The relative insensitivity of NTO to accidental ignition is attributed to a unique crystal structure that holds reactive groups of the molecules apart from each other and forces disruption of the crystal structure (melting) before reaction can take place. A similar mechanism has been found to explain the insensitivity of 2,4-dinitroimizazole compared with its structural isomer, 1,4-dinitroimidazole.

14. SUBJECT TERMS

NTO;infrared spectroscopy; laser; pyrolysis; thin film; explosive; reaction mechanism; sensitivity.

15. NUMBER OF PAGES

57

16. PRICE CODE

17. SECURITY CLASSIFICATION OF REPORT	18. SECURITY CLASSIFICATION OF THIS PAGE	19. SECURITY CLASSIFICATION OF ABSTRACT	20. LIMITATION OF ABSTRACT
UNCLASSIFIED	UNCLASSIFIED	UNCLASSIFIED	UL

Objectives of the Project (Statement of Work)

1. Transmission FTIR and Laser Raman spectra of thin films of NTO will be obtained in order to assess the degree of crystallinity of the NTO.

2. Thin film IR laser pyrolysis experiments will be carried out in order to identify initial reaction products of the thermal decomposition reaction.

3. Single and double-window experiments will be carried out in order to identify those reaction products that are formed in gas phase vs. condensed phase reactions.

4. Pyrolysis experiments will be carried out on amorphous and polycrystalline thin films in order to determine whether the initial products are formed in unimolecular or bimolecular reactions.

Status of Efforts

All four objectives were completed.

The results of task 1 have been described in an article co-authored by Donald Thompson and his group at Oklahoma State University. The article (publication 1, below) has been accepted for publication in the Journal of Molecular Structure. A copy of the article is attached in Appendix 1.

The results of task 2 have been described in a journal article and in the proceedings of the 1995 Materials Research Society meeting (publications 2 and 3, also attached).

Task 3 was completed and it was found that the thermal decomposition of NTO produces CO_2 by a condensed phase mechanism.

Task 4 has been completed. Instead of using amorphous films to distinguish the reaction mechanisms, we measured the concentration dependence of the decomposition yield and found it to be second-order in NTO concentration. This established the mechanism of CO_2 formation as a bimolecular reaction involving two different NTO molecules. This result is described in publication 2. We also carried out an isotopic crossover experiment using ^{13}C and ^{18}O labeled samples of NTO that were synthesized by Professor Ted Burkey (Memphis State University) and ourselves, respectively. These experiments definitively confirmed the bimolecular nature of the reaction mechanism. A publication describing these experiments and additional gas phase decomposition experiments is currently in preparation.

Accomplishments and New Findings

1. NTO Thermal Decomposition
   We have found that NTO has a mechanism of thermal decomposition that is unique among high explosives. Whereas most explosives tend to react by loss of NO_2 (or HNO_2) in a unimolecular reaction, NTO has a bimolecular mechanism in which the nitro group of one molecule reacts with the carbonyl group of another NTO molecule, thereby forming CO_2 as the initial products in the condensed phase. This mechanism may provide an explanation for the low sensitivity of NTO to ignition by impact because the crystal structure is what keeps the reactive groups separated and prevents reaction at temperatures lower than the melting point of NTO (262° C.). The melting point is high because the NTO molecules form a hydrogen-bonded network which resists reorganization. We have suggested that the following characteristics may contribute to reducing the sensitivity of high explosives:
   a. bimolecular reaction mechanism (rate depends on local structure of the crystal)
   b. crystal structure that effectively separates reactive functional groups
   c. high melting point (preferably involving formation of a hydrogen-bonded network)

2. Thermal Decomposition of 2,4-Dinitroimidazole and 1,4-Dinitroimidazole
   Dinitroimidazoles (DNI) form a relatively new class of high explosives. To our knowledge there are no published studies of the thermal decomposition mechanism of these molecules except for a recent paper by Behrens *et al.* in which the thermal rearrangement of 1,4-DNI and 2,4-DNI was investigated. We found experimental evidence of an N-NO_2 bond scission reaction step in the nitramine functional group of 1,4-DNI under high heating rates. No corresponding mechanism was found in 2,4-DNI, which has no N-N bonds and no nitramine functional groups. Under slow heating conditions, the main reaction channel is conversion of 1,4-DNI to 2,4-DNI and subsequent decomposition to form CO_2, N_2O, NO, HCN and other minor products. Our attempts to isolate the initial reaction products were unsuccessful. However, we found absolutely no evidence for formation of NO_2 at any stage in the reaction of 2,4-DNI, so C-NO_2 bond scission is unlikely to play a major role in the decomposition mechanism of 2,4-DNI.

3. Shock-Initiated Chemical Reactions
   A new project to study shock-initiated reactions in thin films of energetic materials is being carried out by a graduate student, Ping Ling. He has investigated the decomposition reactions of a series of azides and nitrate esters. Two preliminary papers have been published describing the initial results (publication 4) and experimental techniques (publication 5). A third paper (publication 6) describes further work on the detonation chemistry of glycidyl azide polymer (GAP). A fourth paper in this series describing the decomposition of polyglycidyl nitrate (PGN) is currently in preparation (publication 7).

Personnel

1. Principal Investigator - Charles A. Wight
2. Postdoctoral Research Associate - Tod R. Botcher (currently at Naval Research Laboratory)
3. Graduate Students - David Beardall and Ping Ling
4. Summer Undergraduates - Matthew Hammond (1995) and Nader Helmi (1996)

Interactions/Transitions

1. The following seminars have been given to describe the results of this research:

   "The Chemistry of Explosives", Naval Research Laboratory, Washington, DC, June 1994.

   "Thin Film Laser Pyrolysis of Propellants", Gordon Research Conference on Energetic Materials, June 1994.

   "The Chemistry of Explosives", Aptus, Inc. (Salt Lake City, UT), September 1994.

   "Detonation Chemistry of Glycidyl Azide Polymer", Materials Research Society 1995 Fall Meeting, Boston, November 1995.

   "Thermal Decomposition Mechanism of NTO", Materials Research Society 1995 Fall Meeting, Boston, November 1995.

   "The Chemistry of High Explosives", Idaho State University, Pocatello, ID, February 1996.

   "The Chemistry of High Explosives", Denison College, Granville, OH, February 1996.

   "The Chemistry of High Explosives", Ohio Wesleyan University, Delaware, OH, February 1996.

   "The Chemistry of High Explosives", Colorado College, Colorado Springs, CO, March1996.

   "The Chemistry of High Explosives", University of Colorado-Colorado Springs, March 1996.

   "The Chemistry of High Explosives", University of California, Riverside, CA, May 1996.

"The Chemistry of Explosives", 1994 HEDM Contractors' Meeting, Cal-neva, NV, June 1994.

"Explosive Thermal Decomposition Mechanism of NTO", Materials Research Society 1995 Fall Meeting, Boston, November 1995.

"The Chemistry of High Explosives", Gordon Research Conference on Energetic Materials, New Hampton, NH, June 1996.

"The Chemistry of High Explosives", High Energy Density Materials Contractors' Conference, Boulder, CO, June 1996.

2. Dr. Scott Shackelford (formerly with Seiler Laboratory at the US Air Force Academy) graciously provided the synthetic procedure for preparation and purification of NTO.

3. We collaborated with the group of Prof. Donald Thompson to determine the vibrational frequencies and normal modes of NTO in the solid state and isolated in solid argon.

4. We have interacted with the group of Prof. Dana Dlott at the University of Illinois to set up the laser-initiated shock wave experiments to determine the detonation chemistry of GAP.

5. Prof. Ted Burkey (Memphis State University) was a collaborator on the NTO thermal decomposition project. The ^{13}C labeled NTO was synthesized in his laboratory.

6. Dr. Surya Bulusu (Army Research Laboratory, Picatinny Arsenal, NJ) provided technical assistance in the preparation of 2,4-DNI and ^{18}O labeled NTO samples.

7. We obtained samples of polyglycidyl nitrate and ammonium dinitramide (ADN) from Dr. Robert Wardle of Thiokol Corp., as well as technical advice on the purification of ADN.

8. We have had discussions with Dr. Don McMillen of SRI to resolve some minor discrepancies between his proposed thermal decomposition mechanism of NTO and ours. These discussions have stimulated additional work in both laboratories to determine the source of the apparent disagreements and to resolve them.

Inventions, Discoveries and Patent Disclosures
(none)

Honors and Awards
Dr. Tod R. Botcher (postdoctoral research associate) was awarded a National Research

Council Postdoctoral Fellowship (September 1995) to work at the Naval Research Laboratory in collaboration with Dr. Tom Russell.

Prof. C. Wight (principal investigator) was elected a Fellow of the American Association for the Advancement of Science in 1994.

Scientific Publications (attached as Appendix)

1. D. C. Sorescu, T. R. L. Sutton, D. L. Thompson, D. Beardall, and C. A. Wight, "Theoretical and Experimental Studies of the Structure and Vibrational Spectra of NTO", J. Mol. Struct., J. Mol. Struct., 384, 87-89 (1996).

2. T. R. Botcher, D. J. Beardall, C. A. Wight, L. Fan, and T. J. Burkey, "Thermal Decomposition Mechanism of NTO", J. Phys. Chem., 100, 8802 (1996).

3. D. J. Beardall, T. R. Botcher, and C. A. Wight, "Explosive Thermal Decomposition Mechanism of NTO", in Decomposition, Combustion and Detonation Chemistry of Energetic Materials, T. B. Brill, T. P. Russell, W. C. Tao, and R. B. Wardle, Eds., (Materials Research Society: Pittsburgh, 1996) p. 379.

4. J. Sakata and C. A. Wight, "Shock-Initiated Chemistry of Energetic Materials", J. Phys. Chem. 99, 6584 (1995).

5. P. Ling and C. A. Wight, "Laser-Generated Shock Waves in Thin Films of Energetic Materials", J. Appl. Phys. 78, 7022, (1995).

6. P. Ling, J. Sakata, and C. A. Wight, "Detonation Chemistry of Glycidyl Azide Polymer", in Decomposition, Combustion and Detonation Chemistry of Energetic Materials, T. B. Brill, T. P. Russell, W. C. Tao, and R. B. Wardle, Eds., (Materials Research Society: Pittsburgh, 1996) p. 363.

7. P. Ling and C. A. Wight, "Laser Photodissociation and Thermal Pyrolysis of Energetic Polymers", J. Phys. Chem. B 101, 2126-2131 (1997).

APPENDIX

Publications citing support of AFOSR Grant F49620-94-1-0125

ELSEVIER

Journal of Molecular Structure 384 (1996) 87–99

Journal of
MOLECULAR
STRUCTURE

Theoretical and experimental studies of the structure and vibrational spectra of NTO

Dan C. Sorescu[1a], Teressa R.L. Sutton[a], Donald L. Thompson[a,*], David Beardall[b], Charles A. Wight[b]

[a]*Dept. of Chemistry, Oklahoma State University, Stillwater, OK 74078, USA*
[b]*Dept. of Chemistry, University of Utah, Salt Lake City, UT 84112, USA*

Received 5 June 1996; accepted 5 June 1996

Abstract

The structure and vibrational spectra of the high explosive 5-nitro-2,4-dihydro-3H-1,2,4-triazol-3-one (NTO) have been determined by ab initio molecular orbital calculations at the Hartree–Fock and second-order Møller–Plesset levels and by density functional theory (B3LYP). Experimental frequencies for the molecule have been determined from infrared spectra of pure NTO films and NTO molecules isolated in an argon matrix at 21 K. A force field for gas phase NTO has been obtained based on calculated results at the MP2/6-311G** level. In addition, a force field for solid state NTO has been constructed using the experimental vibrational frequencies for NTO films and scaled ab initio vibrational frequencies. Differences between the solid state and gas phase results indicate that the environment and preparation procedure exert a marked influence on the spectral characteristics of the NTO molecule.

Keywords: NTO; Infrared spectrum; Potential energy surface; Ab initio molecular orbital calculation; Density functional theory calculation

1. Introduction

The molecular structure of NTO (5-nitro-2,4-dihydro-3H-1,2,4-triazol-3-one) is shown in Fig. 1. In 1985 it was identified as a high explosive with several attractive attributes [1]. It is highly energetic and has explosive performance characteristics similar to RDX (hexahydro-1,3,5-trinitro-1,3,5-triazine). In spite of this, NTO is less sensitive than RDX; it is able to withstand much larger mechanical and thermal shocks without igniting. These characteristics make the material particularly well-suited to a variety of defense and civilian applications [1,2].

Numerous experimental studies of the thermal decomposition of crystalline NTO have been reported [3,9]. The results of these studies suggest a broad range of possible mechanistic steps such as the auto-catalytic mechanism [3], nitrogen–hydrogen bond cleavage [4], NO_2 elimination with formation of amide fragments [5,6], or hydrogen transfer to the nitro groups followed by subsequent loss of HONO [8]. Corresponding to this wide variety of chemical processes reported in the various kinetics studies of NTO [3–7] are significant spreads in the values of the

* Corresponding author.
[1] Present address: Dept. of Chemistry, University of Pittsburgh, Pittsburgh, PA 15260.

PII S0022-2860(96)09343-X

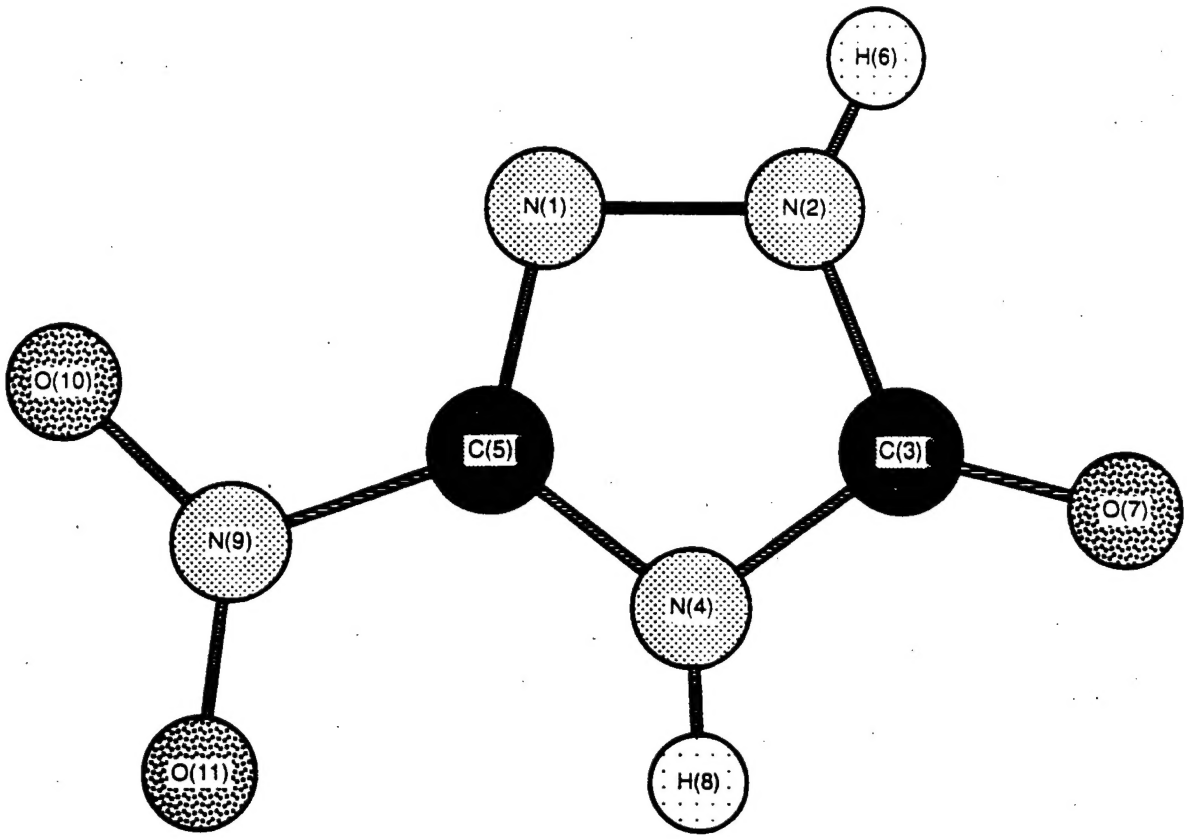

Fig. 1. Atom designation and numbering for NTO.

Arrhenius parameters: activation energies in the range 40.7 to 120.4 kcal mol^{-1} and pre-exponential factors, ln$A$, between 26.9 and 112.1 s^{-1}. However, most of these data can be unified based on a "kinetic compensation effect" [9]. That is, different pairs of values (E_a, $-\ln A$) lie on or close to a compensation regression line, i.e., $\ln A = aE_a + b$. Similar kinetic compensation effects have been found in the case of other energetic materials such as RDX and HMX (octahydro-1,3,5,7-tetranitro-1,3,5,7-tetrazocine) [9]. These demonstrate that kinetic data for thermal decomposition of NTO, RDX and HMX are highly dependent on the experimental conditions and sample characteristics. Thus, it is useful to undertake additional theoretical and experimental studies to elucidate the influence of the physical state of the material and of the reaction conditions on a particular reaction mechanism.

One way to resolve some of the matters is to study the dynamics of thermal decomposition of NTO by using molecular dynamics calculations. This requires the formulation of an accurate potential energy surface (PES) for the thermal decomposition of NTO that describes the main geometric, spectroscopic and thermochemical parameters of the reactant, products and transition states. We have previously used such semiempirical PESs in molecular dynamics and Monte Carlo simulations to study the dynamics of other cyclic nitro and diazo compounds such as RDX [10,11] and 2,3-diazabicyclo(2.2.1)hept-2-ene [12].

The general strategy followed in the construction of semiempirical PESs is to determine a parametrization of the potential terms as functions of the valence coordinates that reproduces the maximum number of known physical and chemical features. The quantities used in the parameter adjustments include the equilibrium bond lengths and bond angles, the experimental or ab initio calculated fundamental vibrational

frequencies for the reactants, products and transition states, the exo- and endothermicities for each of the reaction channels, and the reaction profiles and barrier heights. The main difficulties of this procedure result from the lack of measured or calculated data for the critical regions of the potential, particularly the transition states for reaction channels. This is also true for the case of the NTO molecule. We have performed experimental and theoretical studies to elucidate the geometric and spectroscopic parameters for NTO in the gas and solid phases.

The structure of NTO has been determined experimentally only for the β crystal form [13]. Some efforts have been made to determine the crystal structure of α-NTO, but the structure was refined only to a weighted R index of 17% and the details of the structure have not been given [13]. Some of the geometric parameters for several possible tautomers of NTO as well as some conjugate bases of these compounds have been reported by Ritchie [14] based on molecular orbital calculations at the AM1, 3-21G//3-21G and 6-31G*//3-21G levels. He found that the structure presented in Fig. 1 is the most stable isomer at these levels of theory, irrespective of nitro group substitution.

In an attempt to have a better characterization of the geometric and spectroscopic parameters of NTO in gas phase, in the present study we report the results of ab initio calculations at the Hartree–Fock (HF) and second-order Møller–Plesset (MP2) levels using different types of basis sets. For the purpose of comparison and as an alternative to the computationally demanding MP2 method we have also used density functional theory (DFT), in the Kohn–Sham formulation [15,16]. Recent studies have shown that nonlocal DFT techniques are superior to Hartree–Fock theory for calculating molecular force fields [17–19]. The fundamental vibrational frequencies were calculated using analytical second derivatives for the optimized geometries.

Ideally, the interpretation and the accuracy of the theoretical frequencies should be done in connection to gas-phase experimental results. However, such data are not obtainable. It is, however, possible to mimic to some degree gas-phase conditions by using a rare gas matrix. Thus, we have measured IR spectra of NTO isolated in an argon matrix at 21 K. These spectra consist of well-defined, narrow infrared bands indicative of minimal intermolecular interactions.

As was mentioned before the sample characteristics apparently have significant influence on the kinetic data. We were interested in determining if the spectral features of NTO are influenced by environment and thus we have recorded the experimental spectrum of thin films of pure NTO. We found that this spectrum is significantly different from those for NTO isolated in an argon matrix. Indeed, the infrared bands exhibit extensive broadening and large frequency shifts due to strong intermolecular interactions in the polycrystalline phase.

The ab initio or experimental results for geometries and fundamental frequencies determined in this study were further used in conjunction with the crystallographic results for β-NTO [13] to develop two force fields, one specific for gas-phase NTO and the second for NTO in crystalline phase. The geometry and the scaled theoretical frequencies determined at the MP2/6-311G** level were used for gas-phase NTO. In the case of solid-phase NTO we have used the experimental geometry reported for β-NTO [13] and our experimental vibrational frequencies for NTO films. The frequencies that are missing in the measured spectra were obtained by scaling the fundamental frequencies from the ab initio calculations. The accuracy of these force fields are illustrated by normal-mode analyses and power spectra calculations. These force fields can be used in development of reliable PESs for studying the thermal decomposition of NTO in the gas and solid phases.

2. Theoretical procedure

It was previously shown [20,21] that a proper description of NO_2-containing molecules based on ab initio calculations should be done using multiconfigurational methods, especially when description of a transition state is involved. For the case of NTO molecule such an approach is beyond our computational resources, so we have considered the use of single-reference calculations at the MP2 level. In a recent study [22], Morokuma et al. have shown that for the case of $NH_2 + NO_2$ reaction, involving the H_2NNO_2 intermediate, the use of MP2 optimized geometries is a viable alternative. Similarly, a good description

of the structures and thermochemistry of other systems, such as NH_4NO_2 and $NH_4N(NO_2)_2$, can be obtained using the MP2 level [23].

Standard ab initio molecular orbital calculations were carried out using the Gaussian 92 [24] and Gaussian 92/DFT [25] system of programs. Geometry optimizations were performed with basis sets 3-21G (split valence [26]), 6-31G* (split-valence plus heavy-atom polarization [27]), 6-31G** (split-valence plus polarization [27,28]) and 6-311G** (triple-ζ-valence plus dp-polarization [29]). The structure of NTO was first optimized under C_s symmetry at the restricted Hartree–Fock level using analytical gradients and then refined within the second-order Møller–Plesset (MP2) perturbation theory [30]. An attempt to optimize the structure under C_1 symmetry led to essentially the same configuration and energy as in the case of C_s symmetry.

We have also investigated the use of efficient DFT codes for predicting the geometry and harmonic vibrational frequencies. We used Becke's three parameter exchange functional [31] in combination with the Lee, Yang and Pan correlation functional [32] (B3LYP). In this case the geometry optimizations were performed with 6-311G** and 6-311++G** (triple-ζ-valence plus dp-polarization and diffuse functions [33]) bases. Harmonic frequency analyses using analytical second derivatives were carried out at all stationary points of interest. The calculated frequencies and the corresponding intensities have been used to predict the IR spectra. The values of harmonic vibrational frequencies determined at the HF/6-31G*, MP2/6-31G*, MP2/6-31G** and MP2/6-311G** levels have been uniformly scaled with the factors 0.8929 [34], 0.94 [35], 0.94 [35] and 0.95 [36], respectively, to take into account the over-estimation of vibrational frequencies at these levels of theory. In the case of B3LYP frequencies we used the overall scaling factor 0.963, recently proposed by Pulay [18].

3. Experimental details

NTO (1,2-dihydro-5-nitro-3H-1,2,4-triazol-3-one) is synthesized by adding formic acid (88%, 65 ml) to semicarbazide hydrochloride (13.5 g), according to the method of Lee et al. [2]. The product is reduced to dryness in a rotary evaporator. Nitration is carried out with a mixture of 20% conc. sulfuric acid and 80% conc. nitric acid. The final product, purified by three recrystallizations from boiling water and air dried for 24 h, undergoes decomposition at 260°C [37].

Neat NTO films are deposited in vacuum from a Knudsen oven (120°C) onto a CsI window at room temperature [38]. Typical rate of deposition is $8.14 \cdot 10^{-3}$ cm h^{-1} (determined by HeNe laser interferometry). Some samples were formed by spraying a dilute solution of NTO in acetone onto a room temperature CsI substrate window using an air brush. These samples were allowed to dry several hours at 25°C to completely remove the solvent.

Samples of NTO isolated in solid argon are formed by codeposition of NTO and argon (which is admitted through the oven) onto a CsI window at 21 K. The window is cooled by a closed-cycle helium refrigerator (APD Cryogenics Displex Model DE-202S). Depositions are typically carried out at a rate of $9.86 \cdot 10^{-3}$ cm h^{-1} for 5 h. The mole fraction of NTO in these samples is $\sim 3 \cdot 10^{-4}$. Two blank experiments were performed in which argon was deposited through the oven in order to identify infrared bands of impurity molecules, which were excluded from the assignments of the NTO spectra.

Transmission infrared spectra are obtained with the use of a Mattson Research Series FTIR spectrometer at 0.25 cm^{-1} resolution.

4. Results and discussion

4.1. Structural characterization

The NTO geometries optimized at the HF/3-21G, HF/6-31G*, MP2/6-31G*, MP2/6-31G**, MP2/6-311G**, B3LYP/6-311G** and B3LYP/6-311++G** levels are given in Table 1. The atom designation and numbering used in the discussion here is shown in Fig. 1.

It can be seen by inspecting the data in Table 1 that there are marked variations of geometric parameters going from HF/3-21G and HF/6-31G* to MP2/6-31G*, which reflect the significant effects of electron correlations in this molecule. However, there is little change in going from MP2/6-31G* to MP2/6-311G**.

The DFT calculations using the B3LYP functional provide an excellent description of the NTO molecule compared to the MP2 calculations. For the majority of

Table 1
Geometrical parameters for NTO molecule

Parameter	HF 3-21G*	HF 6-31G*	MP2 6-31G*	MP2 6-31G**	MP2 6-311G**	B3LYP 6-311G**	B3LYP 6-311++G**	Exp.
$r(N_1-N_2)$	1.4004	1.3525	1.3656	1.3656	1.3617	1.3594	1.3581	1.369
$r(N_2-C_3)$	1.3845	1.3703	1.3929	1.3928	1.3935	1.3979	1.3975	1.367
$r(C_3-N_4)$	1.3915	1.3806	1.4053	1.4048	1.4065	1.4048	1.4030	1.378
$r(N_4-C_5)$	1.3640	1.3591	1.3584	1.3580	1.3577	1.3646	1.3656	1.349
$r(C_5-N_1)$	1.2660	1.2577	1.3110	1.3106	1.3058	1.2900	1.2906	1.290
$r(N_2-H_6)$	0.9934	0.9939	1.0129	1.0069	1.0085	1.0077	1.0085	0.875[a]
$r(C_3-O_7)$	1.2039	1.1894	1.2190	1.2188	1.2085	1.2026	1.2046	1.226
$r(N_4-H_8)$	0.9961	0.9952	1.0133	1.0075	1.0093	1.0080	1.0094	0.916[a]
$r(C_5-N_6)$	1.4191	1.4406	1.4407	1.4407	1.4478	1.4514	1.4518	1.447
$r(N_6-O_{10})$	1.2299	1.1824	1.2380	1.2380	1.2244	1.2139	1.2149	1.217
$r(N_9-O_{11})$	1.2504	1.1957	1.2468	1.2467	1.2338	1.2299	1.2300	1.218
$\theta(N_1-N_2-C_3)$	112.96	113.85	115.55	115.59	115.48	114.57	114.47	112.8
$\theta(N_2-C_3-N_4)$	101.55	101.48	100.30	100.27	100.27	100.54	100.70	103.8
$\theta(C_5-N_1-N_2)$	103.16	103.64	101.99	101.94	102.16	103.29	103.38	102.4
$\theta(H_6-N_2-N_1)$	119.77	120.23	119.37	119.50	119.55	120.09	120.06	115.7
$\theta(O_7-C_3-N_2)$	129.10	129.29	129.92	129.95	130.06	129.63	129.49	126.9
$\theta(O_7-C_3-N_4)$	129.35	129.23	129.78	129.78	129.67	129.84	129.81	129.3
$\theta(H_6-N_4-C_3)$	126.59	125.93	125.63	125.74	125.70	126.08	125.93	123.3
$\theta(N_9-C_5-N_4)$	120.76	121.52	121.75	121.70	121.59	121.74	121.88	123.2
$\theta(O_{10}-N_9-C_5)$	118.09	118.03	117.99	117.98	117.88	118.27	118.46	117.4
$\theta(O_{11}-N_9-C_5)$	114.48	114.76	114.91	114.87	114.91	114.67	114.73	116.2
$\theta(O_{10}-N_9-O_{11})$	127.43	127.20	127.10	127.15	127.21	127.05	126.80	126.4
$\tau(N_1-N_2-C_3-N_4)$	0.0	0.0	0.0	0.0	0.0	0.0	0.0	0.06[a]
$\tau(C_5-N_1-N_2-C_3)$	0.0	0.0	0.0	0.0	0.0	0.0	0.0	0.44[a]
$\tau(N_9-C_5-N_1-N_2)$	180.0	180.0	180.0	180.0	180.0	180.0	180.0	178.92[a]
$\tau(O_{10}-N_9-C_5-N_1)$	0.0	0.0	0.0	0.0	0.0	0.0	0.0	− 3.33[a]
$\tau(O_{11}-N_9-C_5-N_4)$	0.0	0.0	0.0	0.0	0.0	0.0	0.0	− 2.53[a]

[a] Calculated using the atomic positions given in [13].

bond lengths the differences between the values found at the MP2/6-311G** and Becke3LYP/6-311G** are smaller than 0.006 Å, with the exception of C_5-N_1 and N_9-O_{10} bonds where differences of 0.015 Å and 0.010 Å are found, respectively. There is similar good agreement for the bond angles, with a maximum deviation of 1.13° between the two sets. The inclusion of the diffuse functions in the Becke3LYP/6-311G** basis set does not have significant effects as can be seen in Table 1 by comparing the geometric parameters in columns 7 and 8.

As mentioned above, the gas-phase structure of NTO has not been measured. The experimental values given in Table 1 correspond to those in the β-NTO crystal determined by single-crystal X-ray methods [13]. As can be seen by comparing the experimental data to the theoretical results at the MP2/6-311G** level, the majority of the crystal bond lengths are smaller than those calculated for the gas-phase geometry. For the heavy atoms the largest difference is 0.0285 Å and occurs for the case of the C_3-N_4 bond. For bond angles, the maximum difference is 3.53° for the $N_2-C_3-N_4$ bond angle.

We cannot compare the values of the calculated N–H bond lengths to the experimental values for the β-NTO due to the fact that the coordinates of hydrogen atoms were not precisely determined. Indeed, it is known [39] that for C–H bonds, X-ray diffraction indicates a shift of electron density into the bond, while other methods such as the neutron diffraction or microwave spectroscopy indicate the nuclear positions.

Table 1 also shows some representative calculated dihedral angles of the crystal structure based on the atomic positions and group symmetry reported in [13]. These results indicate that the crystal structure of NTO is almost planar.

Table 2
Calculated energies (hartrees) and unscaled zero-point vibrational energies (kcal mol^{-1}) of NTO

Calculation level	Energy	ZPE
HF/3-21G*//HF/3-21G*	− 516.1778890	...
HF/6-31G*//HF/3-21G*	− 519.1263198	...
HF/6-31G*//HF/6-31G*	− 519.1378135	46.16321
MP2/6-31G*//MP2/6-31G*	− 520.5899862	42.11600
MP2/6-31G**//MP2/6-31G**	− 520.6082482	42.32594
MP2/6-311G**//MP2/6-31G**	− 520.8258908	42.08552
B3LYP/6-311G**//B3LYP/6-311G**	− 522.1216220	41.75989
B3LYP/6-311++G**//B3LYP/6-311++G**	− 522.1373248	41.58507

4.2. Energy considerations

Calculated total energies and zero-point energies at various levels are presented in Table 2. The values calculated at the HF/3-21G‖3-21G and HF/6-31G*‖3-21G levels are identical to those calculated by Ritchie [14] and are included here for comparison. Based on the group equivalents of Ibrahim and Schleyer [40] and the 6-31G*‖3-21G ab initio calculated energy, Ritchie has estimated a value of − 3.2 kcal mol^{-1} for the gaseous heat of formation of NTO. Recently, Politzer et al. [41] have calculated a gas phase heat of formation of − 5.7 kcal mol^{-1} for NTO based on a nonlocal density functional procedure plus empirical correction terms. Using this last value and the empirical correlation relation between the gaseous and condensed phase heats of formation for NTO [14], $H_f(c) = 1.13H_f(g) - 23.03$, an estimated value $H_f(c) = -29.47$ kcal mol^{-1} is found. This value differs by only 1.46 kcal mol^{-1} from the experimental value of − 30.93 kcal mol^{-1} determined by Finch et al. [42]. When the values of enthalpy of formation in solid [42] and gaseous phases [41] are combined a heat of sublimation equal to 25.23 kcal mol^{-1} is found.

4.3. Vibrational spectra

Experimental infrared spectra of NTO are shown in Fig. 2. Corresponding vibrational frequencies are listed in Table 3 along with the calculated frequencies. The spectrum of matrix-isolated NTO exhibits relatively narrow infrared absorption bands (FWHM typically less than 3 cm^{-1}). Bands were assigned to NTO based on three criteria. First, bands appearing in the blank experiments (deposition of argon only) were attributed to impurities and were eliminated from consideration. Second, the relative band intensities observed in three different matrix-isolated NTO samples were compared and only those bands appearing in all three spectra with comparable relative intensities were included in the assignments. Finally, the observed band frequencies and integrated intensities were compared with the theoretical calculations to make the final assignments.

In contrast, the spectrum of neat NTO exhibits much broader features indicative of strong intermolecular interactions. This spectrum suggests that our NTO crystals have the structure of the alpha polymorph. Indeed, there is a close match between this spectrum and the partial IR spectrum of the alpha polymorph published by Lee and Gilardi [13].

By comparing the spectra in Fig. 2 we observe that many of the frequencies are red- or blue-shifted by 100 cm^{-1} or more. The N–H stretching vibrational

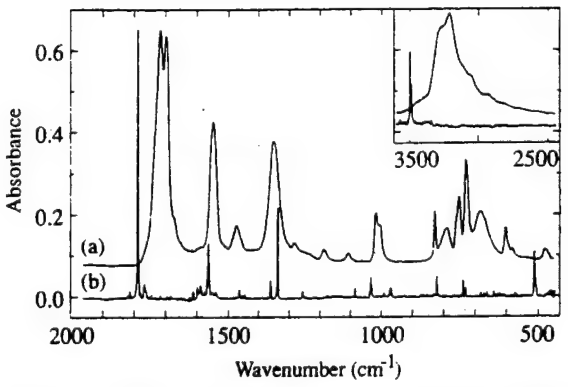

Fig. 2. (a) Infrared spectrum of a neat NTO film at room temperature. The film was deposited onto a CsI substrate window via airbrush from acetone solution. (b) Spectrum of NTO molecules isolated in an argon matrix at 21 K on a CsI window. The mole fraction of NTO is ~3 × 10^{-4}.

Table 3
Fundamental vibrational frequencies of NTO

Mode	MP2[a] 6-31G*	MP2[a] 6-31G**	MP2[a] 6-311G**	B3LYP[b] 6-311G**	B3LYP[b] 6-311++G**	Exp 1[c]	Exp 2[d]	Calc[e]	Calc[f]
1	70.8[g]	70.6[g]	68.5[h]	78.1[i]	77.3[i]	no[j]	no	72.3	72.9
2	132.3	131.8	132.2	137.6	135.0	no	no	139.0	135.5
3	191.3	190.9	191.9	194.5	194.2	no	no	228.7	195.7
4	258.9	258.9	257.6	292.0	287.8	no	no	254.5	263.4
5	385.7	385.7	389.5	390.3	389.1	no	no	385.0	397.4
6	436.5	436.5	413.9	448.7	446.8	no	no	387.6	423.5
7	438.7	440.7	444.1	468.0	469.6	no	no	443.4	455.7
8	517.7	515.9	500.1	522.5	517.1	512	480	499.5	480.9
9	542.9	542.7	552.9	561.9	560.9	573	606	552.9	608.8
10	597.4	597.5	604.4	628.0	624.9	613	693	604.9	686.9
11	651.1	650.0	681.6	716.9	707.6	730	728	681.9	727.0
12	685.0	683.4	709.6	726.5	725.3	no	no	709.0	735.0
13	706.4	705.9	715.3	736.9	726.7	738	751	715.3	751.5
14	772.0	771.6	797.4	813.1	809.8	822	805	796.8	804.6
15	946.7	944.8	946.8	944.1	946.4	971	830	946.8	830.5
16	952.3	951.3	961.5	972.9	970.7	991	1021	961.3	1021.3
17	1093.6	1091.8	1094.8	1045.6	1046.8	1085	1111	1094.8	1110.9
18	1141.4	1141.6	1149.7	1160.0	1162.8	1174	1185	1150.7	1186.9
19	1211.5	1211.7	1215.9	1217.9	1219.3	1257	1282	1216.1	1280.5
20	1296.1	1297.3	1305.8	1322.2	1313.0	1338	1343	1304.9	1341.5
21	1327.1	1331.7	1336.7	1343.1	1344.1	1361	1477	1336.7	1478.2
22	1434.3	1437.6	1436.6	1414.6	1410.6	1463	1550	1437.4	1552.2
23	1508.2	1509.7	1519.5	1557.0	1541.3	1563	1605	1519.7	1604.5
24	1707.5	1707.6	1723.3	1584.2	1570.1	1768	1695	1723.8	1696.2
25	1779.2	1780.9	1794.2	1801.4	1778.5	1789	1716	1794.9	1715.6
26	3452.3	3519.4	3509.5	3525.0	3517.5	3489	3200	3509.7	3193.3
27	3456.0	3523.3	3514.1	3526.8	3518.9	no	no	3514.8	3200.9

[a] Ab initio calculated.
[b] Density functional theory.
[c] NTO/Ar matrix experiment.
[d] Thin solid film experiment.
[e] Predicted by the semiempirical PES (Eq. (1)) for gas-phase NTO.
[f] Predicted by semiempirical PES (Eq. (1)) for thin film NTO.
[g] Values scaled by 0.94.
[h] Values scaled by 0.95.
[i] Values scaled by 0.963.
[j] Not observed.

band observed at 3489 cm^{-1} for the matrix-isolated NTO shifts down to 3200 cm^{-1} in the pure NTO film due to extensive hydrogen bonding. The presence of the hydrogen-bonding in the neat NTO is expected to have a marked effect only on a limited number of frequencies. However, our results suggest that this is not the case. Indeed, the spectral differences between the neat films and matrix-isolated NTO go far beyond that expected for hydrogen bonding. The influences of crystal defects, twinning, dipole–dipole interactions and random orientations of the crystallites with respect to the polarization of the IR beam serve to broaden and shift the spectral lines. This means that the observed frequencies correspond not only to the intramolecular motions, but to collective motions of groups of molecules as well.

The ab initio calculated and experimental vibrational frequencies for NTO isolated in an Ar matrix are compared in Table 3. The root-mean-square deviations for the 18 measured frequencies is 39.4 cm^{-1} at the MP2/6-31G*, 38.8 cm^{-1} at the MP2/6-31G** and 28.4 cm^{-1} at the MP2/6-311G** levels. The calculated

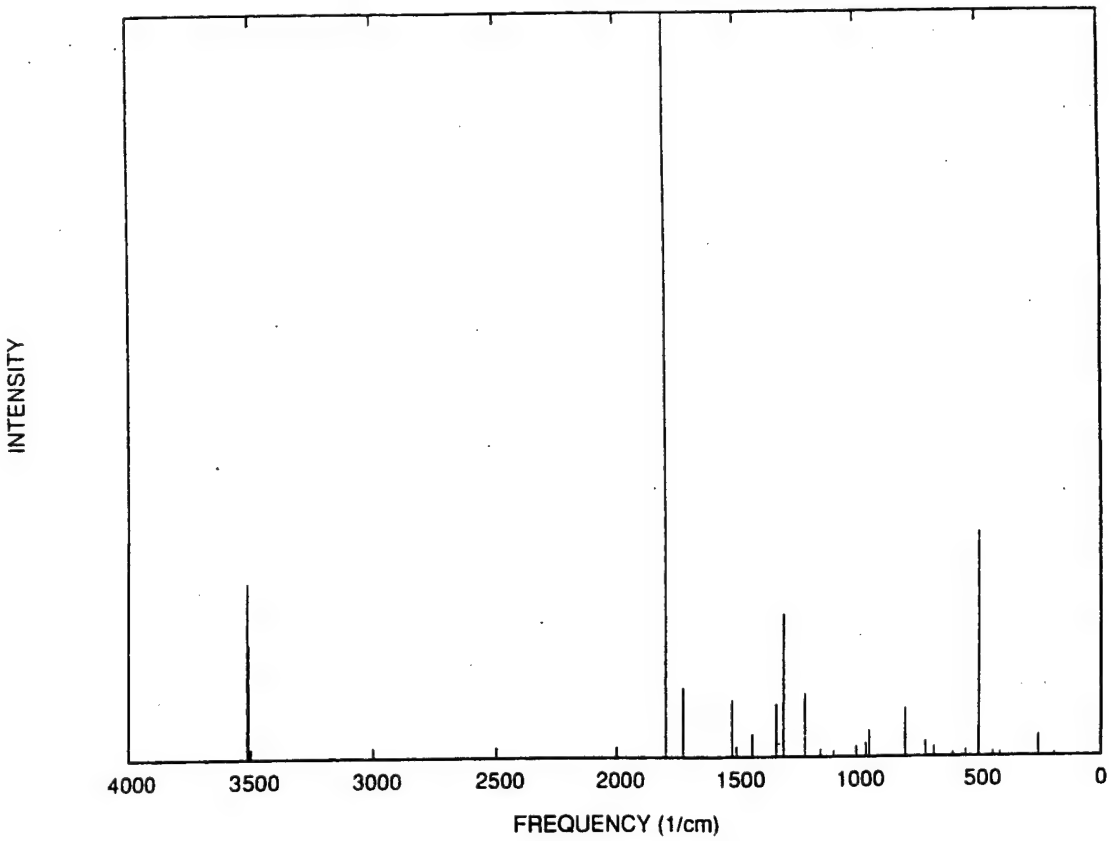

Fig. 3. Theoretical IR spectra of the NTO molecule calculated at the MP2/6-311G** level.

IR spectrum at the MP2/6-311G** level is presented in Fig. 3, while the corresponding eigenvectors are given in Fig. 4.

In Table 3 we present the vibrational frequencies determined by using DFT theory. Generally, there is close agreement between the scaled frequencies determined at the B3LYP/6-311G** and B3LYP/6-311++G** levels and the corresponding scaled MP2/6-311G** values, with root-mean-square deviations (excluding mode 24) of 20.9 cm^{-1} and 18.1 cm^{-1}, respectively. However, there is poor agreement for mode 24, which involves a NO_2 vibration, the DFT value is 1584.2 cm^{-1} compared to 1723.1 cm^{-1} calculated by MP2. The origin of this large deviation is not clear. A direct comparison of the scaled frequencies at MP2/6-311G** and B3LYP/6-311G** with the experimental values, excepting the mode 24, gives root-mean-square deviations of 27.2 and 23.5 cm^{-1}, respectively. These results suggest the possibility of using DFT methods to predict the normal vibrational frequencies with a fairly good accuracy.

4.4. Equilibrium force fields

The values of the geometric and spectroscopic data described above were used to construct equilibrium force fields for isolated NTO molecule (PES1) and for NTO in the neat solid (PES2). The total potential-energy surface is written as a sum of harmonic bond stretches and bond and wag angles and a truncated cosine series for the torsions:

$$V = \sum_{\text{bonds}} \frac{k_b}{2}(r-r_0)^2 + \sum_{\text{bends}} \frac{k_\theta}{2}(\theta-\theta_0)^2 + \sum_{\text{wags}} \frac{k_\gamma}{2}(\gamma-\gamma_0)^2 + \sum_{\text{torsions}} k_\tau(1-\cos(2(\tau-\tau_0))), \quad (1)$$

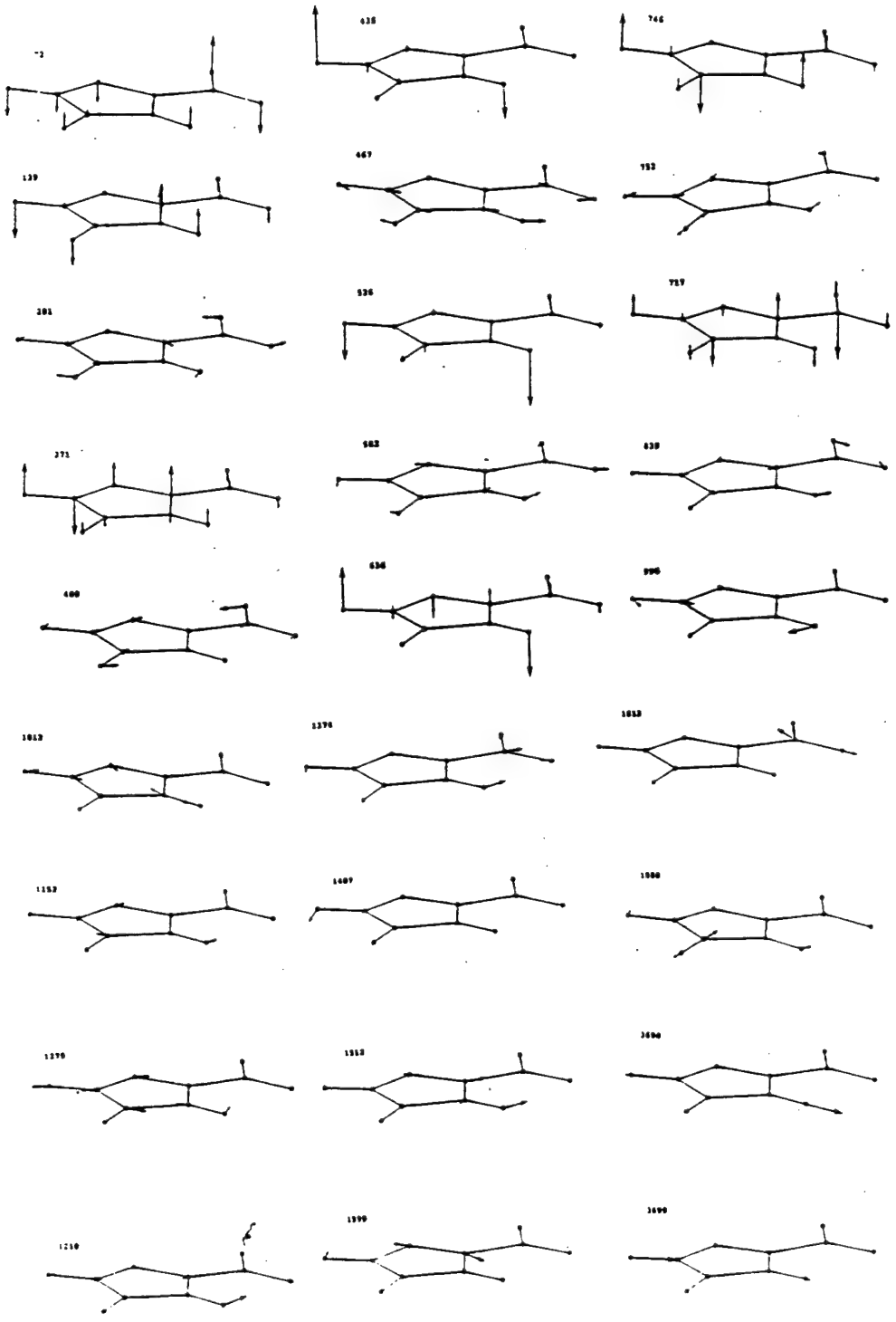

Fig. 4. The normal mode eigenvectors for NTO molecules obtained at MP2/6-311G** level. The indicated numbers correspond to the unscaled values of the frequencies.

Table 4
Geometry and force field parameters

	Gas phase		Thin film	
(a) Diatomic pair	r_0(Å)	k_r (kcal mol^{-1}Å^{-2})	r_0 (Å)	k_r (kcal mol^{-1}Å^{-2})
N_1–N_2	1.36167	625.9044	1.36900	775.6129
N_2–C_3	1.39350	229.2499	1.36712	721.2977
C_3–N_4	1.40657	649.9102	1.37751	510.3781
N_4–C_5	1.35772	434.8855	1.34847	579.9373
C_5–N_1	1.30585	356.8599	1.29031	592.1656
N_2–H_6	1.00854	979.7909	0.87545	810.7909
C_3–O_7	1.20854	769.1578	1.22641	800.6486
N_4–H_8	1.00932	982.6186	0.91564	812.6186
C_5–N_9	1.44785	954.6974	1.44668	760.1933
N_9–O_{10}	1.22444	721.4614	1.21680	709.8978
N_9–O_{11}	1.23380	671.9435	1.21800	747.0553
(b) Bond angle	θ_0 (deg.)	k_θ (kcal mol^{-1} rad^{-2})	θ_0 (deg.)	k_θ (kcal mol^{-1} rad^{-2})
N_1–N_2–C_3	115.48171	277.0935	112.81086	167.6350
N_2–C_3–N_4	100.26662	156.9281	103.79741	152.7514
C_3–N_4–C_5	107.98488	239.2295	105.86817	303.5688
N_4–C_5–N_1	114.10667	203.4175	115.15639	175.4953
C_5–N_1–N_2	102.16015	325.3054	102.35997	180.3936
H_6–N_2–N_1	119.55203	81.8644	115.65136	72.4440
O_7–C_3–N_2	130.05975	230.7410	126.96117	501.1958
H_8–N_4–C_3	125.70094	60.6617	123.30634	78.2801
N_9–C_5–N_1	124.29784	350.7930	121.58074	341.6415
N_9–C_5–N_4	121.59549	278.0675	123.26236	184.1071
O_{10}–N_9–C_5	117.88091	399.1255	117.3358	289.0394
O_{11}–N_9–C_5	114.90927	405.9188	116.33580	190.0737
O_{10}–N_9–O_{11}	127.20990	276.2264	126.48710	331.3401
(c) Wag angle	γ (deg.)	k_γ (kcal mol^{-1} rad^{-2})	γ (deg.)	k_γ (kcal mol^{-1} rad^{-2})
N_1–N_2–C_3–H_6	0.0	75.6128	–0.73486521	66.8019
N_2–C_3–N_4–O_7	0.0	30.5431	–0.80510661	84.2155
C_3–N_4–C_5–H_8	0.0	80.5196	–1.29814287	65.5663
N_4–C_5–N_1–N_9	0.0	81.8644	0.21498770	48.0182
(d) Dihedral angles	τ (deg.)	k_τ (kcal mol^{-1})	τ (deg.)	k_τ (kcal mol^{-1})
N_1–N_2–C_3–N_4	0.0	5.05	0.0634662	2.53
C_5–N_2–N_3–C_3	0.0	3.0	0.4449448	2.17
N_1–N_2–C_3–O_7	180.0	12.05	–178.9289266	15.53
N_9–C_5–N_4–C_3	180.0	0.75	–178.8375920	0.76
N_1–C_5–N_9–O_{10}	0.0	5.0	–3.3314816	4.74
N_4–C_5–N_9–O_{11}	0.0	5.0	–2.5361465	4.74
H_6–N_2–N_1–C_5	180.0	12.05	–178.7398418	15.52
H_8–N_4–C_3–N_2	180.0	3.55	–178.9771500	3.06

where the numbers of terms in the sums are 11 for bond stretches, 13 for bends, 4 for wagging and 8 for torsions.

In the case of gas phase NTO the parameters r_0, θ_0 and τ_0 in Eq. (1) were adjusted to reproduce the MP2/6-311G** equilibrium geometry given in Table 1. The force constants k_b, k_θ, k_γ and k_τ were adjusted to yield reasonable agreement with the scaled ab initio MP2/6-311G** frequencies.

The second force field, PES2, was constructed to reproduce both the experimental geometry of β-NTO [13] and the experimental vibrational frequencies determined in our thin solid films experiments. For the missing experimental frequencies we have used

specific scaling factors for ab initio data, i.e., 0.89 for stretches, 0.97 for bendings and 0.95 for torsions. These values have been obtained as averages of the ratios of the ab initio values and the corresponding experimental values. A complete list of the parameters used in eqn (1) for both PESs are given in Table 4. The variations of the geometry as well as the significant shifts of the infrared peaks in the case of the neat films relative to those for the gas phase made it necessary to adjust different types of force constants in PES2, i.e., N_2–H_6, N_4–H_8, N_2–C_3 bond stretches, O_7–C_3–N_2, C_5–N_1–N_2 bond bendings, etc. As discussed above the observed red or blue-shifts by 100 cm^{-1} of many frequencies cannot be due only to H-bonding. Consequently, there is not a specific set of force constants that describe completely these shifts.

A first check of the accuracy of the calculated force fields is done by performing normal mode analyses at the equilibrium geometries for comparison to ab initio and experimental frequencies. The computed eigenvalues for PES1 and PES2 are given in Table 3, columns 9 and 10, respectively. Analytical derivatives were used in the normal mode analyses.

As a second check we have determined the normal mode frequencies by calculating power spectra at the zero-point energy levels for PES1 and PES2. The composite power spectra shown in Fig. 5 have been obtained by Fourier transforming the averaged autocorrelation function of the time history of the internal coordinates as described in [43]. In this calculation every normal mode was initially assigned zero-point energy and the trajectory was integrated for 18.432 ps, which gives a resolution of 1.8 cm^{-1}. Before calculation of the autocorrelation spectrum the mean value of the data recorded during a trajectory was subtracted off. This procedure provides a set of coordinates which are stationary, with averages of zero.

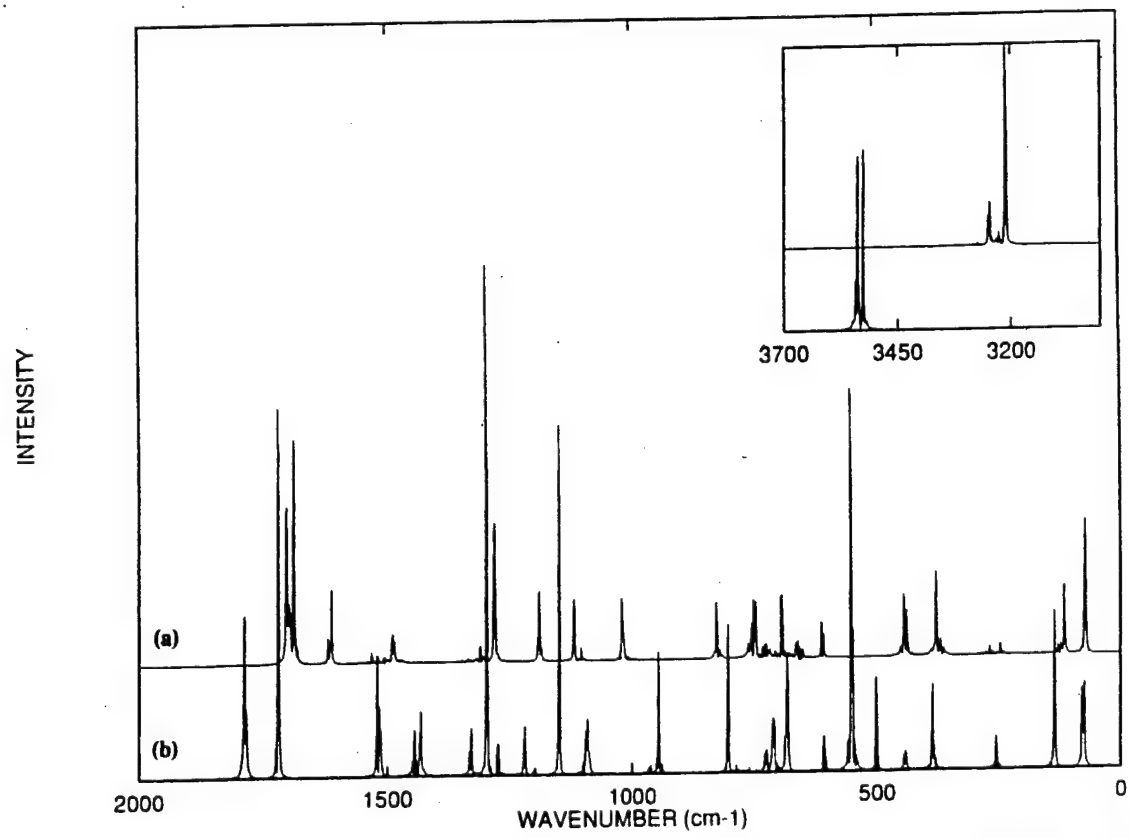

Fig. 5. Composite power spectrum for NTO at the zero-point energy levels using: (a) PES1 (ZPE = 40.00 kcal/mol); (b) PES2 (ZPE = 39.95 kcal mol^{-1}).

As can be seen by inspecting the values presented in Table 3 there is good agreement between the ab initio values and those calculated for PES1 as well as between the experimental frequencies (Exp2) and those obtained from PES2. The overall root-mean-square deviations between respective sets of frequencies are 8.91 cm^{-1} for PES1 and 1.8 cm^{-1} for PES2, with the largest deviations of 26 cm^{-1} and 6 cm^{-1}, respectively. The normal mode eigenvectors for PES1 are in good agreement with the ab initio eigenvectors. The frequency positions in the power spectra (Fig. 5) are in accord with those obtained in the normal mode analyses of PES1 and PES2.

5. Concluding remarks

Ab initio calculations and experimental spectroscopic studies were performed to determine the structure and fundamental vibrational frequencies for the NTO molecule in the gas phase, in a rare gas matrix and in thin films.

The experimental spectra recorded for NTO isolated in an Ar matrix and thin films have significant differences with large red or blue shifts of more than 100 cm^{-1}. The largest variations of the positions of spectral peaks are for N–H stretches. The observed spectral changes are due in part to extensive hydrogen bonding.

There is relatively good agreement between the scaled ab initio frequencies at the MP2/6-311G** level and the values measured for NTO isolated in an argon matrix. Except for the N–H bond lengths, similar good correspondence exists between the experimental geometry of β-NTO [13] and the optimized geometry at MP2/6-311G** level.

The results of DFT calculations demonstrate that the B3LYP exchange-correlation functional provides a description of the NTO molecule similar to that computed at the MP2 level. Indeed, it was found that the calculated values of the geometric parameters and vibrational frequencies at the MP2 and B3LYP levels are in fairly good agreement with each other and with the corresponding experimental values.

The experimental and theoretical results for the geometry and vibrational frequencies have been used to construct two force fields, one for NTO in gas phase and the other one for NTO in the neat phase. The results of normal mode analyses and power spectra at zero-point energies show that the semiempirical potentials accurately reproduce the ab initio and experimental results.

The results of this study provides deeper understanding of the IR spectral differences in NTO in different phases. Furthermore, they will facilitate the development of realistic potential energy surfaces that describe reactions of NTO in both the gas phase and in solid NTO.

Acknowledgements

This work was supported by the U.S. Air Force of Scientific Research (Grant numbers F-49620-95-L-0310, F-49620-92-J-0433 and F-49620-94-1-0125).

References

[1] K.Y. Lee and M.D. Coburn, Los Alamos Report LA-10302-MS, 1985.
[2] K.Y. Lee, L.B. Chapman and M.D. Coburn, J. Energ. Mater., 5 (1987) 27.
[3] E.F. Rothgery, D.E. Audetter, R.C. Wedlich and D.A. Csejka, Thermochim. Acta, 185 (1991) 235.
[4] J.A. Menapace, J.E. Marlin, D.R. Bruss and R.V. Dascher, J. Phys. Chem., 95 (1991) 5509.
[5] H. Östmark, H. Bergman, G. Åqvist, A. Langlet and B. Persson, Proc. Int. Pyrotech. Semin., 16 (1991) 874.
[6] K.V. Prabhakaran, S.R. Naidu and E.M. Kurian, Thermochim. Acta, 241 (1994) 199.
[7] X. Yi, R. Hu, X. Wang, X. Fu and C. Zhu, Thermochim. Acta, 189 (1991) 283.
[8] J.C. Oxley, J.L. Smith and Z. Zhou, J. Phys. Chem., 99 (1995) 10383.
[9] T.B. Brill, P.E. Gongwer and G.K. Williams, J. Phys. Chem., 98 (1994) 12242.
[10] T.D. Sewell and D.L. Thompson, J. Phys. Chem., 95 (1991) 6228.
[11] E.P. Wallis and Thompson, J. Phys. Chem., 99 (1993) 2661; (b) E.P. Wallis and D.L. Thompson, Chem. Phys. Lett., 189 (1992) 363.
[12] D.C. Sorescu, D.L. Thompson and L.M. Raff, J. Chem. Phys., 102 (1995) 7910.
[13] K.Y. Lee and R. Gilardi, in D.H. Lienbenberg, R.W. Armstrong and J.J. Gilman (Eds.), Structure and Properties of Energetic Materials, Materials Research Society, Pittsburgh, PA, Vol. 296, 1993, p. 237.
[14] J.P. Ritchie, J. Org. Chem., 54 (1989) 3553.
[15] R.G. Parr and W. Yang, Density Functional Theory of Atoms and Molecules; Oxford: New York, 1989.

[16] J.K. Labanowski and J.W. Andzelm (Eds.), Density Functional Methods in Chemistry; Springer: New York, 1991.
[17] B.G. Johnson, P.M.W. Gill and J.A. Pople, J. Chem. Phys., 98 (1993) 5612.
[18] G. Rauhut and P. Pulay, J. Phys. Chem., 99 (1995) 3093.
[19] P.J. Stephens, F.J. Devlin, C.F. Chabalowski and M.J. Frisch, J. Phys. Chem., 98 (1994) 11 623.
[20] M.L. McKee, J. Am. Chem. Soc., 108 (1986) 5784.
[21] D.S. Marynick, A.K. Ray and J.L. Fry, Chem. Phys. Lett., 116 (1985) 429.
[22] A.M. Mebel, C.-C. Hsu, M.C. Lin and K. Morokuma, J. Chem. Phys., 103 (1995) 5640.
[23] A.M. Mebel, M.C. Lin, K. Morokuma and C.F. Melius, J. Phys. Chem., 99 (1995) 6842.
[24] M.J. Frisch, G.W. Trucks, M. Head-Gordon, P.M.W. Grill, M.W. Wong, J.B. Foresman, B.G. Johnson, K. Raghavachari, J.S. Binkley, C. Gonzalez, R.L. Martin, D.J. Fox, D.J. Defrees, J. Baker, J.J.P. Stewart and J.A. Pople, GAUSSIAN 92; Gaussian Inc.: Pittsburgh, PA, 1992.
[25] M.J. Frisch, G.W. Trucks, H.B. Schlegel, P.M.W. Gill, B.G. Johnson, M.W. Wong, J.B. Foresman, M.A. Robb, M. Head-Gordon, E.S. Replogle, R. Gomperts, J.L. Andres, K. Raghavachari, J.S. Binkley, C. Gonzalez, R.L. Martin, D.J. Fox, D.J. Defrees, D.J.; J. Baker, J.J.P. Stewart and J.A. Pople, GAUSSIAN 92/DFT; Gaussian Inc.: Pittsburgh, PA, 1993.
[26] J.S. Binkley, J.A. Pople and W.J. Hehre, J. Am. Chem. Soc., 102 (1980) 939.
[27] W.J. Hehre, R. Ditchfield and J.A. Pople, J. Chem. Phys., 56 (1972) 2257. (b) M.M. Frankl, W.J. Pietro, W.J. Hehre, J.S. Binkley, M.S. Gordon, D.J. DeFrees and J.A. Pople, J. Chem. Phys., 77 (1982) 3654.
[28] P.C. Hariharan and J.A. Pople, Theor. Chim. Acta, 28 (1973) 213.
[29] R. Krishnan, M.J. Frisch and J.A. Pople, J. Chem. Phys., 72 (1980) 4244.
[30] (a) C. Møller and M.S. Plesset, Phys. Rev. 46 (1934) 618. (b) J. Binkley and J.A. Pople, Int. J. Quantum Chem., 9 (1975) 229. (c) J.A. Pople, J.S. Binkley and R. Seeger, Int. J. Quantum Chem., Symp. 10 (1976) 1.
[31] A.D. Becke, J. Chem. Phys., 98 (1993) 5648.
[32] C. Lee, W. Yang and R.G. Parr, Phys. Rev., B41 (1988) 785.
[33] T. Clark, J. Chandrasekar, G.W. Spitznagel and P.v.R. Shleyer, J. Comp. Chem., 4 (1983) 294.
[34] J.A. Pople, M. Head-Gordon, D.J. Fox, K. Raghavachari and L.A. Curtiss, J. Chem. Phys., 90 (1989) 5622.
[35] N.V. Riggs, U. Zoller, M.T. Nguyen and L. Radom, J. Am. Chem. Soc., 114 (1992) 4354.
[36] J.W. Gauld and L. Radom, J. Phys. Chem., 98 (1994) 111.
[37] B.M. Dobratz, LLNL Explosives Handbook: Properties of Explosives and Explosive Simulants; UCRL-52997, Lawrence Livermore National Laboratory: Livermore, CA, 1981.
[38] T.R. Botcher and C.A. Wight, J. Phys. Chem., 97 (1993) 9149.
[39] D.E. Williams in R.M. Metzger (Ed.), Crystal Cohesion and Conformational Energies, Springer–Verlag, Berlin, 1981, p. 10.
[40] M.R. Ibrahim and P.v.R. Schleyer, J. Comput. Chem., 6 (1985) 157.
[41] P. Politzer, J.S. Murray and M.E. Grice, Mat. Res. Soc. Symp, 1995 (in press).
[42] A. Finch, P.J. Gardner, A.J. Head and H.J. Majdi, J. Chem. Thermodynamics, 23 (1991) 1169.
[43] K.L. Bintz, D.L. Thompson, T.R. Gosnell and P.J. Hay, J. Chem. Phys., 97 (1992) 6432.

The Journal of
Physical Chemistry

Thermal Decomposition Mechanism of NTO

Tod R. Botcher, David J. Beardall, and Charles A. Wight

Department of Chemistry, University of Utah,
Salt Lake City, Utah 84112

Leimin Fan and Theodore J. Burkey

Department of Chemistry, University of Memphis,
Memphis, Tennessee 38152

Reprinted from
J. PHYS. CHEM., Volume 100, Number 21, Pages 8802–8806

Thermal Decomposition Mechanism of NTO

Tod R. Botcher, David J. Beardall, and Charles A. Wight*

Department of Chemistry, University of Utah, Salt Lake City, Utah 84112

Leimin Fan and Theodore J. Burkey

Department of Chemistry, University of Memphis, Memphis, Tennessee 38152

Received: October 9, 1995; In Final Form: March 13, 1996[⊗]

Thin films of NTO (5-nitro-2,4-dihydro-3*H*-1,2,4-triazol-3-one) are subjected to transient pyrolysis using a pulsed infrared laser in order to determine the initial steps of the thermal decomposition mechanism under rapid heating conditions. After heating, the film is quenched to 77 K in about 2 ms, thereby trapping reaction products which are subsequently detected by transmission Fourier-transform infrared spectroscopy. The first observed product of the decomposition is CO_2; no evidence has been found for formation of NO_2 or HONO in the early stages of thermal decomposition. The experimental results show that the CO_2 reaction product is formed by bimolecular oxygenation of the carbonyl group by the nitro group of an adjacent NTO molecule. This conclusion is contrasted with mechanisms proposed by other research groups based on slow heating experiments.

Introduction

NTO (5-nitro-2,4-dihydro-3*H*-1,2,4-triazol-3-one)[1] is a relatively new high explosive that has several desirable attributes, including a high heat of formation,[2,3] high density,[4] and relatively low sensitivity to shock or impact-induced ignition.[5] The fundamental characteristics which determine the sensitivity of explosives are poorly understood and are the subject of current research. One hypothesis is that sensitivity is related to the shear strength and molecular orientations of the crystalline material.[6] Another is that defects can sensitize a crystal by creating "hot spots" for concentration of mechanical energy and local heating of molecules. Yet another is that the sensitivity can be strongly influenced by the reaction mechanism, for example by early steps that either release large amounts of heat or create catalytic radical species. All of these factors may ultimately play a role in determining the performance characteristics of energetic materials. The focus of this paper is the chemical decomposition mechanism of NTO at high heating rates, i.e., conditions which simulate a thermal explosion.

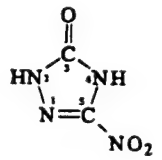

NTO

Several studies of NTO decomposition have been reported previously.[7−12] It has been suggested that the first step in the thermal decomposition of NTO is scission of the C−NO_2 bond, either by direct thermal activation[13,14] or catalyzed by H atom transfer and loss of HONO. Evidence for the latter reaction pathway comes from observations of a deuterium kinetic isotope effect (DKIE) in the global thermal decomposition rate[15] and from direct observation of NTO hydroxy nitroxide radicals by EPR spectroscopy in acetone solution.[6] Additional clues to the decomposition mechanism were provided by Fan *et al.* who synthesized isotopically labeled NTO and showed that N_2 produced during the decomposition originates predominantly from the 1 and 2 positions in the NTO ring.[17] Curiously, most experiments have found that the major gas phase products of decomposition are CO_2 and N_2, whereas NO_2 and HONO have been detected only in small amounts[13] or not at all.[9]

Although there is ample evidence for loss of HONO in the rate determining step of the decomposition reaction, it is difficult to determine the *initial* steps in the decomposition mechanism on the basis of the global kinetics. It is the initial steps that are more likely to influence the sensitivity of the material, whereas global kinetics are more closely associated with burn rates. With this in mind, we initiated a study of NTO decomposition by thin film laser pyrolysis (TFLP). This technique was used previously in our group to prove that the initial step in the decomposition mechanism of RDX (a widely used military high explosive) is scission of an N−NO_2 bond.[18−21] In that study, we detected condensed phase N_2O_4 which arose from dimerization of free NO_2 radicals produced in the initial step of the reaction mechanism. We expected that if C−NO_2 bond scission were the initial step in NTO decomposition, then it should be possible to observe condensed phase NO_2, N_2O_4, or HONO by IR spectroscopy following pulsed laser pyrolysis of thin film samples of NTO.

Our TFLP technique has two significant advantages for detecting initial reaction decomposition products compared with other techniques. First, the experiments are carried out at high heating rates, so the reaction mechanism is likely to be the same as that under actual ignition conditions. Second, the reaction products are detected by condensed phase spectroscopy, which nicely complements other techniques such as SMATCH/FTIR,[22] in which gas phase products are detected with high sensitivity.

Experimental Section

The experimental technique, which has been described in detail elsewhere,[19] involves preparation of a thin film (~10 μm) of explosive on the surface of an inert optical window. The sample is cooled to 77 K in vacuum and irradiated with a pulsed CO_2 laser having a 35 μs pulse duration. The laser heating initiates condensed phase reactions in the film, which are then

* Author to whom correspondence should be addressed.

⊗ Abstract published in *Advance ACS Abstracts,* May 1, 1996.

S0022-3654(95)02984-4 CCC: $12.00

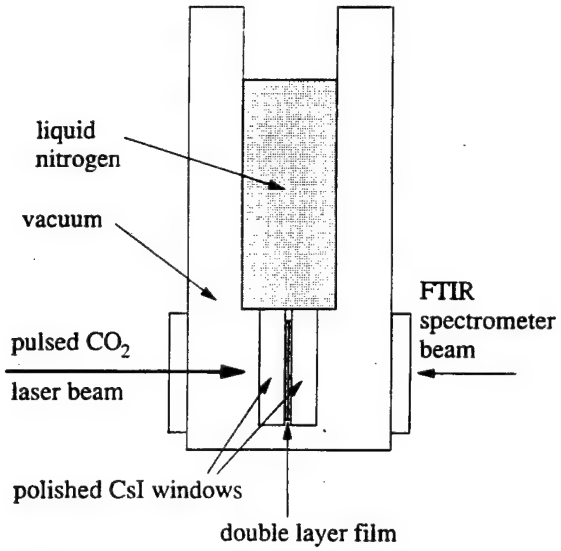

Figure 1. Schematic drawing of a layered sample of K_2HPO_4 and NTO inside the vacuum dewar vessel used for laser pyrolysis.

quenched on a millisecond time scale by conduction of the heat from the hot film to the cold supporting window. Transmission FTIR spectra of the film obtained before and after laser pyrolysis are used to detect the initial reaction products.

Thin films of NTO do not exhibit an appreciable infrared absorption band within the tuning range of a pulsed carbon dioxide laser. Therefore, our thin film laser pyrolysis technique was modified to incorporate two layered films: an inner layer of inert material which is heated by the laser and an outer layer of NTO, which undergoes decomposition as a result of heat transfer from the inner layer. Three different materials were used for the inert inner layer: dibasic potassium phosphate salt (K_2HPO_4), poly(vinyl chloride) (hereafter abbreviated PVC), or sodium tetrafluoroborate salt ($NaBF_4$). A thin film was formed by airbrushing a methanol solution of the salt onto a 25 mm diameter CsI optical window. A second layer of NTO was airbrushed onto the window from methanol solution. Most of the solvent evaporated during the airbrushing steps, and the samples were typically heated to 70 °C. to remove the remaining methanol. Thin films of PVC were deposited from *N,N*-dimethylformamide (DMF) solution, and in one experiment a film of $NaBF_4$ was deposited from acetone solution.

After drying, the sample was covered with a second CsI window and mounted in a copper retainer at the cold tip of a liquid nitrogen dewar vessel as shown in Figure 1. The vessel was typically evacuated overnight and then cooled to 77 K. The sample was irradiated with a single pulse from a carbon dioxide laser (Pulse Systems Model LP140G) through KBr windows mounted on the outside of the vacuum shroud. The dewar vessel was then placed in the sample compartment of an FTIR spectrometer (Mattson Model Polaris or Mattson Model RS-10000) and a spectrum of the film obtained by averaging 64 scans at 0.5 cm^{-1} resolution. In most experiments, spectra of the irradiated films were obtained before pyrolysis (77 K), after pyrolysis (77 K), and after warming to room temperature. More than 50 different experiments were carried out at laser fluences ranging from 0.41 J/cm^2 to 3.2 J/cm^2 in several different variations of the sample preparation conditions (a variety of film thicknesses and solid solutions of NTO in salts or PVC at different concentrations).

NTO was synthesized by nitration of TO (2,4-dihydro-3*H*-1,2,4-triazol-3-one) using a mixture of nitric and sulfuric acids. The TO was formed by a no-solvent condensation reaction of semicarbizide hydrochloride with formic acid. The final NTO product was purified by recrystallization from boiling aqueous solution. The indicated melting point was 262 °C, though some decomposition occurs below this temperature. The analytical mass spectrum and infrared spectrum were consistent with formation of the alpha polymorph of NTO.[23] A sample of isotopically labeled NTO-$^{13}C_1$ was synthesized in which the ^{13}C label was introduced exclusively at the carbonyl group (position 3 in the NTO ring). An analytical mass spectrum of this compound showed that the ^{13}C isotopic purity was greater than 99%.

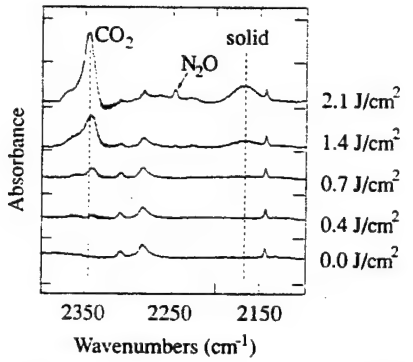

Figure 2. Spectra of reaction products formed after successive laser pyrolysis pulses of a double-layered sample (NTO on K_2HPO_4) at increasing fluence.

Results

Layered Samples. The first set of experiments was conducted using layered thin films of NTO with K_2HPO_4. At laser fluences above 0.4 J/cm^2 a small product band appears at 2345 cm^{-1}, as shown in Figure 2. This band is assigned to solid carbon dioxide trapped in the solid NTO sample at 77 K. At higher fluences, additional products are observed. A small band near 2250 cm^{-1} was tentatively identified as N_2O (gas phase frequency is 2224 cm^{-1}). As expected, the bands assigned to CO_2 and N_2O disappear when the sample is warmed to room temperature because the gases escape from the sample and are pumped out of the vacuum dewar vessel. A third product observed in the infrared spectrum exhibits a broad unstructured absorption band centered at 2168 cm^{-1}. This band is essentially unchanged after warming to room temperature, so it is attributed to a solid phase reaction product of NTO. Layered NTO/PVC samples exhibited no laser pyrolysis products other than a small yield of CO_2 (approximately 1% of the initial NTO concentration); the most likely reason for this is that the relatively small absorption coefficient of PVC at the laser frequency limited the extent of heating to produce CO_2 but no secondary reaction products. Layered NTO/$NaBF_4$ films that were pyrolyzed at 0.4 J/cm^2 also formed CO_2, as shown in Figure 3. The large absorption coefficient of $NaBF_4$ at the laser frequency allowed high temperature pyrolysis to the extent that the NTO absorption bands were attenuated to less than 50% of their original intensities, and samples pyrolyzed at fluences greater than 1.0 J/cm^2 exhibited several new bands in the spectral region 2000–2400 cm^{-1}. These were attributed to solid phase reaction products because they persisted after warming the sample to room temperature; however, none matched the 2168 cm^{-1} band observed previously using K_2HPO_4. No other reaction products were unambiguously identified under these extreme pyrolysis conditions.

Several control experiments were carried out to confirm that the CO_2 product arises from decomposition of NTO. Pyrolysis of a thoroughly dried K_2HPO_4 film (without NTO) at 2.6 J/cm^2 produced no new absorption bands, though samples that were

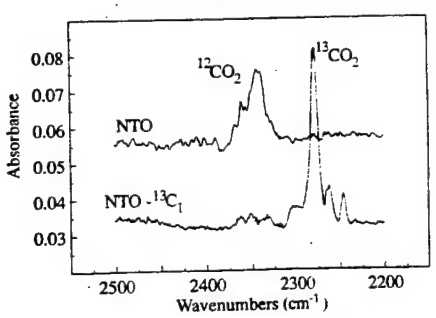

Figure 3. Post-pyrolysis infrared spectra of double layer films of sodium tetrafluoroborate with unlabeled NTO and with ^{13}C-labeled NTO in which the isotopic label is incorporated exclusively at the carbonyl position.

not completely dry produced observable CO_2 product bands, presumably due to pyrolysis of residual methanol solvent. Similar experiments on neat, dry PVC and $NaBF_4$ films produced no CO_2.

The second type of control experiment was designed to test if the CO_2 was produced by reaction of NTO with the phosphate salt. In one experiment, the K_2HPO_4 salt layer was coated with a layer of poly(tetrafluoroethylene) by spraying it with Teflon Dry Lube from an aerosol can. The NTO film was deposited on top of the Teflon layer, and the sample was pyrolyzed at 2.1 J/cm^2 in the usual manner at 77 K. In a second experiment, the K_2HPO_4 layer was covered with a layer of Teflon tape (sold commercially as pipe thread sealant) over the salt. The NTO film was deposited on the tape, and the sample was pyrolyzed at 77 K. In both of these experiments, CO_2 was observed as the only detected reaction product, though the yield was significantly lower than when the NTO was in direct contact with the K_2HPO_4 layer.

In three experiments, double-layer samples of ^{13}C-labeled NTO on $NaBF_4$ were pyrolyzed. At low fluence (less than 0.6 J/cm^2), the infrared spectra obtained after pyrolysis showed that the initial product was exclusively $^{13}CO_2$ (greater than 95% isotopically pure). However, at higher fluence, about 10% of the CO_2 observed after pyrolysis was unlabeled. In one experiment, two separate samples were prepared in which the NTO films (one containing the ^{13}C label and the other unlabeled) were deposited from tetrahydrofuran (THF) solution instead of methanol. The samples were then pyrolyzed at low fluence under identical experimental conditions. The labeled sample produced exclusively $^{13}CO_2$, whereas the unlabeled sample gave only $^{12}CO_2$ product.

Solid Solutions of NTO. In one series of experiments, samples were prepared by airbrushing mixtures of NTO with PVC in DMF solvent, thereby depositing a single film containing a mixture of the two compounds. The purpose of these experiments was to test whether CO_2 can be generated by isolated NTO molecules (in the host matrix), or whether intermolecular interactions between NTO molecules are required.

A stock solution was prepared, which contained 1.25×10^{-2} g/ml PVC in DMF solvent. The most concentrated solution was prepared for deposition by airbrush onto a CsI window by dissolving 0.39 g of NTO in 30 mL of stock solution. The resulting NTO/PVC film contained 0.51 mass fraction NTO. Additional solutions were prepared by successive dilutions with the PVC stock solution to produce a series of NTO/PVC films on CsI windows at 0.20, 0.11, 0.06, 0.03, 0.015 and 0.008 mass fraction NTO. After deposition, the films were dried and the amounts of NTO deposited were estimated using the integrated band intensities at 1548 and 1720 cm^{-1}. The PVC concentration was similarly estimated using an infrared band at 1425 cm^{-1}. The band intensities of PVC and NTO were converted to mol/cm^2 using conversion factors derived from standard samples of the pure compounds, and the thicknesses of the films were estimated using the known densities of PVC and NTO. The films were then pyrolyzed in the usual manner at 3.2 J/cm^2. CO_2 product bands were observed in each case. The results of this series of experiments are given in Table 1. Note that the yields of CO_2 were small (a few percent) in comparison with the amount of NTO initially present.

TABLE 1. Summary of Experimental Results from Pyrolysis of NTO/PVC Mixtures

mass fraction NTO[a]	film thickness[b] (μm)	NTO concn[c] (μmol/cm^2)	post-pyrolysis yield[d] of CO_2 (nmol/cm^2)
0.20	134	18.3 ± 9.0	150 ± 50
0.11	69	4.6 ± 2.3	148 ± 50
0.06	81	2.2 ± 1.1	11.5 ± 5
0.03	76	8.8 ± 4.0	40.0 ± 20
0.015	67	1.8 ± 0.9	1.9 ± 1.5
0.008	100	0.9 ± 0.4	0.32 ± 0.3

[a] Based on solution concentrations prior to sample deposition. [b] Calculated on the basis of PVC band intensity at 1425 cm^{-1}. [c] Estimated using NTO band intensities at 1548 and 1720 cm^{-1}. [d] Calculated on the basis of CO_2 band intensity at 2345 cm^{-1}.

A second series of experiments was carried out by preparing solid solutions of NTO in K_2HPO_4 (mole fraction 0.005 to 0.2). However, laser pyrolysis of residual amounts of methanol solvent produced significant amounts of CO_2, even in the absence of NTO. Therefore, the dependence of CO_2 product formation on the NTO concentration could not be reliably measured, and the results were discarded.

Gas Phase Detection of NTO Decomposition Products. Four experiments were conducted in which gas phase decomposition products were collected following transient laser pyrolysis of NTO crystals that were placed on one (horizontal) window of a sealed room temperature gas cell (5 cm path length) equipped with NaCl windows. The absorption coefficient of NTO is quite small, so the sample was subjected to 30 laser pulses in order to generate a significant quantity of CO_2 product. No other products were observed (e.g., CO, which could have been lost to vaporization in the 77 K experiments). Laser pyrolysis of a similarly prepared ^{13}C-labeled NTO sample resulted in formation of $^{13}CO_2$ in the gas cell. In a third experiment, the ^{13}C-labeled NTO was recrystallized from $^{18}OH_2$ solvent in order to test a hypothesis that residual water in the NTO crystal (left over from the final recrystallization/purification step of synthesis) might be responsible for hydrolysis of the carbonyl group of the NTO. The sample was placed in the gas cell and briefly evacuated. The infrared spectra obtained after pyrolysis showed bands attributable to $^{13}CO_2$ and a small quantity of $^{12}CO_2$, but no other isotopomers of CO_2 were observed. Based on the signal-to-noise ratio of the spectra, the maximum amount of $^{18}O^{13}C^{16}O$ that could have been produced was less than 5% of the $^{13}CO_2$ observed. In the fourth room temperature gas cell experiment, a double-layered sample of ^{13}C-labeled NTO on $NaBF_4$ was prepared on the surface of one of the NaCl windows. In order to minimize the possibility of including ordinary water in the films, the $NaBF_4$ layer was deposited from acetone solvent, and the NTO was deposited from THF solution. The sample was then thoroughly dried. Prior to assembly of the gas cell, a small drop of $^{18}OH_2$ was placed on top of the NTO film. The cell was quickly assembled and briefly evacuated. Post-pyrolysis spectra exhibited absorption bands of $^{18}OH_2$ and $^{13}CO_2$ but no evidence for $^{18}O^{13}C^{16}O$ or any other ^{18}O-containing species.

Discussion

The experiments described in the preceding section all share a common theme: transient laser pyrolysis of NTO results in the formation of carbon dioxide as a conspicuous product in the infrared absorption spectrum. Other reaction products have been detected following high fluence pyrolysis, but below about 0.7 J/cm^2 fluence, CO_2 is the only product detected by infrared spectroscopy. In almost all experiments, the fraction of NTO molecules pyrolyzed was small (less than 5%), but a few experiments were carried out under more severe conditions (greater than 50% reaction).

We made a careful search for the possible formation of HONO, NO_2, and N_2O_4 in each experiment because these molecules are the expected initial products of C−NO_2 bond scission (possibly catalyzed by H atom transfer to NTO). No evidence for these products was found in the infrared spectra. We had observed N_2O_4 in our earlier study of RDX thermal decomposition.[18-21] It is easily detected at low concentration (less than 1% of the precursor concentration) by a characteristic triplet of bands near 1735 cm^{-1}. The parent NTO molecule has a strong carbonyl absorption band at 1709 cm^{-1} that extends toward the region where N_2O_4 would be expected. The shape of this NTO band is particularly sensitive to slight changes in the crystal morphology that are induced by the laser pulse. This unfortunate source of spectral interference made it difficult to completely eliminate the possibility that N_2O_4 was being formed from pyrolysis of normal NTO. However, in the ^{13}C-labeled NTO, the carbonyl band shifts to 1656 cm^{-1}, and the spectral region where N_2O_4 would be expected is completely devoid of absorption bands both before and after pyrolysis, even at high fluence. Therefore, we can state with confidence that if N_2O_4 is formed under these experimental conditions, its concentration must be less than 5% that of the CO_2 product.

Having established carbon dioxide as a major reaction product that is formed early in the decomposition mechanism, we now turn our attention to showing that it is the first product that is detected by infrared spectroscopy. The integrated infrared absorption coefficient for the ν_3 fundamental of CO_2 is unusually large, so experiments of this type are particularly sensitive to detection of this product. In order to confirm that CO_2 is the first product formed, and not simply the first product detected, the integrated intensities of the two other products (spectra shown in Figure 2) were scaled by the integrated intensity of the CO_2 band in each spectrum and then plotted as a function of laser fluence. If a product is formed concurrently with CO_2, then its scaled intensity should be a constant function of fluence. Products formed in mechanistic steps following CO_2 formation should have a monotonically increasing fluence dependence, whereas those formed earlier than CO_2 should have a monotonically decreasing fluence dependence. The data shown in Figure 4 clearly demonstrate that the product corresponding to the 2168 cm^{-1} band is formed subsequent to CO_2 and that the threshold for N_2O formation is significantly higher than for the other two products.

The experiments carried out using ^{13}C-labeled NTO (where the label is incorporated exclusively at the carbonyl position) show that the CO_2 product formed early in the reaction comes exclusively from the carbonyl group. We note that after high fluence pyrolysis of labeled samples, a significant fraction (~10%) of the CO_2 formed is unlabeled. Therefore, oxidation of the ring carbon (position 5) apparently does occur in the later stages of the mechanism. However, near the pyrolysis threshold, essentially all of the CO_2 observed comes from the carbonyl position.

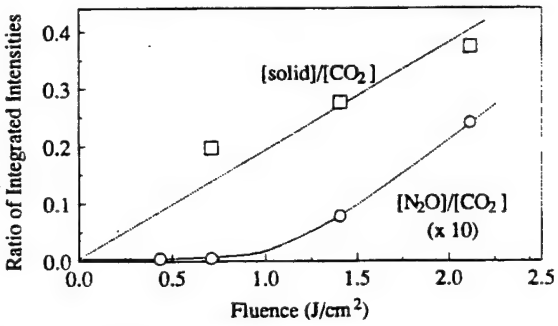

Figure 4. Integrated intensities of spectral features in Figure 2 attributed to N_2O (2250 cm^{-1}, circles) and an unidentified solid product (2160 cm^{-1}, squares), normalized to the integrated intensity of the CO_2 band (2345 cm^{-1}), and plotted as a function of laser fluence to determine the order of product formation (see text). Values for the N_2O band have been multiplied by 10 for clarity of presentation.

What is the reaction that converts the carbonyl group of NTO to CO_2? The synthesis of NTO calls for recrystallization of the material from aqueous solution as the final step of purification. We have observed significant outgassing of water and other gases from NTO crystals during heating in a Knudsen oven to about 65 °C. Therefore, the suggestion[24] that water may be involved in the initial reaction step is perfectly plausible. However, the room temperature gas cell experiments carried out with isotopically labeled NTO and H_2O offer convincing proof that impurity water molecules are not responsible for formation of CO_2 in the initial stages of reaction because none of the labeled oxygen in the water appears in the CO_2 product.

The reasonable alternatives to this are intermolecular or intramolecular oxygenation[25] of the carbonyl group by a nitro group. Our pyrolysis experiments on solid solutions of NTO in PVC were designed to determine whether the initial step of the decomposition is unimolecular or bimolecular. If the order of this reaction is n, then we can write a formal kinetic equation

$$n\text{NTO} \rightarrow \text{CO}_2 + \text{other products} \quad (1)$$

where n would be 1 for a unimolecular reaction and 2 for a bimolecular reaction. For a series of experiments carried out under identical pyrolysis conditions, the initial amount of CO_2 product detected should be proportional to the nth power of the initial NTO concentration

$$[\text{CO}_2]_i = k[\text{NTO}]^n \quad (2)$$

where k is a constant that depends on experimental conditions such as laser fluence, thermal conductivity, heat capacity, and thickness of the sample. For a series of experiments at sufficiently low NTO concentrations, these factors are essentially the same. Taking the logarithm of both sides, eq 2 becomes

$$\ln [\text{CO}_2]_i = \ln (k) + n \ln [\text{NTO}] \quad (3)$$

Therefore, a logarithmic plot of the initial CO_2 concentration (as measured by its integrated infrared band intensity) as a function of mass fraction NTO in PVC should give a straight line with slope equal to n, the order of reaction. This plot is shown in Figure 5, and the corresponding value of n is 1.9 ± 0.3. On this basis, we conclude that the initial step is bimolecular in nature. In other words, oxygenation of the carbonyl group to CO_2 occurs by reaction with the −NO_2 functional group on a neighboring molecule, viz.

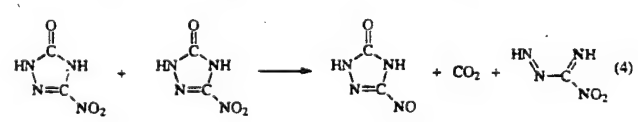

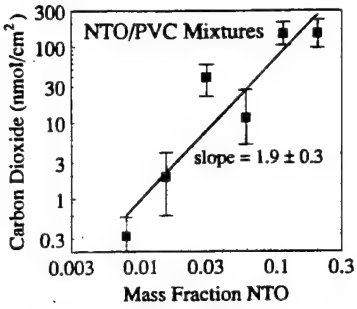

Figure 5. Pyrolysis yield of CO_2 (nmol/cm^2) as a function of mass fraction NTO in solid solutions with PVC. Data are taken from Table 1 and plotted on logarithmic scales. The solid line is a least-squares fit of the logarithmic data, and the slope of 1.9 ± 0.3 indicates that CO_2 is produced by bimolecular reaction of two NTO molecules (see text).

Subsequent decomposition steps may generate free radicals that initiate polymerization reactions in the solid. Polymeric residues have been reported by several groups following slow thermal decomposition. Williams *et al.* have shown that NTO and a large number of related materials produce large thermally stable cyclic azines (melamine and melon) during their decomposition.[26] These polymers consist of highly cross-linked C=N functional groups and may act as burn rate stabilizers in novel propellant formulations. The polymerization process is believed to liberate NH_3, which has been detected by NMR spectroscopy by Fan *et al.*[17] In our high fluence experiments conducted with K_2HPO_4 and $NaBF_4$ salt films, we observed several infrared bands due to solid phase reaction products that could be precursors to the melamine or melon polymers reported by Williams *et al.*[9] Their presence in the spectral region 2000–2400 cm^{-1} is consistent with the formation of products containing C=N double bonds. However, the position and shape of the bands were different for the two different salts, so we cannot rule out participation of the salts in the decomposition reactions themselves. A small band tentatively identified as N_2O was observed in the K_2HPO_4/NTO experiments but not in the $NaBF_4$/NTO experiments.

Acknowledgment. This research is support by the Air Force Office of Scientific Research under Contract No. F49620-94-1-0125. We thank Dr. Leanna Minier (Sandia National Laboratory) for several enlightening discussions during the course of this project.

References and Notes

(1) The name for NTO currently used by Chemical Abstracts Service (CAS, Registry No. 932-64-9) is 1,2-dihydro-5-nitro-3*H*-1,2,4-triazol-3-one. Other commonly used names include 5-nitro-1,2,4-triazol-3-one, 3-nitro-1,2,4-triazol-5-one, and 2,4-dihydro-5-nitro-3*H*-1,2,4-triazol-3-one. The last of these describes the most stable structure (refs 2 and 4), which is a tautomer of the structure indicated by the official CAS name.

(2) Ritchie, J. P. *J. Org. Chem.* **1989**, *54*, 3553.

(3) Finch, A.; Gardner, P. J.; Head, A. J.; Majdi, H. S. *J. Chem. Thermodynamics* **1991**, *23*, 1169.

(4) Lee, K.-Y.; Gilardi, R. In *Structure and Properties of Energetic Materials*; Liebenberg, D. H., Armstrong, R. W., Gilman, J. J., Eds.; Materials Research Society: Pittsburgh, PA, 1993; Vol. 296, p 237.

(5) Lee, K.-Y.; Chapman, L. B.; Coburn, M. D. *J. Energetic Mat.* **1987**, *5*, 27.

(6) Dick, J. J.; Ritchie, J. P. *J. Appl. Phys.* **1994**, *76*, 2726.

(7) Rothgery, E. F.; Audette, D. E.; Wedlich, R. C.; Csejka, D. A. *Thermochim. Acta* **1991**, *185*, 235.

(8) Yi, X.; Rongzu, H.; Xiyou, W.; Xiayun, F.; Chunhua, Z. *Thermochim. Acta* **1991**, *189*, 283.

(9) Williams, G. K.; Palopoli, S. F.; Brill, T. B. *Combust. Flame* **1994**, *98*, 197.

(10) Burkey, T. J.; Shackelford, S. A. Thermal Decomposition of NTO and NTO/TNT Mixtures. Report on contract F49620-88-C-0053, 1992.

(11) Prabhakaran, K. V.; Naidu, S. R.; Kurian, E. M. *Thermochim. Acta* **1994**, *241*, 199.

(12) Williams, G. K.; Brill, T. B. *J. Phys. Chem.* **1995**, *99*, 12536.

(13) Östmark, H.; Bergman, H.; Åqvist, G.; Langlet, A.; Persson, B. *Proceedings of the 16th International Pyrotechnics Seminar*; 1991, p 874.

(14) Östmark, H. *FOA Report D-20178 2.3*; National Defense Research Establishment: Sundbyberg, Sweden, Nov 1991.

(15) Oxley, J. C.; Smith, J. L.; Zhou, Z.;McKenney, R. L. *J. Phys. Chem.* **1995**, *99*, 10383.

(16) Menapace, J. A.; Marlin, J. E.; Bruss, D. R.; Dascher, R. V. *J. Phys. Chem.* **1991**, *95*, 5509.

(17) Fan, L.; Dass, C.; Burkey, T. J. *J. Labelled Compd. Radiopharm.* **1995**, *38*, 87.

(18) Wight, C. A.; Botcher, T. R. *J. Am. Chem. Soc.* **1992**, *114*, 8303.

(19) Botcher, T. R.; Wight, C. A. *J. Phys. Chem.* **1993**, *97*, 9149.

(20) Botcher, T. R.; Wight, C. A. In *Structure and Properties of Energetic Materials*; Liebenberg, D. H., Armstrong, R. W., Gilman, J. J., Eds; Materials Research Society: Pittsburgh, PA, 1993; Vol. 296, p 47.

(21) Botcher, T. R.; Wight, C. A. *J. Phys. Chem.* **1994**, *98*, 5441.

(22) Timken, M. D.; Chen, J. K.; Brill, T. B. *Appl. Spectrosc.* **1990**, *44*, 701.

(23) Sorescu, D. C.; Sutton, T. R. L.; Thompson, D. L.; Beardall, D. J.; Wight, C. A. Unpublished.

(24) We are grateful to Dr. Leanna Minier for bringing this possible mechanism to our attention in a private communication.

(25) The term oxygenation is used here instead of oxidation because the formal oxidation state of the carbon atom in the carbonyl group of NTO is the same as in CO_2.

(26) Stoner, C. E., Jr.; Brill, T. B. *Combust. Flame* **1991**, *83*, 302.

JP952984Y

EXPLOSIVE THERMAL DECOMPOSITION MECHANISM OF NTO

DAVID J. BEARDALL, TOD R. BOTCHER AND CHARLES A. WIGHT
Chemistry Department, University of Utah, Salt Lake City, UT 84112,
wight@chemistry.utah.edu

ABSTRACT

The initial step of the thermal decomposition of NTO (5-nitro-2,4-dihydro-3*H*-1,2,4-triazol-3-one) is determined by pulsed infrared laser pyrolysis of thin films. Rapid heating of the film and quenching to 77 K allows one to trap the initial decomposition products in the condensed phase and analyze them using transmission Fourier-transform infrared spectroscopy. The initial decomposition product is CO_2; NO_2 and HONO are not observed. We propose a new mechanism for NTO decomposition in which CO_2 is formed.

INTRODUCTION

NTO, shown in Figure 1, is an energetic material similar to RDX (hexahydro-1,3,5-trinitro-1,3,5-triazine), having a high density[1] and heat of formation.[2,3] However, NTO is much less sensitive to impact-induced ignition than RDX, which has prompted several recent investigations into the decomposition mechanism of NTO.[4-9]

Östmark, *et al.* used laser induced mass spectrometry to study NTO decomposition.[10,11] They observed formation of CO_2 and NO_2, and postulated that C-NO_2 bond cleavage is the initial step of thermal decomposition, followed by breakup of the azole ring. Menapace, *et al.* studied the decomposition of neat NTO and NTO dissolved in acetone or trinitrotoluene.[12] Their work indicated that the decomposition is bimolecular, beginning with H atom transfer and subsequent loss of HONO. The work by Oxley, *et al.*[13] is of special interest, in that they observed the formation of CO_2, N_2 and a polymeric solid which defied characterization. They also measured a primary deuterium kinetic isotope (DKIE) in the thermal decomposition of NTO, concluding that H atom transfer occurs in the rate determining step.

Of further interest is the work of Fan, Dass and Burkey,[14] in which they isotopically labelled NTO and found that N_2 formed during decomposition comes primarily from the adjacent nitrogen atoms in the ring. In addition, Brill and co-workers studied NTO thermal decomposition using Fast Thermolysis/FTIR[6] and found no evidence that NO_2 or HONO are generated. Instead, they report that CO_2 is the principal gas phase product.

With so little direct evidence for formation of NO_2 or HONO, the generally accepted decomposition mechanism (which requires the C-NO_2 bond be one of the first to break) must be called into question. This paper will address the issue of C-NO_2 bond cleavage and present an alternative mechanism of NTO decomposition.

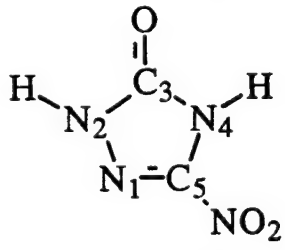

Figure 1 - NTO ring numbering.

In previous work,[15-18] thin-film laser pyrolysis (TFLP) was used to determine that the initial step in the decomposition of RDX was cleavage of an N-NO_2 bond. TFLP is an elegant technique for trapping the initial decomposition products formed at high heating rates, which closely mimics actual detonation conditions. A thin (1-5 μm) film of explosive is deposited onto a thick (3 mm) transparent window (usually CsI), cooled to 77K in

vacuum, and irradiated using a pulsed CO_2 laser, which causes rapid (35 μs) heating to several hundred Kelvin and initiates NTO decomposition. As the film cools to 77K over several milliseconds, the decomposition products are trapped by a CsI cover window placed on the film, and products are identified by Fourier-transform infrared spectroscopy.

EXPERIMENTAL

Because NTO does not have strong absorbance bands accessible to a pulsed carbon dioxide laser, it is necessary to deposit a thin film of absorbing substrate onto the window under the NTO layer to convert the energy of the laser pulse into heat, which then diffuses into the NTO film and initiates decomposition. Three different absorbing substrates are used during the course of these experiments: dibasic potassium phosphate salt (K_2HPO_4), low molecular weight poly(vinyl chloride) (PVC, Aldrich Chemical Co.) and sodium tetrafluoroborate salt ($NaBF_4$). Layered samples (using K_2HPO_4, PVC or $NaBF_4$) and solid solutions (K_2HPO_4 or PVC only) are studied.

NTO isotopically labelled with ^{13}C at the carbonyl position (NTO-^{13}C) used in this work was synthesized by T. Burkey at the University of Memphis. Normal NTO (NTO or NTO-^{12}C, m.p. 262°C) was synthesized by us according to a procedure communicated to us by T. Burkey. The mass and infrared spectra of NTO-^{12}C match those of the α-polymorph of NTO.[1]

All films studied in this work were deposited from solutions of the pure compound or mixtures onto polished CsI windows using an airbrush (Paasch type H with a #1 needle). All pure K_2HPO_4 films were deposited from methanol, as were K_2HPO_4/NTO solutions, and dried at 70°C after each deposition. Layered films of K_2HPO_4 and NTO were also dried at 70°C. Thin films of pure PVC and PVC/NTO solution were deposited from N,N-dimethylformamide (DMF) and placed in a beaker in a 140°C sand bath to drive off solvent. Layered films of NTO on PVC were similarly dried. $NaBF_4$ films were deposited from methanol and NTO films were deposited from methanol or tetrahydrofuran. Layered $NaBF_4$/NTO films were dried in a manner identical to PVC films. All films were mounted at the tip of a vacuum cell shown in Figure 2, evacuated overnight and cooled to 77K before pyrolysis. Spectra of the films were taken at 298K and 77K before and after pyrolysis using a Mattson RS-10000 spectrometer with 64 scans at 0.5 cm^{-1} resolution.

A Pulse Systems Model LP140G carbon dioxide laser (35 μs pulse length) was used to irradiate all of the samples reported in this work. Laser fluence for any given experiment was determined by measuring the power of several laser pulses with a Scientech absorbing disk calorimeter and placing the sample at the required distance from a gold focusing mirror (1 m radius of curvature). At high fluences, the beam profile was smaller than the area of the window, so the beam was rastered across the sample in such a way that the entire sample area probed by infrared spectrometer bean had been subjected to a single laser pulse.

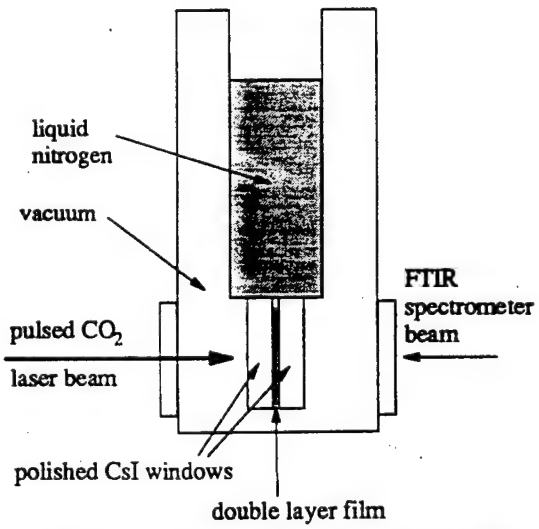

Figure 2 - Schematic of vacuum cell.

RESULTS

Layered Samples

Initially, thin layered films of K_2HPO_4 and NTO were prepared as described above and pyrolyzed. Three decomposition products were detected: CO_2 (s, 77K, 2345 cm^{-1}, fluence ≥0.4 J/cm^2), N_2O (s, 77K, 2250 cm^{-1}, fluence >0.4 J/cm^2) and an unidentified solid (77K, 2168 cm^{-1}, fluence >0.4 J/cm^2). Because CO_2 was an unexpected product, several control experiments were conducted to determine its source. The first consisted of pyrolysis at fluence up to 2.6 J/cm^2 of thin neat K_2HPO_4 films prepared as described above, sometimes yielding trace amounts of CO_2 from pyrolysis of methanol trapped in the film. In the second set of control experiments a layer of Teflon® was either sprayed (aerosol form) or stretched (teflon tape) between the salt and NTO layers. Subsequent pyrolysis yielded relatively large amounts of CO_2, coming presumably from the NTO.

PVC and NTO were layered on windows from DMF and methanol solutions, respectively. Pyrolysis of pure PVC films at fluence up to 3.1 J/cm^2 produced no detectable CO_2, while pyrolysis of layered films at 3.1 J/cm^2 produced measurable amounts of CO_2 in all cases. In no case was NO_2 detected.

Pyrolysis of ~1μm neat $NaBF_4$ films at 3.0 J/cm^2 produced no measurable CO_2. Experiments using normal and ^{13}C-labelled NTO were conducted to eliminate ambiguity about the source of CO_2. Pyrolysis of layered films of $NaBF_4$ and NTO-^{13}C yielded >95% $^{13}CO_2$ (s, 77K, 2279 cm^{-1}) at low laser fluence (~0.6 J/cm^2) and 90% $^{13}CO_2$ at high fluence (2.4 J/cm^2). Figure 3 shows that simultaneous pyrolysis of separate samples of NTO-^{12}C and NTO-^{13}C on $NaBF_4$ at 0.6 J/cm^2 produced exclusively $^{12}CO_2$ and $^{13}CO_2$, respectively.

Solid Solutions

Deposition and pyrolysis of single-layer, two component films of K_2HPO_4 and NTO was carried out. The mole fraction NTO in the prepared films (0.233, 0.066, 0.016, 0.0041 and 0.0046) was determined by measuring the integrated intensities of some NTO and K_2HPO_4 bands and comparing them to reference bands in spectra of pure NTO or K_2HPO_4 films of known mass. All pyrolyses were at a laser fluence of 1.03 J/cm^2. The yield of CO_2 (molecules CO_2/ initial number NTO molecules) is plotted as a function of NTO mole fraction in Figure 4.

Deposition of thin films of NTO/PVC solution was carried out as described. Pyrolysis was at 3.2 J/cm^2. Mass percent NTO was 0.20, 0.11, 0.06, 0.03, 0.015 and 0.008. The yield of CO_2 relative to the amount of NTO present in sample films was calculated as described above and appears in Figure 5.

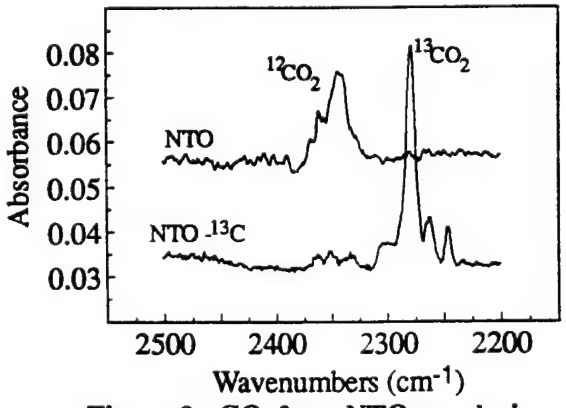

Figure 3 - CO_2 from NTO pyrolysis

Gas Phase Decomposition Products

Gas phase decomposition products of NTO were collected after pyrolysis of thin films and crystals of NTO in an evacuated gas cell fitted with NaCl windows. Pyrolysis was carried out by multiple (~30) laser pulses at 3.0 J/cm^2. Gaseous CO_2 produced

was always $^{12}CO_2$ or $^{13}CO_2$ from pyrolysis of NTO-^{12}C or NTO-^{13}C, respectively. Some samples of NTO-^{13}C were refluxed in and
recrystallized from $^{18}OH_2$. Pyrolysis of these NTO-^{13}C samples (wet with $^{18}OH_2$) showed the presence of gas phase $^{18}OH_2$ in addition to $^{13}CO_2$ in the gas cell. No evidence for the formation of $^{13}C^{18}O^{16}O$ or other isotopomers of CO_2 was observed.

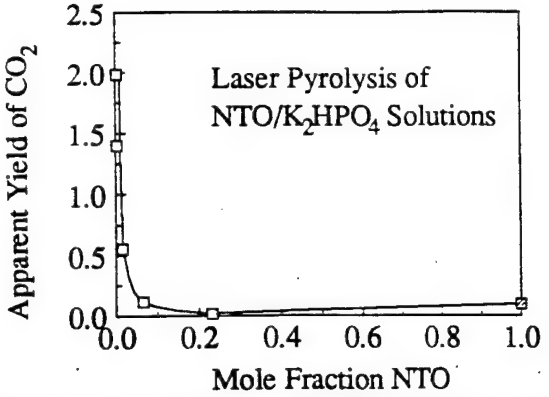

Figure 4 - CO_2 yield from NTO/K_2HPO_4 solution

CONCLUSION

In all experiments conducted, CO_2 was the initial decomposition product detected by infrared spectroscopy. Other products were detected, but only at higher energies. In experiments conducted just above the threshold for thermal decomposition, CO_2 was the only product detected. There was no evidence for formation of NO_2 (1617 cm^{-1}), N_2O_4 (1735 cm^{-1}) or HONO (1117 cm^{-1}). Experiments using NTO-^{13}C are ideal for detection of N_2O_4 because the carbonyl band shifts from 1717 cm^{-1} to 1656 cm^{-1}, clearing a spectral region between 1715 cm^{-1} and 1800 cm^{-1} which makes possible ready detection of small amounts of N_2O_4.

CO_2 can be demonstrated to be the initial I.R. active product formed during thermal decomposition by comparing the scaled intensity of product peaks as a function of laser fluence. Products formed concurrently with CO_2 will have a constant value as laser fluence changes, while products formed before or after CO_2 in the thermal decomposition will have monotonically decreasing or increasing slopes, respectively. Figure 6 shows that both N_2O and the product associated with the 2168 cm^{-1} band appear after the CO_2 formation step, and that N_2O has a formation threshold much higher than that for carbon dioxide.

Experiments have shown that the CO_2 formed during thermal decomposition includes the carbonyl group carbon, and most likely the carbonyl oxygen as well. Possible sources of oxygen which participate in oxidation of the carbonyl group to CO_2 include the -NO_2 group in the same or a neighboring NTO molecule, or impurities in NTO film (most likely water, because NTO is recrystallized from water). Control experiments with a Teflon® barrier between K_2HPO_4 and NTO films eliminate the possibility of this salt oxidizing NTO.

The gas cell experiments were conducted to test whether water is a source of oxygen for CO_2 formation. The presence of $^{18}OH_2$ vapor in the cell without incorporation of the ^{18}O label in product CO_2 indicates that water participation in carbonyl oxidation is not significant.

Thus, we can clearly state that carbonyl oxidation must be by interaction with a -NO_2 group in the same or a neighboring NTO molecule. The pyrolysis of solid solutions of NTO in K_2HPO_4 or PVC over a broad range of NTO concentrations can indicate whether or not the yield of CO_2 is dependent on the initial concentration of NTO in the sample. If

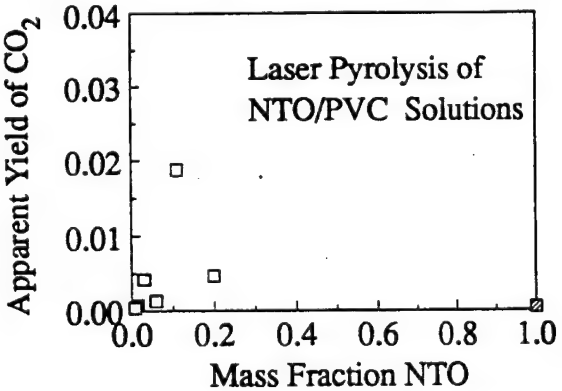

Figure 5 - PVC solution CO_2 yields.

CO_2 formation is independent of NTO concentration the reaction must be unimolecular, while an intramolecular reaction would show a concentration dependence. Considering all the data in Figure 4 and 5, we conclude that CO_2 formation is unimolecular.

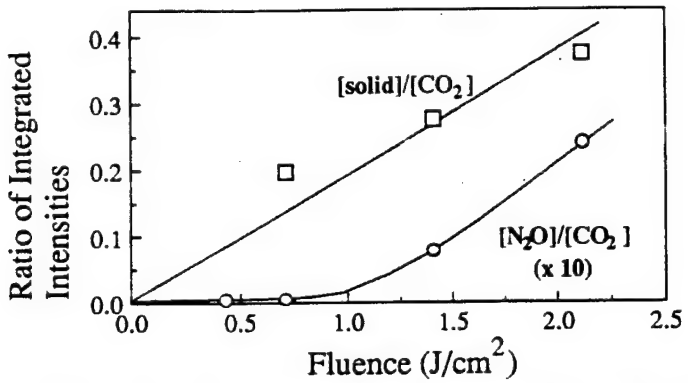

Figure 6 - Determination of product formation order.

A mechanism based on this data is shown in equation (1) below, beginning with ring opening and oxidation of the carbonyl group.

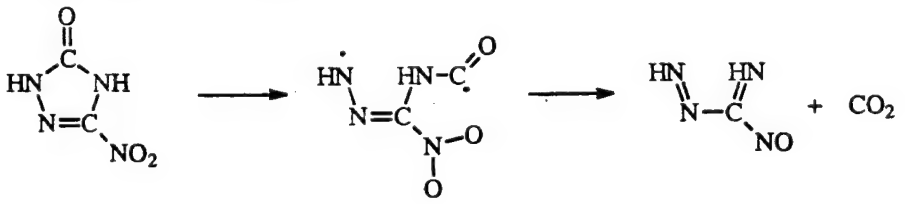

(1)

Formation of N_2 from the adjacent nitrogen atoms as described in equation (2) is consistent with the isotopic work done by Fan et al.

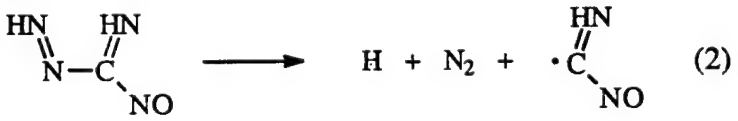

(2)

ACKNOWLEDGMENTS

This research is supported by the Air Force Office of Scientific Research. We thank Ted Burkey at the University of Memphis and Leanna Minier at Sandia/Lawrence Livermore National Labs for important discussions during the course of this work.

REFERENCES

1. K.-Y. Lee and R. Gilardi in Structure and Properties of Energetic Materials, edited by K.H. Liebenberg, R.W. Armstrong, and J.J. Gilman (Mater. Res. Soc. Proc. **296**, Pittsburgh, PA, 1993) p. 237.
2. J.P. Ritchie, J. Org. Chem. **54**, 3553, (1989).
3. A. Finch, P.J. Gardner, A.J. Head, and H.S. Majdi, J. Chem. Thermodynamics **23**, 1169 (1991).

4. E.F. Rothgery, D.E. Audette, R.C. Wedlich and D.A. Csejka, Thermochimica Acta, **185**, 235 (1991).
5. X. Yi, H. Rongzu, W. Xiyou, F. Xiayun and Z. Chunhua, Thermochimica Acta, **189**, 283 (1991).
6. G.K. Williams, S.F. Palopoli and T.B. Brill, Combust. Flame, **98**, 197 (1994).
7. T.J. Burkey and S.A. Shackelford, Thermal Decomposition of NTO and NTO/TNT Mixtures, Report No. 49620-88-C-0053, 1992.
8. K.V. Prabhakaran, S.R. Naidu and E.M. Kurian, Thermochimica Acta, **241**, 199 (1994).
9. G.K. Williams and T.B. Brill, J. Phys. Chem. **99**, 12536 (1995).
10. H. Östmark, H. Bergman, G. Åqvist, A. Langlet and B. Persson, in Proceedings of the 16th International Pyrotechnics Seminar, (1991) p. 874.
11. H. Östmark, FOA Report D-20178 2.3, National Defense Research Establishment, Sundbyberg, Sweden, 1991.
12. J.A. Menapace, J.E. Marlin, D.R. Bruss and R.V. Dascher, J. Phys. Chem. **95**, 5509 (1991).
13. J.C. Oxley, J.L. Smith, Z.Zhou and R.L.Mckenney, J. Phys. Chem. **99**, 10383 (1995).
14. L. Fan, C. Dass and T. Burkey, private communication.
15. C.A. Wight and T.R. Botcher J. Am. Chem. Soc., **114**, 8303 (1992).
16. T.R. Botcher and C.A. Wight, J. Phys. Chem., **97**, 9149 (1993).
17. T.R. Botcher and C.A. Wight in Structure and Properties of Energetic Materials, edited by D.H. Liebenberg, R.W. Armstrong and J.J. Gilman (Mater. Res. Soc. Proc.**296**, Pittsburgh, PA, 1993) p. 47.
18. T.R. Botcher and C.A. Wight, J. Phys. Chem., **98**, 5441 (1994).

Reprinted from The Journal of Physical Chemistry, 1995, 99.

Shock-Initiated Chemistry of Energetic Materials

Jill Sakata and Charles A. Wight*,†

Department of Chemistry, University of Utah, Salt Lake City, Utah 84112

Received: November 28, 1994; In Final Form: February 6, 1995®

The initial step of a reaction sequence initiated by a strong acoustic shock has been observed for the first time in a condensed phase energetic material. Shocks are generated by pulsed laser vaporization of thin aluminum films and launched into adjacent films of glycidyl azide polymer at 77 K through an inert spacer material. Changes in the composition of the polymer films are monitored by transmission FTIR spectroscopy. Comparison of spectra obtained before and after the shock reveals that the initial reaction sequence involves elimination of molecular nitrogen from the azide functional groups on the polymer.

Introduction

Elucidation of the individual chemical steps that occur during a condensed phase explosion or detonation presents an extremely challenging problem. Reactions occur on a fast time scale and in an environment that is generally unfriendly from the standpoint of spectroscopic interrogation. Much of the recent interest in this field stems from a desire to understand the sensitivity of explosives toward accidental ignition by impact, heat, or spark.[2] At the present time, there seems to be little consensus among researchers in this field regarding what are the most important characteristics of energetic materials that determine their sensitivity. Some groups are focusing on structural aspects and physicochemical interactions that occur during shear banding of organic crystals.[3] Others focus on localized heating that results from plastic relaxation in the vicinity of crystals defects or vacancies during the shock process.[4] Still others are investigating enhanced rates of vibrational energy transfer from phonon modes to intramolecular modes in the vicinity of structural defects.[5] The approach taken in our laboratory (and several others) is to investigate the chemical mechanisms of explosions and detonations. One of the common themes shared by all of these studies is that attaining a fundamental knowledge of combustion and explosion mechanisms at the molecular level will aid the development of new insensitive energetic materials that are safer to manufacture, handle, and store.

Recently, two experimental techniques have been developed for investigating some of the initial steps in the thermal decomposition mechanisms of explosives and propellants at high heating rates that are characteristic of the conditions under which these materials are often used. Brill and co-workers developed the SMATCH/FTIR technique in which a small amount of explosive is heated on a platinum ribbon at rates up to 2000 K/s. Gaseous reaction products are probed by transmission FTIR spectroscopy just above the burning surface. By use of this technique, specific chemical reactions have been identified that control the burning rate of the material.[6]

In our laboratory, we have developed a pulsed laser pyrolysis technique in which thin films of explosives are heated to several hundred degrees in a few microseconds to initiate thermal reactions.[7-9] The films are then rapidly quenched to 77 K by conduction of the excess heat into the supporting substrate in order to trap the initial products for spectroscopic detection. This thin film laser pyrolysis (TFLP) technique complements the SMATCH/FTIR method insofar as TFLP detects the initial reaction products in the condensed phase explosive rather than in the gas phase. Using this approach, we showed that the first step in the thermal decomposition mechanism of RDX is unimolecular scission of an N−N bond. An important feature of the TFLP method is that films of explosives are heated at extremely high rates ($\sim 10^7$ K/s) that simulate conditions of a thermal explosion;[10,11] however, rapid conduction of the heat through the thin film into the supporting substrate prevents any explosion from taking place. In this way, we can investigate the chemistry of explosives under relatively safe experimental conditions.

In this paper, we extend the technique to investigations of shock-initiated chemistry of energetic materials. The principal motivation for doing this is to develop a methodology for comparing the mechanism of ordinary thermal decomposition to that initiated by a shock wave. One might suppose that the reactions that occur during deflagration (ordinary thermal combustion) might be the same as that for detonation, in which heating occurs as a result of a strong shock. However, if bimolecular reaction pathways are kinetically competitive with unimolecular reactions, the high pressures associated with the detonation shock wave might cause a shift in the overall reaction mechanism. Theories that describe how the mechanical energy of a shock is utilized to initiate chemical reactions on a molecular level are in their infancy.[12-15] Likewise, experimental investigations of energy transfer in shocked materials[16,17] are only beginning to reveal processes that are important in the initial stages of a detonation wave. It seems clear to us that it will be necessary to elucidate the chemical mechanisms of both deflagration and detonation in order to fully understand issues of sensitivity in this class of materials.

Our application of thin film techniques to understanding the chemistry of shock waves in explosives borrows liberally from techniques developed in other laboratories.[18] Techniques for generating planar shock waves using lasers to explode thin metal foils have been known for some time.[19] Dlott and co-workers have recently developed the use of optical nanogauges for measuring the velocity of laser-generated shock waves in solids.[20,21] This group has also used picosecond CARS spectroscopy to make the first direct detection of a chemical reaction product in a polymer during laser ablation.[22] They have demonstrated that pulsed lasers are capable of generating brief but intense shock waves having velocities in the range 4000

† Alfred P. Sloan Fellow 1990−1994. Electronic mail: wight@chemistry.utah.edu.

® Abstract published in *Advance ACS Abstracts,* April 1, 1995.

0022-3654/95/2099-6584$09.00/0

m/s and shock pressures in the range 10−20 GPa that are capable of initiating chemical reactions.

By applying some of these experimental techniques to energetic materials, we hope to reveal some of the chemically important steps relevant to initiation and propagation of detonation. Once again, the thin film geometry of these experiments makes it possible to investigate chemical reactions that may be associated with a detonation without ever initiating a sustained detonation. For our first study, we chose glycidyl azide polymer (GAP), which has the molecular structure

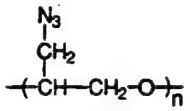

GAP

This material is marketed by the 3M Company as an energetic binder for rocket propellants, explosives, and pyrotechnics.[23,24] In this study we have used the uncured hydroxy-terminated polymer, which is a liquid at room temperature.[25] Although most inorganic azides (e.g., PbN_3) are sensitive primary explosives, GAP is reportedly insensitive to impact-induced detonation. Nevertheless, we anticipated that the initial chemical reaction might be loss of N_2, as it is for most inorganic azides. This supposition is supported by an earlier study of pulsed IR laser decomposition of GAP carried out by Haas *et al.*[26] They concluded that ordinary thermal decomposition of GAP proceeds by initial rupture of azide functional groups, which releases N_2 and forms a reactive species leading to an imine polymer and several gas phase products. The distribution of small molecule reaction products detected in the gas phase (mainly N_2, CO, and C_2H_4) is consistent with earlier work reported by Brill and co-workers.[27,28]

Experimental Section

A 20 g sample of GAP was generously supplied by Specialties Chemicals Division of 3M. Samples are prepared by placing a small drop of GAP onto a CaF_2 optical window (25 mm diameter × 3 mm thick). Next, a film of aluminized Mylar is stretched over the surface of a second CaF_2 window, and two halves are assembled in the manner shown schematically in Figure 1. The layered sample is mounted in an oxygen-free high-conductivity (OFHC) copper retainer inside a Dewar vessel shown in Figure 2. This apparatus is evacuated and the sample cooled to 77 K by pouring liquid nitrogen into the reservoir.

The cold sample is irradiated with a single pulse from a Nd:YAG laser (Continuum Model Surelite) at 1.064 μm. The total energy of the laser pulse is typically 100 mJ, and the spatial profile of the beam was measured to be nearly Gaussian with a 1/e diameter of 4.2 mm. The peak fluence (at the center of the beam) is 0.71 J/cm^2.

Each laser pulse is absorbed by the thin layer (50 nm) of aluminum on the Mylar sheet, generating a rapidly expanding plasma which launches a shock wave into the GAP film. After cooling and relaxation of the shock, the irradiated area is nearly transparent because the aluminum film rearranges to clusters aggregated on the Mylar.[29] The nominal laser pulse duration is 10 ns, which is long in comparison to the time required for the shock to traverse the thickness of the GAP sample (13 μm). Therefore, the duration of the shock is approximately the same as the duration of the laser pulse. The shock pressure in the GAP film has contributions from the original wave (emanating from the aluminized Mylar layer) and from the wave that is partially reflected from the GAP/CaF_2 interface. Gupta and co-workers have described step-wave loading and unloading criteria

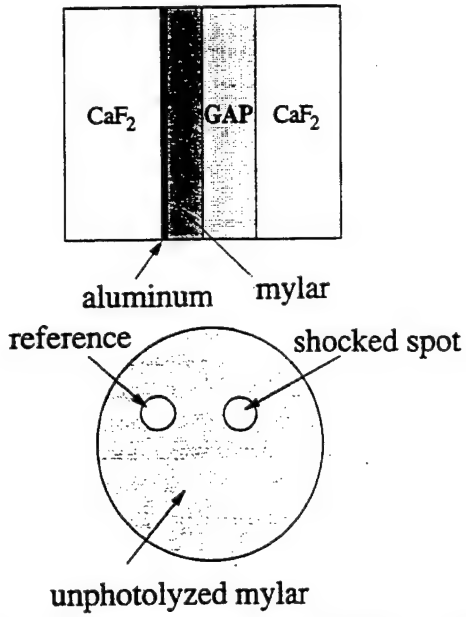

Figure 1. Schematic drawing of the sample assembly including a 13 μm layer of GAP, a layer of aluminized Mylar (6 μm Mylar film coated on one side with a 50 nm layer of aluminum), and two supporting CaF_2 windows (each 3 mm thick). The lower drawing illustrates how the laser beam is used to create transparent holes in the otherwise reflective aluminum layer. Infrared spectra obtained through the shocked spots are compared with spectra obtained through the reference spot, which is created prior to assembly of the sample.

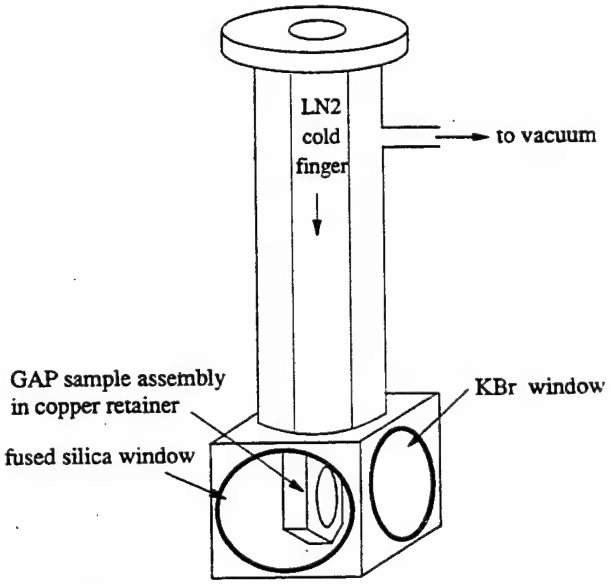

Figure 2. Schematic drawing of the Dewar vessel in which samples are mounted prior to laser irradiation. Following evacuation of the cell, liquid nitrogen is poured into the top of the Dewar to cool the sample to 77 K. This allows trapping of the initial shock-initiated reaction products for spectroscopic detection. The sample window can be rotated to face the fused silica window for laser irradiation or to face a pair of KBr windows for obtaining transmission FTIR spectra.

for shocks impinging on thin film samples. A modified treatment (which takes into account the relatively long laser pulse duration) can be used to model the shock pressures achieved in our apparatus. Experiments designed to quantify the shock pressures and shock velocities are currently underway in our laboratory.[30]

Following irradiation with a single laser pulse, the sample is placed into the sample chamber of an FTIR spectrometer (Mattson RS/10000) and the IR beam directed through the

"hole" formed by the laser. This geometry ensures that the resulting spectrum is obtained only for that portion of the GAP that was subjected to the shock wave. Prior to assembly of each sample, a hole is formed in the bare Mylar film (again, by laser ablation of the aluminum layer). This makes it possible to record a reference infrared spectrum of the GAP film in the sample holder prior to laser generation of the shock wave. It is possible to conduct up to four separate experiments on each sample simply by irradiating different areas of the window assembly and comparing the spectrum of each shocked zone to that of the reference spot. Spectra of the reference spot are obtained before and after creation of the shocked spots in order to detect any changes in sample thickness or chemical composition that may occur in areas that are remote from the irradiated spots. The thickness of the GAP film was determined to be 10 $\pm$ 3 μm by obtaining infrared spectra of a GAP sample in a liquid cell having a calibrated path length.

It should be noted that 100 mJ is the largest pulse energy that could be used in the experiment. Attempts to increase the fluence by increasing the laser pulse energy or focusing the beam to a smaller diameter resulted in cracking of the CaF_2 windows. Even at 100 mJ, several sets of CaF_2 windows were destroyed in the course of this study.

Approximately 45 separate experiments were conducted using variations on this basic experimental sample geometry. In some experiments, thin films of aluminum were deposited directly onto the supporting CaF_2 windows; this geometry produced satisfactory results but was not as convenient as using the aluminized Mylar. In three experiments, the supporting windows were replaced with ZnSe in an attempt to expand the useful range of infrared wavelengths that could be probed; however, the laser shock caused extensive damage (spalling, pitting, and cracking) to the ZnSe surface so the spectra obtained were of little practical value due to extensive light scattering in the shocked spots. In many experiments, two layers of Mylar were used with their aluminum sides in contact with each other in order to prevent the hot aluminum plasma from coming into direct contact with either the CaF_2 or the GAP; this modification made no difference to the spectral changes that were observed in the GAP layer but helped to extend the useful life of the CaF_2 windows.

In several experiments, an inert spacer (a glass microscope cover slip 100 μm thick) is placed between the aluminized Mylar and the GAP layer. The thermal conductivity and heat capacity of this inert layer are sufficient to prevent heat from the plasma from reaching the GAP layer. A worst-case calculation shows that if the entire 100 mJ pulse energy is converted to heat in the inert layer, the sample temperature would rise to only about 100 K (far below the 513 K temperature required to initiate thermal combustion). This experiment is useful for distinguishing whether observed chemical changes are attributable to ordinary thermal combustion or are caused by passage of the shock wave.

We found that propagation of the shock wave across the interface between any two dry solid surfaces in the sample assembly was unreliable, as evidenced by irreproducible results. To circumvent this, all such interfaces were filled with mineral oil or silicone oil. The latter proved beneficial in terms of minimizing the extent of spectral interference in the region above 1500 cm^{-1}, which is transmitted by the CaF_2 support windows, the Mylar, and the inert spacer.

Results

Representative FTIR spectra of GAP before and after the sample is subjected to a laser-generated shock wave are shown in Figure 3. The most obvious difference between the two spectra is a 45% reduction in the integrated intensity of the band at 2100 cm^{-1}. This band is associated with the azide functional groups of the polymer. The band near 2900 cm^{-1}, which is associated with C—H stretching vibrations along the polymer backbone, remains essentially unchanged. It should be emphasized that the comparison of spectra such as those presented in Figure 3 is indirect, because the reference spot is in a different location than the shocked spot. Small variations in the thickness of the GAP between the reference and shocked spots were noted. However, the relative intensity of the azide band (compared with the C—H stretching band) was always less in the shocked spot.

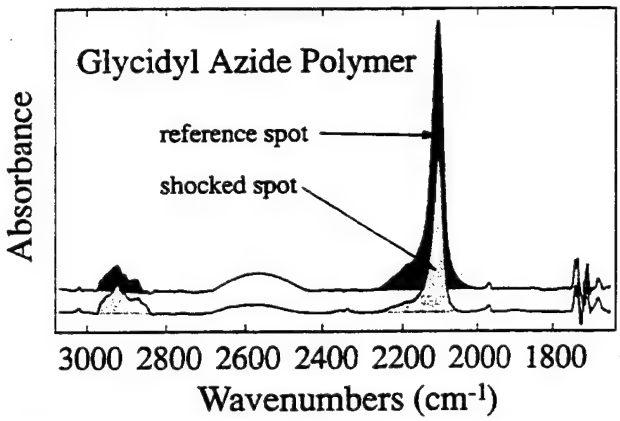

Figure 3. Infrared spectra of a GAP film showing the reduction of the 2100 cm^{-1} azide band as a result of laser irradiation. Note that the intensity of the C—H stretching band near 2900 cm^{-1} is nearly the same in both spots. The feature near 1700 cm^{-1} is an artifact caused by imperfect spectral subtraction of an intense band of the Mylar film.

Control experiments showed that there was no significant change in the band intensities recorded in the reference spot as a result of irradiating the shocked spot. In other words, the laser had no effect on the sample characteristics in regions other than the irradiated zone. Also, irradiation of the sample in the absence of the aluminum layer had no effect (because the GAP sample and windows are transparent at the 1.064 μm laser wavelength).

In order to show that the loss of azide functionality is due to the shock wave and not associated with bulk heating, several samples were constructed having an inert glass layer 100 μm thick between the aluminum and the GAP. A spectrum of such a sample is shown in Figure 4. Again, subjecting the sample to a laser-generated shock wave results in a 29% reduction in the intensity of the band at 2100 cm^{-1}. Although the reactive yields (loss of azide) were highly variable from experiment to experiment, they were generally lower in experiments using the spacer than in those without it. There are at least two reasonable mechanisms that could account for this. The first is that the shock wave is partially reflected from the glass/GAP interface due to a mismatch in shock impedance, thereby reducing the shock pressure in the sample. The second is that the intensity of the shock may be attenuated by a rarefaction wave because the transit time through the 100 μm glass (about 20 ns) is longer than the duration of the driving laser pulse (about 10 ns). In addition, it is not possible to rule out a small component of thermal reaction in experiments where the GAP is in contact with the aluminized Mylar layer.

In several experiments, infrared spectra of the shocked GAP sample were obtained after warming from 77 K to room temperature. These samples exhibited a further reduction in the band at 2100 cm^{-1}. For the sample illustrated in Figure 4, warming produced an additional 27% reduction, for a total 56%

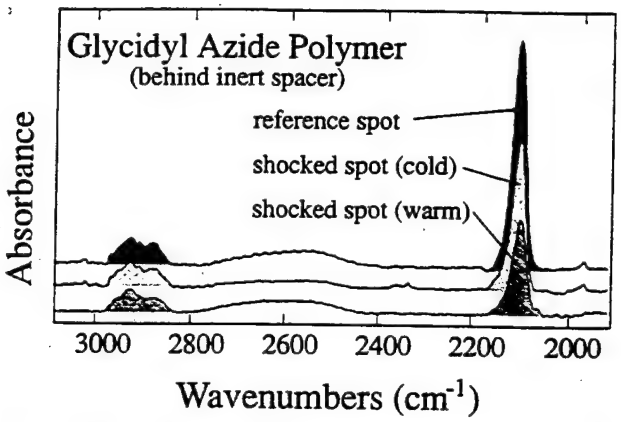

Figure 4. Infrared spectra of a GAP sample assembly containing an inert glass spacer between the aluminized Mylar and GAP layers. Infrared bands associated with the Mylar, glass, and silicone oil layers have been removed by spectral subtraction of reference samples. Note that reduction in the azide band occurs following shock initiation and during warmup from 77 K to room temperature.

reduction in intensity relative to the reference spot. In a few experiments, reduction of the 2100 cm^{-1} band during warmup was as much as 5 times greater than that caused directly by the laser-generated shock wave.

Discussion

The principal goal of this study was to subject a thin film of energetic material to a brief but intense shock wave in order to determine the initial chemical step in the decomposition of the material under these conditions. Although shock-induced chemical reactions have been observed in other studies, to our knowledge, this is the first *in situ* measurement in which the first step has been isolated using an energetic solid.

The principal observation is that the polymer undergoes loss of azide functionality,

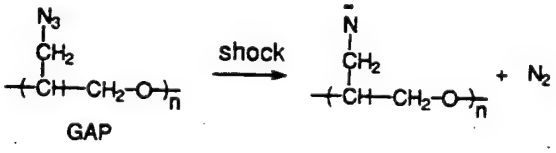

as evidenced by reduction of the band at 2100 cm^{-1}. This is not particularly surprising. Elimination of N_2 proceeds by breaking the weakest bond in the molecule, and this reaction is entirely consistent with the known thermal chemistry of azides in general and with GAP in particular.[31,32]

One might suppose that the nitrene radical might rearrange to an imine structure by a 1,2 hydrogen atom shift,

Evidence for this type of rearrangement was obtained by Haas *et al.*[25] in their study of the thermal decomposition of GAP. Although we made an extensive search for new NH stretching vibrations near 3400 cm^{-1}, we could find no convincing evidence of formation of imines in our shocked samples.

One of the interesting aspects of our study is that reactive species such as nitrene radicals are trapped at 77 K immediately following passage of the shock wave. Subsequent warming of the sample results in reactions that further destroy azide functional groups of the polymer. Unfortunately, our attempts to expand the spectral range of our experiments by using ZnSe support windows failed, so we have been unable to detect the nitrene radicals directly, and we are unable to determine the final reaction products. As mentioned in the Results section above, there was at least one instance in which the amount of azide destroyed during warmup exceeded that destroyed during passage of the shock wave. This observation implies that reactive intermediates formed during the shock are able to catalyze the decomposition of azide functional groups at relatively low temperatures, perhaps by a chain reaction process.

Conclusions

Thin films of glycidyl azide polymer at 77 K have been subjected to laser-generated shock waves. Infrared spectra of the shocked regions exhibit substantial loss of the azide functionality, presumably by elimination of molecular nitrogen and formation of nitrene radicals. No evidence for formation of imine functional groups was obtained under these conditions. Loss of azide occurs even in the presence of an inert spacer between the shock generator and the polymer film; this proves that the reactions are initiated by passage of the shock and not by an ordinary thermal wave. During warmup to room temperature, reactive species trapped in the energetic film cause reactions that further destroy the azide functional groups of the polymer. However, our initial attempts to identify the intermediates by infrared spectroscopy were unsuccessful.

Acknowledgment. This research is supported by the Air Force Office of Scientific Research (Grant No. F-49620-94-10125). The authors thank Dr. Rob Hunter (3M Company) for providing samples of the GAP polymer and for helpful advice. We also thank Professor Dana Dlott for stimulating discussions and for advice in setting up the laser-generated shock apparatus.

References and Notes

(1) Several articles about mechanical and thermal sensitivity of explosives can be found in *Structure and Properties of Energetic Materials*, Materials Research Society Symposium Proceedings; Liebenberg, D. H., Armstrong, R. W., Gilman, J. J., Eds.; Materials Research Society: Pittsburgh, 1993; Vol. 296.
(2) Dick, J. J. *J. Phys. Chem.* **1993**, *97*, 6193.
(3) Tsai, D. H.; Armstrong, R. W. *J. Phys. Chem.* **1994**, *98*, 10 997.
(4) Dlott, D. D.; Fayer, M. D. *J. Chem. Phys.* **1990**, *92*, 3798.
(5) Brill, T. B.; Patil, D. G.; Duterque, J.; Lengelle, G. *Combust. Flame* **1993**, *95*, 183.
(6) Wight, C. A.; Botcher, T. R. *J. Am. Chem. Soc.* **1992**, *114*, 8303.
(7) Botcher, T. R.; Wight, C. A. *J. Phys. Chem.* **1993**, *97*, 9149.
(8) Botcher, T. R.; Wight, C. A. *J. Phys. Chem.* **1994**, *98*, 5441.
(9) Brill, T. B.; James, K. J. *Chem. Rev.* **1993**, *93*, 2667.
(10) Wenograd, J. *Trans. Faraday Soc.* **1961**, *57*, 1612.
(11) Takmakoff, A.; Fayer, M. D.; Dlott, D. D. *J. Phys. Chem.* **1993**, *97*, 1901.
(12) Coffey, C. S. *Phys. Rev. B: Condens. Matter* **1994**, *49*, 208.
(13) Sharma, J.; Forbes, J. W.; Coffey, C. S. *J. Phys. Chem.* **1987**, *91*, 5139.
(14) Coffey, C. S. *J. Appl. Phys.* **1991**, *70*, 4248.
(15) Pangilinan, G. I.; Gupta, Y. M. *J. Phys. Chem.* **1994**, *98*, 4522.
(16) Yoo, C. S.; Gupta, Y. M. *J. Phys. Chem.* **1990**, *94*, 2857.
(17) Shoen P. E.; Campillo, A. J. *Appl. Phys. Lett.* **1984**, *45*, 1049.
(18) Several articles on the subject of laser-generated shock waves can be found in *Shock Compression of Condensed Matter - 1991*; Schmidt, S. C., Dick, R. D., Forbes, J. W., Tasker, D. G., Eds.; North-Holland: Amsterdam, 1991.
(19) Hare, D. E.; Franken J.; Dlott, D. D.; Chronister, E. L.; Flores, J. J. *Appl. Phys. Lett.* **1994**, *65*, 3051.
(20) Lee, I.-Y. S.; Hill, J. R.; Dlott, D. D. *J. Appl. Phys.* **1994**, *75*, 4975.
(21) Hare, D. E.; Dlott, D. D. *Appl. Phys. Lett.* **1994**, *64*, 715.
(22) Gadiot, G. M. H. J. L.; Mul, J. M.; Meulenbrugge, J. J.; Korting, P.; Schnorkh A. J.; Schoyer, H. F. R. *Acta Astron.* **1993**, *29*, 771.
(23) Ger, M. D.; Hwu, W. H.; Huang, C. C. *Thermochim. Acta* **1993**, *224*, 127.

(24) Although the polymer is linear, it is formed from a branched initiator, so the average number of OH terminating groups per molecule is 2.7. The average molecular weight of the polymer is 700, and each polymer molecule has an average of seven azide functional groups.

(25) Haas, Y.; Eliahu, Y. B.; Welner, S. *Combust. Flame* **1994**, *96*, 212.

(26) Chen, J. K.; Brill, T. B. *Combust. Flame* **1991**, *87*, 157.

(27) Oyumi, Y.; Brill, T. B. *Combust. Flame* **1987**, *65*, 127.

(28) Tolbert, W.; Diott, D. D. *J. Imaging Sci.* **1993**, *37*, 411.

(29) Ling, P.; Wight, C. A. Unpublished results.

(30) Kubota, N.; Sonobe, T. *Propellants Explos. Pyrotech.* **1988**, *13*, 172.

(31) Farber, M.; Harris, S. P.; Srivastava, R. D. *Combust. Flame* **1984**, *55*, 203.

JP943142M

Laser-generated shock waves in thin films of energetic materials

Ping Ling and Charles A. Wight[a)]
Department of Chemistry, University of Utah, Salt Lake City, Utah 84112

(Received 31 May 1995; accepted for publication 24 August 1995)

Shock waves are generated in thin films of glycidyl azide polymer (GAP) by pulsed laser vaporization of a thin aluminum film. The rapidly expanding aluminum plasma launches a shock wave into the adjacent layer of GAP, initiating chemical reactions. The shock velocity has been measured by use of a velocity interferometer as a function of the thickness of the GAP layer and the fluence of the Nd:YAG laser pulse. Shock pressures as high as 8 GPa have been generated in this manner. Detonation of thick GAP samples has been observed, providing important information about the chemical reaction rates and the thickness of the reaction zone. © *1995 American Institute of Physics.*

INTRODUCTION

Much of the current research in the field of energetic materials is directed toward understanding the microscopic mechanisms of explosion sensitivity towards heat, spark, and impact. This research is driven in part by the need to develop insensitive explosives, propellants, and pyrotechnics that are safer to manufacture, handle, and store. Whereas much of this research has focussed on understanding the structural and mechanical characteristics of energetic compounds, there is now an increased emphasis on understanding the chemical mechanisms of combustion, thermal explosion, and detonation.

Shock-initiated detonation has been widely studied, and laser-generated shock waves have been used to investigate detonation of insensitive high explosives.[1] Studies have shown that strong shocks (0.1–50 GPa) can be generated in confined films using nanosecond or picosecond laser pulse drivers at moderate fluence.[2–5] Besides detonation, this general method has applications in simulating high velocity impacts[6] that alter the mechanical properties and microstructure of metal alloys and ceramics.[7] Theoretical studies of the shock wave generation process by lasers have been reported, and molecular dynamics simulations have revealed some of the specific features of shock wave formation and propagation on a microscopic scale.[3–10]

Recently, we demonstrated that laser-generated shock waves are a useful tool for determining the initial chemical reactions induced by shock waves.[11] We used a Nd:YAG laser pulse to vaporize a thin aluminum film, thereby launching an acoustic shock wave into a thin film of glycidyl azide polymer (GAP). The shocks were sufficiently strong to initiate chemical reactions in the film, but did not cause explosion or detonation of the sample. Transmission FTIR spectra of the films obtained before and after the laser shocks showed that the first step in the reaction sequence is elimination of molecular nitrogen from the azide groups of the polymer. We were able to show that the chemical reactions are caused by the propagating shock wave (not an ordinary thermal wave) by inserting an inert spacer 100 μm thick between the aluminum film and the GAP layer. However, at the time of our initial report[11] we did not have the means to experimentally characterize the shock velocity or pressure in this type of experiment. The purpose of this article is to report the experimental techniques and initial results on the characterization of shock velocities and pressures in experiments designed to reveal the initial chemical steps involved in the detonation of energetic materials.

EXPERIMENTAL DETAILS

A schematic diagram of the experiment is shown in Fig. 1. The 25-mm-diameter target array begins with a 3-mm-thick quartz window, which supports a 100-μm-thick microscope cover slip. The cover slip has a 0.1 μm aluminum film vacuum deposited on one side which absorbs the laser pulse. Next comes a layer of GAP inside a spacer ring that determines the thickness of the GAP layer (15 μm–2 mm), followed by a second quartz window that has a mirror coating on the side facing the GAP. The array is held pressure tight by clamping the entire assembly in a stainless steel cylinder held by a threaded retaining ring.

GAP is obtained from the 3M Company, which markets the material as an energetic binder for propellants. The material used in our study is the uncrosslinked polyol,

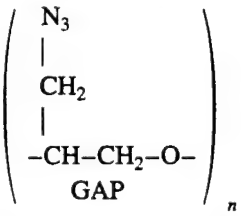

which is a viscous liquid at room temperature. Although the polymer is linear, it is formed from a branched initiator. The average number of OH terminating groups per molecule is 2.7, and the average molecular weight of the polymer is 700. Therefore, each polymer molecule has an average of seven azide functional groups.

The laser driver pulse is from a Nd:YAG laser (Continuum Model Surelite) at 1.064 μm. The laser pulse duration is 7 ns and the total energy per pulse is 90 mJ. A lens is used to focus the beam to the desired fluence. The spatial profile of the beam is determined by recording the average laser power (Scientech Model 38-0101 disk calorimeter) at

a)Electronic mail: wight@chemistry.utah.edu

 0021-8979/95/78(12)/7022/4/$6.00

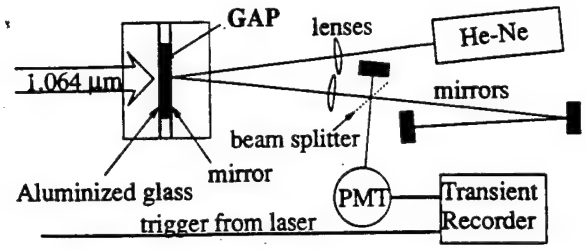

FIG. 1. Schematic diagram of the sample target array, pulsed Nd:YAG laser, and velocity interferometer detector.

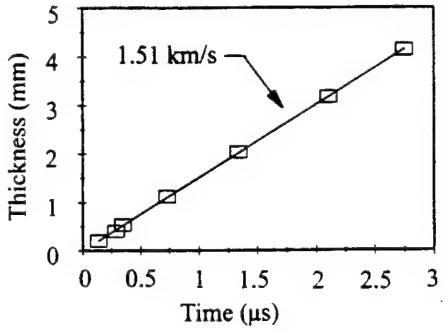

FIG. 2. Transit time of an ordinary sound impulse through different thicknesses of GAP. The slope of the linear least-squares fit gives the speed of sound in GAP. An average of three such measurements gives $c_0=1.55\pm0.05$ km/s.

10 Hz pulse repetition rate while a razor blade is scanned across the beam at the position of the sample. The data are differentiated and fit to a Gaussian function to determine the $1/e$ diameter of the beam. Laser fluences quoted here are determined by dividing the measured pulse energy by the beam area.

Each laser pulse is absorbed by the aluminum film on the disposable glass cover slip, generating a rapidly expanding gas plasma. The plasma launches a shock into the GAP layer, setting the material into motion in the direction of the laser beam. When the pressure wave reaches the opposite side, it disturbs the mirrored surface of the second quartz window. This disturbance is detected as a Doppler shift of the 632 nm He-Ne laser beam propagating in a home-built velocity interferometer. The change in the fringe pattern of the interferometer is detected by a fast photomultiplier tube (Hamamatsu R928 tube wired to give a rise time of 1.5 ns), and recorded by a digital storage oscilloscope (Tektronix Model TDS 540, 1 G sample/s at 500 MHz bandwidth).

The velocity interferometer has a delay leg of 90–150 cm, corresponding to a time delay of 3–5 ns. According to the criteria of velocity resolution,[12] it is capable of detecting a velocity as low as about 50 m/s. Usually, the particle velocity associated with a strong shock is much greater than this value. In principle, it is possible to measure the acceleration of the mirrored surface; however, shock fronts in condensed phase materials typically have widths that are comparable to atomic dimensions,[13,14] and our detection system is not fast enough to resolve the fringes associated with such a rapid change in velocity. Also, the multilayered structure of the sample causes the velocity interferogram to have a complicated structure, so we were unable to determine the particle velocity from the rarefaction wave. However, we are able to record the arrival time of the shock (transit time through the GAP layer) to within an experimental uncertainty of 2–3 ns. By changing the thickness of the spacer that defines the thickness of the GAP layer, the velocity of the shock is determined from the measured transit times. Each single-shot data point is repeated ten times in order to determine acceptable average values and uncertainties in the transit time data. The "zero time" is determined by omitting the GAP layer and the second quartz window from the target array. In this configuration, the interferometer beam is reflected directly from the aluminum film that is vaporized by the laser pulse.

We attempted to use a Michelson interferometer (with equal length delay lines) to record the transit time by detecting the movement of the mirrored surface. The measured times were the same as for the velocity interferometer, but the sensitivity of the method was lower, due to the relatively high immunity of the velocity interferometer to vibrations of the optics.

The speed of sound in GAP is measured by a similar method. The first quartz window and glass cover slip are replaced with a 25 mm diameter×1.5-mm-thick aluminum disk. The shock wave induced by laser irradiation of the disk is dissipated to an ordinary sound impulse prior to reaching the GAP layer. However, the impulse is still strong enough to disturb the mirrored surface on the second quartz window, allowing detection by the velocity interferometer. Records of transit time as a function of GAP thickness in this configuration provided an accurate measurement of the sound speed in GAP at room temperature.

RESULTS AND DISCUSSION

Experimental data showing the transit time of an ordinary sound impulse through GAP as a function of thickness are shown in Fig. 2. The speed of sound, determined from the average of three series of measurements, is $c_0=1.55\pm0.05$ km/s. This value is comparable to other liquids such as castor oil (1.488 km/s) and nitrobenzene (1.463 km/s).[15] Measurement of the sound speed in water by our method gave 1.52 km/s, which is less than 2% greater than the literature value.[15]

Transit times for laser-generated shock waves are shown in Fig. 3 for data obtained at a total laser fluence of 0.75 J/cm^2 (the lowest value used in this study). For relatively large thicknesses (>1 mm) the shock velocity approaches the ordinary sound speed. However, at thicknesses less than 100 μm the velocity of the shock is greater than 2 km/s, as shown in the inset of Fig. 3. The linear dependence of arrival time on sample thickness shows that for sample thicknesses less than 100 μm, the shock velocity is constant.

Shock transit times were measured for GAP films at higher laser fluence (up to 11 J/cm^2) using spacers of 100 μm or less. The experimentally determined shock velocities are shown as a function of laser fluence in Fig. 4.

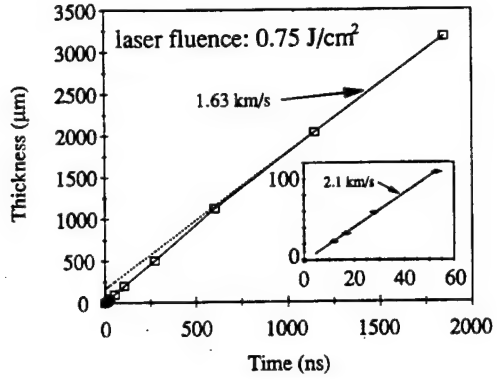

FIG. 3. Measured transit time of laser-generated shock waves through different thicknesses of GAP at a total laser fluence of 0.75 J/cm^2. Inset shows data obtained for GAP film thicknesses less than 100 μm.

The particle velocities achieved in these experiments are calculated from the transit times by use of the universal liquid state Hugoniot equation[16]

$$\frac{U_s}{c_0}=1.37-0.37e^{-2U_p/c_0}+\frac{1.62U_p}{c_0}, \tag{1}$$

where c_0 is the speed of sound, and U_s and U_p are the shock and particle velocities, respectively. The shock pressure is calculated from these quantities by use of the relation

$$P_s=\rho U_s U_p, \tag{2}$$

where ρ is the density of GAP (1.34 g/cm^3, measured in our laboratory). If U_s and U_p are expressed in km/s and ρ in g/cm^3, then the resulting value of P is in GPa. The shock pressures calculated in this manner are shown on the right hand side of Fig. 4. Although the experimental uncertainties are large for high fluence laser pulses, the relationship between shock velocity (or pressure) on laser fluence is highly nonlinear.

The fluence dependence is qualitatively consistent with the following simple model. Let us first express the absorbed laser fluence (energy per unit area) as the sum of two terms:

$$\Phi=\phi_0+\phi_1, \tag{3}$$

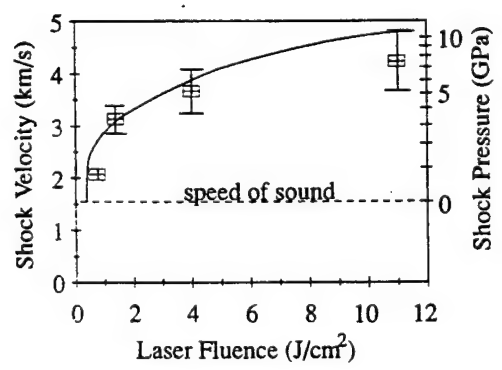

FIG. 4. Measured shock velocities for GAP samples up to 100 μm thick as a function of laser pulse fluence. Calculated shock pressures are given on the right hand axis. The solid curve is a plot of Eq. (8).

where ϕ_0 represents the energy required to vaporize the aluminum target material, and ϕ_1 is the work associated with setting the surrounding GAP material into motion. The latter is given approximately by

$$\phi_1\approx P_s U_p \Delta t, \tag{4}$$

where Δt is the laser pulse duration (7 ns in our work). For relatively weak shocks (i.e., when $U_p \ll c_0$), Eq. (1) can be simplified and substituted into Eq. (2) to give

$$P_s=\rho(c_0+2U_p)U_p. \tag{5}$$

Solving for U_p and substituting into Eq. (4) we obtain

$$\phi_1=\frac{1}{2}P_s\left(\sqrt{\frac{c_0^2}{4}+\frac{2P_s}{\rho}}-\frac{c_0}{2}\right)\Delta t. \tag{6}$$

For an estimate of ϕ_0 we note that the fluence required to vaporize a 0.1 μm film of Al is about 0.33 J/cm^2. The choice of this thickness Al film for the target material was based partly on the fact that this layer is thicker than the optical penetration depth of aluminum[5] but less than the thermal penetration depth

$$d\approx\sqrt{\kappa\Delta t} \tag{7}$$

during the laser pulse. The relationship between laser fluence and shock pressure under our experimental conditions may be written in the form

$$\Phi=0.33\ \text{J/cm}^2+\frac{1}{2}P_s\left(\sqrt{\frac{c_0^2}{4}+\frac{2P_s}{\rho}}-\frac{c_0}{2}\right)(7\ \text{ns}). \tag{8}$$

A plot of P_s as a function of Φ calculated from this relationship is shown as the solid curve in Fig. 4. The calculated values and the shock pressures that are derived from the experimental data show that values as high as 8 GPa can be achieved in GAP films using driver pulses at moderate fluence (~11 J/cm^2).

Finally, we learned that it is possible to induce sustained detonations in thick films of GAP using laser-generated shock waves. When this occurs, the supporting windows are fractured, and large amounts of gas are released from the sample. Based on previous studies of thermal decomposition of GAP,[17–19] these gases are principally N_2, CO, and C_2H_4. The entire target array is covered with burned polymer, even well outside the region irradiated by the Nd:YAG laser. The fluence threshold for detonation decreases dramatically and nonlinearly with increasing film thickness, as shown in Fig. 5.

Of course, it is not possible to distinguish between a laser-induced detonation and an ordinary thermal explosion solely on the basis of our experimental measurements. However, the strongest evidence for having initiated a sustained detonation is the fact that the sensitivity is much lower for a 2-mm-thick layer as compared with a 0.5 mm layer. The entire energy of a 90 mJ laser pulse distributed over a GAP sample volume of 62.5 mm^3 (125 mm^2×0.5 mm thick) should raise the temperature by only 3 K based on the estimated heat capacity of GAP (0.4 J/g/K). GAP is known to be thermally stable to 200 °C. Therefore, it is difficult to imagine how this difference in sample thickness can affect the

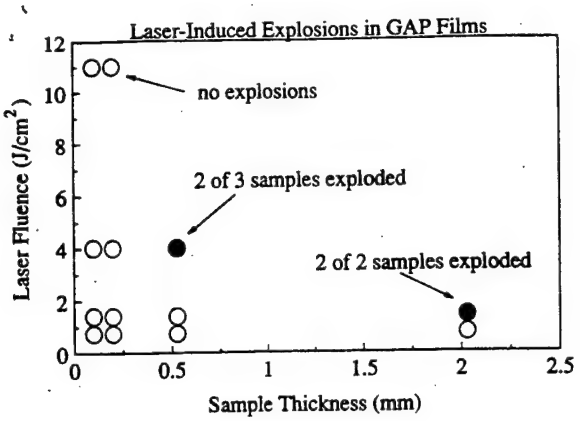

FIG. 5. Sensitivity of GAP samples to detonation by laser-generated shocks. Open circles represent experimental conditions under which no explosions were observed. The solid circle represents conditions for observed explosions in 2 of 2 samples. The cross-hatched circle represents observed explosions in 2 of 3 samples.

probability of initiating a thermal explosion. A transient temperature rise much greater than 3 K undoubtedly occurs as a result of shock compression, but relaxation to atmospheric pressure occurs in a matter of a few nanoseconds.

A sustained detonation depends on the rate of reaction behind the shock front, because it is this energy that must be transmitted to the front in the form of a pressure wave to sustain the shock. Hare and Dlott have demonstrated that some reactions occur on a ns time scale behind shock fronts in poly(methyl methacrylate).[20] It is not known whether enough heat can be released on this time scale to sustain a shock, even in energetic materials. In principle, reactions that occur well behind the front can contribute energy to the shock in the freely detonating material. This is because the sum of the flow velocity and the sound speed in the reaction zone is higher than the velocity of the front. If the thickness of the sample is less than the characteristic reaction zone thickness in the freely detonating material, detonation can only be achieved by overdriving the system (e.g., with a high fluence laser pulse). In other words, the fluence required to initiate detonation should decrease as the sample thickness increases, but only to the point where the sample thickness is roughly equal to the reaction zone thickness in the freely detonating material. This is consistent with the sensitivity behavior illustrated in Fig. 5. This argument suggests that the steady-state detonation velocity in GAP lies between 1.55 km/s (the sound speed) and 3.1 km/s (the initial shock velocity at 1.25 J/cm^2 for the 2 mm sample that exploded). In turn, this argument suggests that the thickness of the reaction zone in freely detonating GAP is greater than 2 mm. Considering the fact that our earlier study of shock-initiated reaction in GAP showed extensive reaction on a nanosecond time scale in samples as thin as 10 μm,[11] a 2 mm thickness for the reaction zone in freely detonating GAP might appear to be a surprisingly large value. However, it is comparable to values obtained for the high explosives RDX (0.8 mm) and TNT (2 mm).[21]

Additional experiments on this system and other liquid energetic materials will provide a clearer picture of the rates and mechanisms of chemical reactions involved in detonation. It is hoped that such fundamental investigations of the chemistry of energetic materials will eventually lead to the development of a new generation of insensitive energetic materials that incorporate greater safety margins for the people who handle them.

ACKNOWLEDGMENTS

This research is supported by the Air Force Office of Scientific Research and by the National Science Foundation.

[1] L. C. Yang and V. J. Menichelli, Appl. Phys. Lett. **19**, 473 (1971).
[2] L. C. Yang, J. Appl. Phys. **45**, 2601 (1974).
[3] B. P. Fairand and A. H. Clauer, J. Appl. Phys. **50**, 1497 (1979).
[4] P. E. Shoen and A. J. Campillo, Appl. Phys. Lett. **45**, 1049 (1984).
[5] I.-Y. S. Lee, J. R. Hill, and D. D. Dlott, J. Appl. Phys. **75**, 4925 (1994).
[6] A. N. Pirri, Phys. Fluids **20**, 221 (1977).
[7] B. P. Fairand, B. A. Wilcox, W. J. Gallagher, and D. N. Williams, J. Appl. Phys. **43**, 3893 (1972).
[8] R. T. Harrach, J. Appl. Phys. **47**, 2473 (1976).
[9] M. Peyrand, S. Odiot, E. Oran, J. Boris, and J. Schnur, Phys. Rev. B **33**, 250 (1986).
[10] M. L. Elert, D. M. Deaven, D. W. Brenner, and C. T. White, Phys. Rev. B **39**, 1453 (1989).
[11] J. Sakata and C. A. Wight, J. Phys. Chem. **99**, 6584 (1995).
[12] J. N. Johnson and L. M. Barker, J. Appl. Phys. **40**, 4321 (1969).
[13] Molecular dynamics simulations such as those presented in Ref. 10 have demonstrated that the change in pressure and particle velocity associated with a detonation shock occurs on a length scale that is comparable to the dimensions of the molecules that comprise the solid. Also, Lee *et al.* have recently shown that the intrinsic rise time of a 2 GPa shock is less than 60 ps (Ref. 14).
[14] I.-Y. S. Lee, R. Hill, H. Suzuki, D. D. Dlott, B. J. Baer, and E. L. Chronister, J. Chem. Phys. (in press).
[15] *CRC Handbook of Chemistry and Physics*, 74th ed. (CRC, Boca Raton, FL, 1993).
[16] R. W. Woolfolf, M. Cowperwaite, and R. Shaw, Thermochimica Acta **5**, 409 (1973).
[17] Y. Haas, Y. B. Eliahu, and S. Welner, Combust. Flame **96**, 212 (1994).
[18] J. K. Chen and T. B. Brill, Combust. Flame **87**, 157 (1991).
[19] Y. Oyumi and T. B. Brill, Combust. Flame **65**, 127 (1987).
[20] D. E. Hare and D. D. Dlott, Appl. Phys. Lett. **64**, 715 (1994).
[21] B. Lewis, R. N. Pease, and H. S. Taylor, *Combustion Processes* (Princeton University Press, Princeton, NJ, 1956), p. 592.

DETONATION CHEMISTRY OF GLYCIDYL AZIDE POLYMER

PING LING, JILL SAKATA, CHARLES A. WIGHT
Chemistry Department, University of Utah, Salt Lake City, UT 84112, wight@chemistry.utah.edu

ABSTRACT

The initial step of chemical reaction initiated by laser-generated shock waves has been observed in glycidyl azide polymer (GAP) in condensed phase. Shocks are generated by pulsed laser vaporization of thin aluminum films and launched into adjacent films of GAP at 77 K. Comparison of FTIR spectra obtained before and after shock passage shows that initial reaction involves elimination of molecular nitrogen from the azide functional groups of the polymer. The shock arrival time has been measured by a velocity interferometer as a function of thickness of GAP and laser fluence. The shock pressure has been calculated by using a universal liquid state Hugoniot. A simple model is proposed to calculate shock velocity and pressure as a function of laser fluence. The results are in agreement with experimental data.

INTRODUCTION

Elucidation of individual chemical steps during an explosion or detonation is important for understanding the microscopic mechanism of explosion sensitivity towards heat, spark, and impact. This research is driven in part by the need to develop insensitive explosives, propellants and pyrotechnics that are safer to manufacture, handle and store. While much of the research has focused on understanding the structural and mechanical characteristics of energetic compounds, recent progress has also been made to understand the chemical mechanisms of combustion, thermal explosion and detonation.

Recently, we developed a thin film laser pyrolysis technique for determining initial condensed phase reaction products under conditions that mimic a thermal explosion.[1] The methodology is complementary to other methods such as SMATCH/FTIR developed by Brill and co-workers,[2] in which gas phase products are detected. These methodologies have been successful in revealing initial steps in the mechanism of thermal decomposition of energetic materials like RDX [2-4] and NTO.[5] However, there are limited experiments on initial chemical steps during an impact or shock wave. In spite of some theoretical approaches that could in some extent reveal relationships between chemical reactions and propagation of detonation waves on a microscopic level, [6-13] in general it is unknown whether the chemistry of detonation is the same as that of thermal explosion. One might guess that in many cases it is, but if bimolecular reaction pathways are competitive with unimolecular reactions, then the high pressure conditions of detonation should favor the bimolecular pathways. Fundamental issues of impact sensitivity may hinge on detailed knowledge of chemical reaction mechanism associated with rapid loading of high pressure shock waves.

The basic idea of the experiment is to subject a thin film of aluminum to a strong laser pulse. Rapid absorption of laser energy causes the aluminum film to explode, generating an expanding plasma and launching a shock wave into an adjacent film of energetic material. Laser-generated shock waves have been known for a long time, and studies have shown strong shocks (up to 50 GPa) can be generated in confined films using nanosecond or picosecond laser pulses.[14-16] Shock waves of this type have been used to investigate detonation of insensitive high explosives.[17] Recently we demonstrated that laser-generated shock waves are capable of initiating

chemical reaction in glycidyl azide polymer.[18] This paper will further characterize the shock strength and discuss the reaction mechanism.

EXPERIMENT

In this section, we first describe how to initiate shock waves in GAP film and detect the chemical reaction. Then we show the method of measuring shock velocity by using a velocity interferometer.

Chemical Reaction in Laser-Generated Shock Waves

The GAP was from Specialties Chemicals Division of 3M, which markets the material as an energetic binder for propellants. The material used in our study is the uncrosslinked polyol,

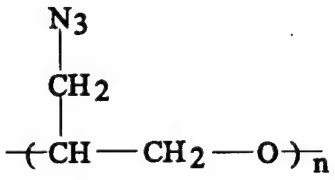

GAP

which is a viscous liquid at room temperature. Although the polymer is linear, it is formed from a branched initiator. The average number of OH terminating groups per molecular is 2.7, and the average molecular weight of the polymer is 700. Therefore, each polymer molecular has an average of seven azide functional groups.

Samples are prepared by placing a small drop of GAP onto a CaF_2 optical window (25mm dia., 3 mm thick). Next, a film of aluminized mylar is stretched over the surface of a second CaF_2 window, and the two halves are assembled in the manner shown schematically in Figure 1. The layered sample is mounted in an OFHC copper retainer inside a dewar vessel. This apparatus is evacuated and the sample is cooled to 77 K by pouring liquid nitrogen into the reservoir.

The cold sample is irradiated with a single pulse from a Nd:YAG laser (Continuum Surelite) at 1.064μm. The laser pulse duration is 7 ns. The average power of the pulse is measured with a disk calorimeter (Scientech Model 38-0101) at 10 Hz pulse repetition rate. A lens is used to focus the beam to the desired fluence. The spatial profile of the beam is determined by recording the average laser power while a razor blade is scanned across the beam at the position of the sample. The data are differentiated and fit to a Gaussian function to determine the 1/e diameter of the beam. Laser fluence quoted here are determined by dividing the measured pulse energy by the beam area.

Each laser pulse causes a region of aluminum on mylar to explode, generating a shock wave in mylar which is transmitted to the adjacent GAP film. Following the irradiation, the sample is placed into the sample chamber of a FTIR spectrometer (Mattson RS/10000) and the IR beam directed through the hole in the aluminum layer produced by the laser. This geometry ensures that the spectrum is obtained

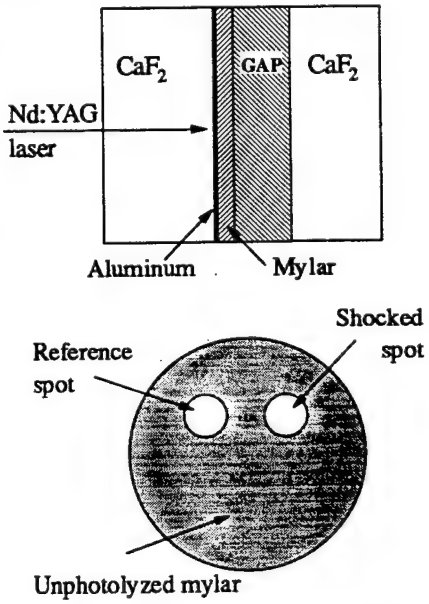

Figure 1 - Sample target assembly.

only for that portion of the GAP subjected to the shock wave. Prior to assembly of each sample, a transparent region is formed on the aluminized mylar film (again by laser ablation of the aluminum). This makes it possible to record a reference IR spectrum of GAP prior to irradiation of the sample. The spectrum of the reference spot is checked after the formation of the shocked spot in order to detect any changes in sample thickness or composition that may occur in areas remote from the irradiated spot. The thickness of the GAP film was determined to be 10±3 μm by obtaining IR spectra of GAP sample in a liquid cell with a calibrated path length.

It was found that 0.75 J/cm^2 is about the highest laser fluence that could be used in the experiment. Attempts to increase the fluence resulted in cracking of the CaF_2 windows. We found that propagation of shock across the interface between any two dry solid surface was unreliable. To circumvent this, all solid interfaces were filled with a thin layer of mineral oil or silicone oil.

Shock Velocity Measurement

A schematic diagram of the apparatus is shown in Figure 2. The 25mm dia. target array begins with 3 mm thick quartz window, which supports a 100 mm thick microscope cover slip. On one side, the cover slip has a 0.1 μm vacuum-deposited aluminum film which absorbs the laser pulse. Next comes a layer of GAP inside a spacer ring that determines the thickness of the GAP layer (15 μm to 2 mm), followed by a second quartz window that has a mirror coating on the side facing the GAP. The array is held pressure tight by clamping the entire assembly in a stainless steel cylinder held by a threaded retaining ring.

Each laser pulse is absorbed by the aluminum film on the disposable glass cover slip, generating a rapidly expanding plasma gas. The expanding plasma gas launches a shock wave into the GAP layer, setting the material into motion in the direction of laser beam. When the pressure wave reaches the opposite side, it disturbs the mirrored surface of the second quartz window. This disturbance is detected as a Doppler shift of the 632 nm He-Ne laser beam propagating in a home-built velocity interferometer. The change in fringe pattern of the interferometer is detected by a fast photomultiplier tube (Hamamatsu R928 tube wired to give a rise time of 1.5 ns), and recorded by a digital storage oscilloscope (Tektronix Model TDS 540, 1 Gsample/s at 500 MHz bandwidth).

The velocity interferometer has a delay leg of 90 to 150 cm, corresponding to a time delay of 3-5 ns. It is capable of detecting a velocity as low as about 50 m/s.[19] Usually, the particle velocity associated with a strong shock is much greater then this value. Shock fronts in condensed media typically have widths that are comparable to atomic dimensions,[7,20] and our detection system is not fast enough to record the acceleration of the mirrored surface. Also, the multilayered structure of the sample causes the velocity interferogram to have a complicated structure, and we are unable to identify the rarefaction wave in order to determine the particle velocity information. However, we are able to record the shock arrival time to within an experimental uncertainty of 2-3 ns. By changing the thickness of the spacer ring that defines the thickness of the GAP layer, the velocity of the shock is determined from the measured transit times. The "zero time" is determined by

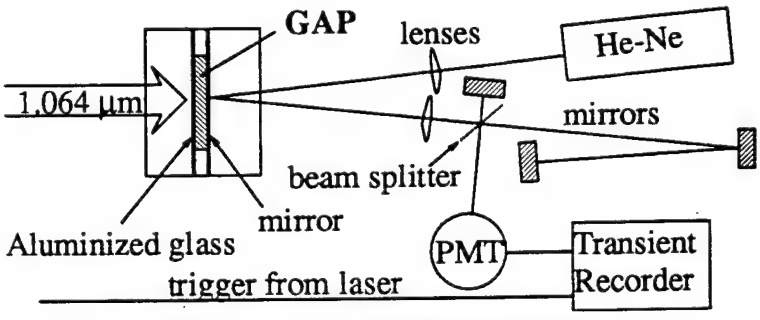

Figure 2 - Velocity interferometer setup.

omitting the GAP layer and the second quartz window from the array. In this configuration, the interferometer beam is reflected directly from the aluminum film that is vaporized by the laser pulse.

The speed of sound in GAP is measured in a similar way. The first quartz window and glass cover slip are replaced with a 1.5 mm thick aluminum desk. The shock wave induced by laser irradiation of the disk is dissipated to an ordinary sound impulse prior to reaching the GAP layer. However, the impulse is still strong enough to disturb the mirrored surface on the second window, allowing detection by the velocity interferometer. Records of transit time as a function of GAP thickness in this configuration provided an accurate method of measuring sound speed.

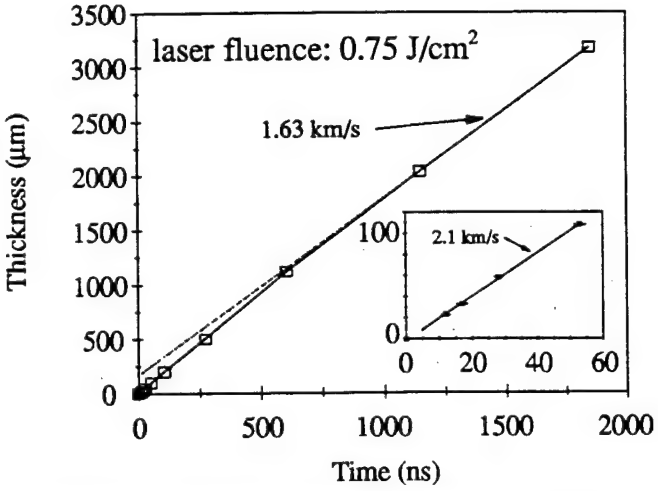

Figure 3 - Measured shock transit times for GAP.

RESULTS

Shock Velocity and Pressure

Experimental data show that the transit times of ordinary sound impulses through GAP layers are linearly dependent on the thickness of the layers. Linear fitting gives the sound speed in GAP to be $c_0 = 1.55 \pm 0.05$ km/s. For comparison, measurement of the sound speed in water by this method gives 1.52 ± 0.02 km/s, which is within 2% of the literature value.[21]

Transit times for laser-generated shock waves are shown in Figure 3 for data obtained at laser fluence 0.75 J/cm^2. For relatively large thicknesses (>1 mm) the shock velocity approaches the sound speed. However, at thicknesses less than 100 μm the velocity of shock is greater than 2 km/s, as shown in the inset of Figure 3. The linear dependence of arrival time on sample thickness shows that for sample thickness less than 100 μm, the shock velocity is constant.

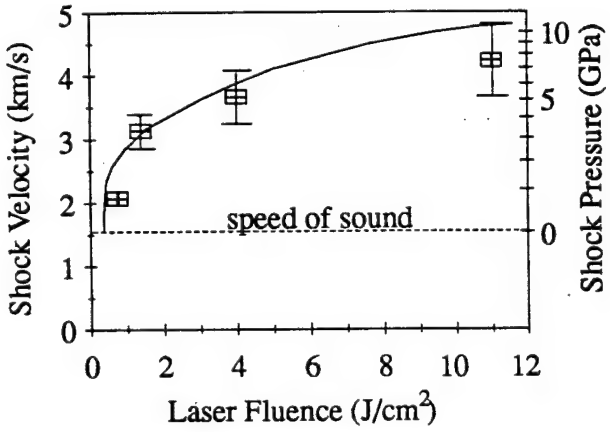

Figure 4 - Measured shock velocities and calculated shock pressures.

Shock transit times were measured for GAP films at higher laser fluence (up to 11 J/cm^2) using spacers of 100 μm or less. The experimentally determined shock velocities are shown as a function of laser fluence in Figure 4.

The particle velocities achieved in these experiments are calculated from shock velocities by use of the universal liquid state Hugoniot equation.[22]

$$\frac{U_S}{c_0} = 1.37 - 0.37\, e^{\frac{-2U_p}{c_0}} + 1.62\,\frac{U_p}{c_0} \qquad (1)$$

where c_0 is the speed of sound, and U_s and U_p are the shock and particle velocities, respectively. The shock pressure is calculated from these quantities by use of the relation

$$P_S = \rho\, U_S U_p \tag{2}$$

where ρ is the density of GAP (1.34 g/cm^3, measured in our lab). If U_s and U_p are expressed in km/s and ρ in g/cm^3, then the resulting value of P_s is in GPa. The shock pressure calculated in this manner are shown on the right hand side of Figure 4.

The laser fluence dependence of the shock pressure is qualitatively consistent with the following simple model. Let us first express the absorbed laser fluence as the sum of two terms

$$\Phi = \phi_0 + \phi_1 \tag{3}$$

where ϕ_0 represents the energy per unit area required to vaporize the aluminum target material, and ϕ_1 is the work associated with setting the surrounding GAP material into motion. We neglect the motion of supporting glass because the shock impedance of glass is about 6 times as that of GAP; therefore the particle velocity in glass is only about 1/6 of that in GAP. The work term is given approximately by

$$\phi_1 \approx P_S U_p \Delta t \tag{4}$$

where Δt is the laser pulse duration (7 ns in this work). For shock velocity from zero to about 5 km/s, the Hugoniot of Eq. (1) can be rewritten in the usual linear form without much error,

$$U_S = a\, c_0 + b\, U_p \tag{5}$$

where a=1.03, b=1.92 ±0.03. Substituting this expression into Eq.(2) we obtain

$$P_S = \rho\, (a\, c_0 + b\, U_p)\, U_p \tag{6}$$

Solving for U_p and substituting into Eq.(4) we obtain

$$\phi_1 = \frac{1}{2} P_S \left[\left(\frac{a^2 c_0^2}{b^2} + \frac{4 P_S}{b \rho} \right)^{\frac{1}{2}} - \frac{a\, c_0}{b} \right] \Delta t \tag{7}$$

For an estimate of ϕ_0, we note that the fluence required to vaporize a 0.1 μm film of Al is about 0.33 J/cm^2. The choice of this thickness Al film for the target material was based partly on the fact this layer is thicker than the optical penetration depth of Al,[16] but less than the thermal penetration depth

$$d \approx (\kappa\, \Delta t)^{\frac{1}{2}} \tag{8}$$

during the laser pulse duration. The relationship between laser fluence and shock pressure under our experimental conditions may be written in the form

$$\Phi\ (J/cm^2) = 0.33 + \frac{1}{2} P_S \left[\left(\frac{a^2 c_0^2}{b^2} + \frac{4 P_S}{b \rho} \right)^{\frac{1}{2}} - \frac{a\, c_0}{b} \right] (\Delta t) \tag{9}$$

A plot of P_s as a function of Φ calculated from this relationship is shown as the solid curve in

Figure 4. The prediction of the simple model is in reasonable agreement with the experimental results. Together, they show that shock pressures of several GPa can be generated in GAP at moderate laser fluence.

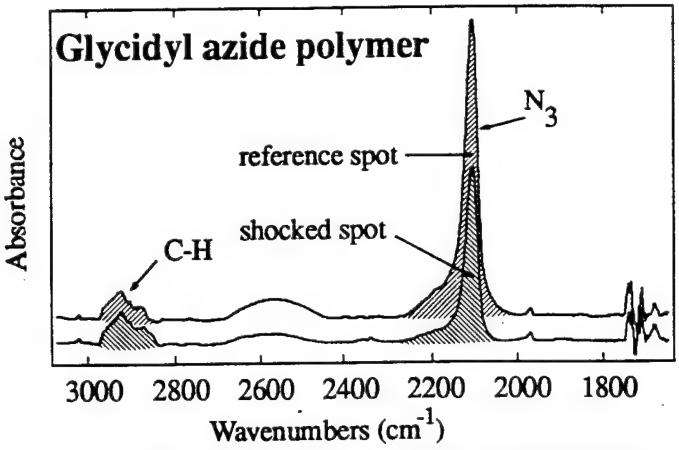

Figure 5 - IR spectra of 10 μm GAP film showing loss of azide groups following laser-induced shock.

Loss of Azide Functional Group after Passage of Shock

Representative FTIR spectra of GAP before and after shock are shown in Figure 5. The most obvious difference is a 29-45% reduction in the integrated intensity of the band at 2100 cm^{-1}. This band is associated with the azide functional groups of the polymer. The band near 2900 cm^{-1}, which is associated with C-H stretching vibrations along the polymer backbone, remains essentially unchanged.

Infrared spectra of shocked samples were obtained after warming from 77 K to room temperature. This warming is accompanied by 20-30 % further reduction in the intensity of the 2100 cm^{-1} band.

Finally, we learned that it is possible to induce sustained explosion in confined thick films of GAP by laser-generated shock waves. These experiments were conducted at room temperature. When explosion occurs, the supporting windows are fractured and large amounts of gas are released from the sample. Based on previous studies of thermal decomposition of GAP,[23-25] these gases are principally N_2, CO and C_2H_4. The entire target array is covered with burned polymer, even well outside the area of the sample irradiated by laser. The fluence threshold for explosion decreases dramatically and nonlinearly with increasing film thickness, as shown in Figure 6.

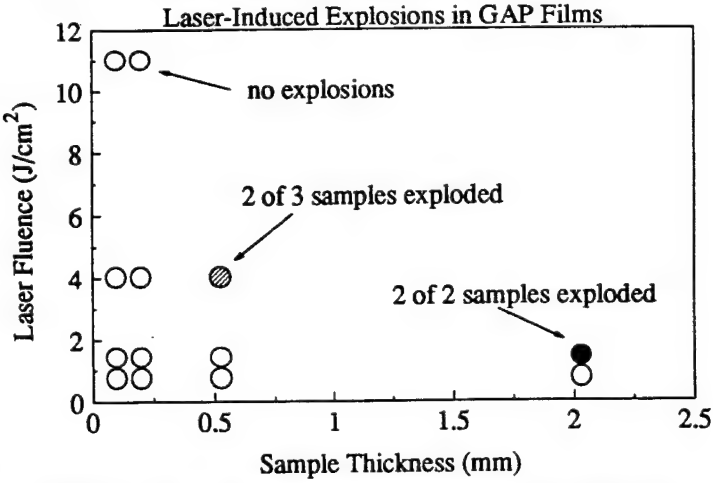

Figure 6 - Sensitivity of GAP to laser-induced explosions.

DISCUSSION

As mentioned in above, the principal observation of chemical changes after passage of shock is loss of azide functional groups as evidenced by reduction of the 2100 cm^{-1} band.

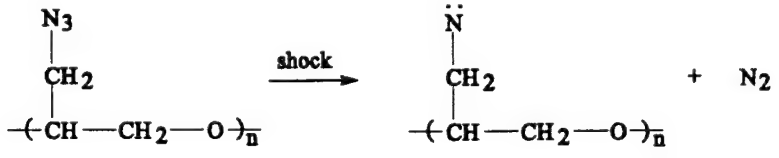

One might suppose that the nitrene radical might rearrange to an imine structure by a 1,2-

hydrogen atom shift,

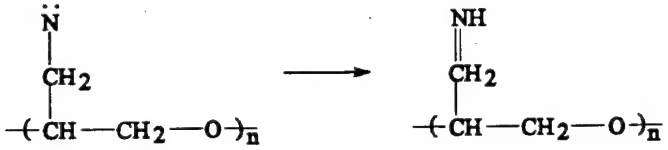

Evidence for this type of rearrangement was obtained by Haas et al. in their study of thermal decomposition of GAP.[23] Although we made an extensive search for new NH stretching bands near 3400 cm^{-1}, we obtained no convincing evidence of formation of imines in our shocked samples.

The laser fluence used in the above experiment is about 0.71 J/cm^2, which corresponds to an experimental value of shock pressure 0.6-0.9 GPa.. Although this value was measured at room temperature, we may use Eq.(9) to estimate pressure at low temperature. When the samples are cooled to 77 K , usually the density and speed of sound of the sample increases, and the form of the Hugoniot may also change. According to Eq.(9), the increasing of density and speed of sound results in higher pressure generated at given laser fluence. For a worst case, let us assume that the density of GAP at 77 K increases by 10 % and speed of sound increases by 1 km/s. If the parameter b lies in the range 1 to 2, the pressure generated at 0.71 J/cm^2 will be about 20 % greater in the cold solid compared with the room temperature liquid. Therefore, the shock pressure at 77 K may be in the range around 1 GPa.

In order to look for the mechanism of losing azide functional group after passage of shock, let us first examine the possibility of reaction due to temperature increase associated with shock waves. Calculation of temperature increase due to shock compression requires quantities such as Grüneisen parameter, specific heat $C_v(T)$, as well as the Hugoniot equation. Unfortunately, these data are not available for GAP. However, a comparison with other materials might be helpful. For example, the temperature increase for TNT is about 50 K/GPa, for carbon tetrachloride about 120 K/GPa, for nitromethane about 70 K/GPa, and for water about 54 K/GPa.[26,27] The pressure of shock initating chemical reaction in our 77 K experiment is about 1 GPa, so it seems unlikely that the temperature increase will exceed 100-200 K. GAP is known to be stable to 473 K, so the driving force for eliminating azide functional group is not likely the ordinary thermal force. Shock initiated reactions require transfer of substantial amounts of mechanical energy from the shock front to the internal vibrational states of the molecules.[8-13] Dlott and co-worker have proposed that, especially in large molecular energetic materials, energy could be transferred from a shock produced phonon bath to the molecule's internal vibrations by multiphonon up-pumping. The mechanism of up-pumping is anharmonic coupling of excited phonon modes with low-frequency molecular vibrations, termed doorway modes. Once the doorway modes are excited, typically by two-phonon absorption, the molecule could absorb more phonons to reach higher energy levels, and so on [12,13] According to this model, shock energy is quickly channeled to the phonon bath with a quasitemperature θ_p before other processes can occur. If the specific heat of the phonon bath is 1/3 to 1/5 of the total specific heat,[13] then for the estimated 100 K temperature increase in GAP associated with the 1 GPa shock wave, the initial phonon bath quasitemperature will be 377 to 577 K, which corresponds to a characteristic phonon energy of 260 to 400 cm^{-1}. The polymeric nature of GAP allows for the possibility of very low-frequency doorway modes, so it is reasonable to expect that motions of the polymer backbone will allow this energy to be coupled into the higher frequency bond stretching modes, which would be required to induce loss of azide groups.

For the explosions occurring in thick samples, generally it is not possible to distinguish between a thermal explosion and detonation solely on the basis of a threshold measurement. However, the strongest evidence for detonation is the fact that sensitivity is much lower for a 2 mm thick layer as compared with a 0.5 mm layer. The entire energy of a 90 mJ laser pulse distributed over a GAP sample volume of 62.5 mm^3 (125mm^2 area, 0.5mm thick) should raise the temperature by only 3 K, based on the estimated heat capacity of GAP (0.4 J/g/K). Therefore, it is difficult to imagine how a four-fold increase in sample thickness can significantly affect the probability of initiating a thermal explosion by the laser.

A sustained detonation depends on the rate of reaction behind the shock front, because it is this energy that must be transmitted to the front in the form of a pressure wave to sustain the shock. Hare and Dlott have demonstrated that some reactions occur on a nanosecond time scale behind a shock front in PMMA.[13] It is not known whether enough heat can be released on this time scale to sustain a shock, even in energetic materials. In principle, reactions that occur well behind the shock front can contribute energy to the shock front in a freely detonating solid. This is because the sum of the local sound speed and the particle velocity in the reaction zone is greater than the shock front velocity. If the thickness of sample is less than the characteristic reaction zone thickness in the freely detonating material, detonation can only be achieved by overdriving the system (e.g. with a high laser fluence). In other words, the fluence required to initiate detonation should decrease as sample thickness increases, but only to the point where the sample thickness is roughly equal to the reaction zone thickness in free detonation. This is consistent with the sensitivity behavior in Figure 6. It suggests that reaction zone of GAP in free detonation is greater than 2 mm.

Additional experiments on this system and other energetic materials will provide a clearer picture of the rates and mechanism involved in detonation. Such fundamental investigations of the chemistry of energetic materials are in important prerequisite to the rational design of less sensitive explosives.

CONCLUSIONS

Thin films of glycidyl azide polymer at 77 K have been subjected to laser-generated shock waves. Infrared spectra show substantial loss of azide functional groups after passage of the shock waves, presumably by elimination of molecular nitrogen and formation of nitrene radicals. The shock wave velocity has been measured by use of a velocity interferometer and shock pressures calculated. Shock-induced detonation has been observed in thick GAP samples.

ACKNOWLEDGMENT

This research is supported by the Air Force Office of Scientific Research.

REFERENCES

1. C. A. Wight, T. R. Botcher, J. Am. Chem. Soc. **114**, 8803 (1992).

2. T. B. Brill, D. G. Patil, J. Duterque, and G. Lengelle, Combust. Flame **95**, 183 (1993).

3. T. R. Botcher, C.A.Wight, J. Phys. Chem. **97**, 9149 (1993).

4. T. R. Botcher, C.A.Wight, J. Phys. Chem. **98**, 5441 (1994).

5. T. R. Botcher, D. Beardall, C.A.Wight, L. Fan, and T. J. Burkey, J. Phys. Chem. in press

6. M. Peyrand, S. Odiot, E. Oran, J. Boris, and J. Schnur, Phys. Rev. **B 33**, 250 (1986).

7. M. L. Elert, D. M. Deaven, D. W. Brenner, and C. T. White, Phys. Rev. **B 39**, 1435 (1989).

8. C. S. Coffey and E. T. Toton, J. Chem. Phys. **76**, 949 (1982)

9. S. F. Trevino and D. H. Tasi, J. Chem. Phys. **81**, 348 (1984)

10. F. J. Zerilli and E. T. Toton, Phys. Rev. **B 29**, 5891 (1984)

11. D. D. Dlott and M. D. Fayer, J. Chem. Phys. **92**, 3798 (1990).

12. A. Tokmakoff, M. D. Fayer, and D. D. Dlott, J. Phys. Chem. **97**,1901 (1993)

13. D.E.Hare and D.D.Dlott, Appl. Phys. lett. **64**, 715 (1994)

14. L. C. Yang, J. Appl. Phys. **45**, 2601 (1974).

15. P. E. Shoen and A. J. Campillo, Appl. Phys. Lett. **45**, 1049 (1984).

16. I.-Y. S. Lee, J. R. Hill, and D. D. Dlott, J. Appl. Phys. **75**, 4925 (1994).

17. L. C. Yang and V. J. Menichelli, Appl. Phys. Lett. **19**, 473 (1971)

18. J. Sakata and C. A. Wight, J.Phys. Chem. **99**, 6584 (1995).

19. J. N. Johnson and L. M. Barker, J. Appl. Phys. **40**, 4321 (1969).

20. I.-Y. S. Lee, J. R. Hill, H. Suzuki, D. D. Dlott, B. J. Baer, and E. L. Chronister, J. Chem. Phys., in press.

21. CRC Handbook of Chemistry and Physics, 74th ed. (CRC, Boca Raton, FL 1993).

22. R. W. Woolfolf, M. Cowperwaite, and R. Shaw, Thermochimica Acta **5**, 409 (1973).

23. Y. Haas, Y. B. Eliahu, and S. Welner, Combust. Flame **96**, 212 (1994).

24. J. K. Chen and T. B. Brill, Combust. Flame **87**, 157 (1991).

25. Y. Oyumi and T. B. Brill, Combust. Flame **65**, 127 (1987)

26. R. Shaw, J. Chem. Phys, **54**, 3657 (1971).

27. M. Cowperthwaite and R.Shaw, J. Chem. Phys. **53**, 555 (1970).

Laser Photodissociation and Thermal Pyrolysis of Energetic Polymers

Ping Ling and Charles A. Wight

Department of Chemistry, University of Utah,
Salt Lake City, Utah 84112

The Journal of
Physical Chemistry®B

Reprinted from
Volume 101, Number 12, Pages 2126–2131

J. Phys. Chem. B **1997**, *101*, 2126−2131

Laser Photodissociation and Thermal Pyrolysis of Energetic Polymers

Ping Ling and Charles A. Wight*

Department of Chemistry, University of Utah, Salt Lake City, Utah 84112

Received: September 24, 1996[⊗]*; In Final Form: January 13, 1997*

Decomposition reactions of glycidyl azide polymer (GAP) and poly(glycidyl nitrate) (PGN) have been investigated by pulsed infrared laser pyrolysis and ultraviolet laser photolysis of thin films at 17−77 K. Reactions are monitored by transmission FTIR spectroscopy. Photolysis of GAP at 266 nm shows that the initial reaction steps are elimination of molecular nitrogen with subsequent formation of imines. Warming leads to loss of the imines, most likely as a result of secondary polymerization reactions. Thermal decomposition of GAP by infrared laser pyrolysis reveals products similar to the UV experiments after warming. Laser pyrolysis of PGN indicated that the main steps of decomposition are elimination of NO_2 and CH_2O from the nitrate ester functional group, followed by rearrangement of the polymer backbone to form carbonyl functional groups. Higher order reactions form numerous small molecule products including NO, CO, CO_2, N_2O, H_2O, HNCO, HCN, HCNO, HONO, and CH_4. UV laser photolysis of PGN shows the major products to be CO, CO_2, N_2O, and polymeric carbonyls. A mechanism is suggested to account for the difference between products in the UV and infrared laser experiments. Quantum yields for destruction of the azide group in GAP and for destruction of the nitrate ester group in PGN are 8×10^{-3} and 1×10^{-3}, respectively, for 266 nm excitation.

Introduction

Glycidyl azide polymer (GAP) and poly(glycidyl nitrate) (PGN) are energetic polymers that have been proposed for use as binders in solid rocket motors. The un-cross-linked oligomers used in this study are viscous liquids at room temperature.

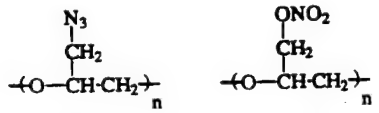

GAP PGN

GAP and other azide-containing polymers have been the subject of several studies over the years. Brill and co-workers[1,2] found that GAP decomposes at about 250 °C during rapid heating; the major products are N_2, CO, HCN, NH_3, CH_2O, CH_4, C_2H_2, and C_2H_4. Thermal decomposition at high temperature and high pressure produces N_2, H_2, CO, C, and other minor products.[3] Although these studies have proved valuable for understanding the gas phase decomposition kinetics, it has been difficult to determine the initial steps of the decomposition mechanism because the time scale of reactions is short and the products are not usually detected in the condensed phase. Haas and co-workers[4] studied the thermal decomposition of GAP by pulsed CO_2 laser irradiation and found that both gaseous products and smoke powder are formed. The gaseous products are mainly N_2, CO, C_2H_4, HCN, CH_4, and C_2H_2. The smoke powder was assigned to be principally imines, as indicated by a broad infrared absorption band near 1650 cm^{-1}. However, early studies of methyl azide decomposition show that there are other strong bands associated with imines[5] that were not reported by Haas and co-workers, casting some doubt on this assignment.

Thermal decomposition of a series of nitrate esters was studied by Oxley and co-workers recently.[6] They concluded that the rate-determining step in nitrate ester thermolysis is usually homolytic cleavage of the RO−NO_2 bond. Chen and Brill studied the thermal decomposition kinetics of PGN and found the reaction to be first-order for slow heating rates[7] but second-order for rapid heating.[8] Under rapid heating conditions, the gaseous decomposition products were determined to be CO, CO_2, NO, NO_2, H_2CO, HCN, HONO, and HCO_2H. However, the mechanism by which these products are formed is still not well established. In earlier work on nitrocellulose, Gelernter *et al.*[9] had proposed that rupture of NO_2 from the side chain is the first step of thermal decomposition. However, a more recent study suggested that the reaction begins with second-order reaction of nitrate ester groups.[10]

Recently, transient thin film laser pyrolysis techniques, which use CO_2 laser pyrolysis of target materials, following by rapid thermal quench of reaction products, has restricted reaction time at high temperatures to within a millisecond scale.[11] Just as shock heating is suitable for studying gaseous reactions at high temperatures for short periods, this technique has been proved successful in studying initial thermal reaction in the condensed phase.

Laser photolysis is also a useful tool in studying the decomposition mechanism of molecules. Although it is not likely to involve electronically excited states in normal thermal decomposition, it is suggested that electronic excited states may play an important role in detonation.[12] On the other hand, if internal conversion of electronically excited states to a vibrationally excited ground electronic state is important, then the photolytic decomposition product ratios should bear a strong similarity to those resulting from thermal decomposition.

Because GAP and PGN polymers have the same backbone structure, it is appropriate and helpful to use transient thin film laser pyrolysis and laser photolysis techniques to study initial reactions in both materials in one set of experiments.

Experimental Section

GAP was obtained from the 3M Company, which markets the material as an energetic binder for propellants. The material used in our study is the un-cross-linked polyol, which has a linear repeating structure but is synthesized using a branched

* Author to whom correspondence should be addressed.

[⊗] Abstract published in *Advance ACS Abstracts*, February 15, 1997.

S1089-5647(96)02936-7 CCC: $14.00

initiator. PGN was supplied by Dr. Robert Wardle of Thiokol Corp. Both GAP and PGN are viscous liquids at room temperature.

Pulsed Infrared Laser Pyrolysis. The details of the apparatus have been described elsewhere.[11] Briefly, a thin film of GAP or PGN is sandwiched between two salt windows (CsI or CaF_2) and mounted at the cold tip of an evacuated liquid nitrogen Dewar vessel. The vacuum enclosure has two infrared windows mounted on opposite sides for obtaining transmission FTIR spectra and one or two quartz windows mounted on the two remaining sides of the cell for photolysis. The vacuum cell is pumped to 10^{-4} Torr; then the cold finger is cooled to 77 K by liquid nitrogen. In some experiments, the sample was cooled to 17 K by a closed cycle helium refrigerator in a similar vessel.

Pyrolysis of the sample is carried out by pulsed CO_2 laser irradiation (Pulse Systems Model LP140-G). The laser was tuned to 1039.5 cm^{-1}, and the pulse length is about 35 μs. The laser beam size can be adjusted by means of a spherical mirror and is measured by irradiating a target of thermally sensitive paper. The average energy per pulse is calculated from the beam power, as measured by a Scientech Model 38−0101 disk calorimeter. Typically, laser fluences in the range 0.5−2.3 J/cm^2 were used in these experiments.

Neither GAP nor PGN has any strong infrared absorption bands within the tuning range of the pulsed CO_2 laser (900−1100 cm^{-1}). Therefore, infrared laser pyrolysis experiments were conducted using two different methods. In the first method, we deposit a thin film of salt ($NaBF_4$, which has very strong absorption at the laser frequency) on the IR window prior to sample preparation. The salt film is in good contact with the GAP or PGN to ensure efficient thermal conduction during laser pyrolysis. The second method is to use a relatively thick sample of GAP or PGN ($\geq$15 μm). Although the energy deposition per unit volume of sample is the same as for thin films, the rate of conduction out of the sample is much slower, so reactions have a greater time to take place. Usually in the first method, a single shot is enough to reach maximum concentration of reaction products, whereas the second method normally requires five to seven shots at the highest available fluence (2.3 J/cm^2) to achieve similar results.

Transmission FTIR spectra were recorded before and after pyrolysis by means of a Mattson Model Polaris FTIR spectrometer. Spectra are obtained by averaging 32 scans at 0.5 cm^{-1} resolution.

Pulsed UV Laser Pyrolysis. The sample assembly is the same as for laser pyrolysis. Before photolysis, the sample is turned to face one of the quartz windows. After photolysis, the sample is turned to face both IR windows before recording the infrared spectrum. Photolysis is carried out by using the fourth harmonic of a Nd:YAG laser (Continuum Model Surelite) at 266 nm. The laser pulse duration is 7 ns, and the laser power is typically 35 mW at 10 Hz repetition rate, as measured by the disk calorimeter. The spatial profile of the beam is determined by recording the laser power while a razor blade is scanned across the beam. The data are differentiated and fit to a Gaussian function to determine the 1/*e* diameter of the beam, which was determined to be 3.9 mm. A lens is used to expand the beam to the desired fluence, which was typically 1 mJ/cm^2 in this study. The bulk temperature change of the sample due to absorption of laser light is estimated not to exceed 1 K.[13]

Ordinary Thermal Decomposition Experiments. A drop of GAP or PGN is placed in a glass tube, and the tube is evacuated and sealed. The end of the tube with material inside is immersed in an oil bath at 170 °C for GAP or 160 °C for PGN. After about 30 min the evolved gas is admitted to an evacuated IR gas cell for detection. In some experiments the gas phase products were condensed onto a 17 K cold window in a deposition chamber for IR detection in the condensed phase. The pyrolysis temperatures were chosen as the lowest temperatures at which gas bubbles can be observed to evolve from the GAP or PGN.

At higher temperatures, it is easy to induce explosive thermal decomposition. For example, when a tube containing GAP is placed in a hot bath at 230 °C, an explosion occurs in seconds, and all of the GAP is consumed.

TABLE 1: Integrated Infrared Absorption Coefficients

molecule	band position (cm^{-1})	integrated absorption coefficient (cm/μmol)
CO_2	2344	19.
CO	2138	2.3
N_2O	2238	13.
H_2CO	1720	2.8
	1495	1.2
$(NO)_2$	1861	0.93
	1755	4.5
N_2O_3	1861	6.4
	1594	5.1
	1300	4.2
	784	0.62
$(NO_2)_2$	1874	0.8
	1738	6.2
	1255	6.5
	747	2.2

Supplementary Experiments. GAP exhibits weak absorption around 285 nm; this transition has been assigned to the n−π^* transitions in the azide functional groups.[14] Similarly, PGN exhibits a weak n−π^* absorption at 270 nm. The absorption cross sections at 266 nm were measured by a Hewlett-Packard diode array UV−visible to be 7.5×10^{-20} cm^2 and 8.8×10^{-20} cm^2 per functional group for GAP and PGN, respectively.

Calibration experiments were carried out in order to determine the relative integrated infrared absorption coefficients for CO, CO_2, N_2O, NO, NO_2, CH_2O, and some gas mixtures. Samples containing 1−10 μmol of the authentic compounds were deposited onto a 2.5 cm diameter infrared window at 17 K at a rate not exceeding 5 μmol/min. Formaldehyde was made by thermal depolymerization of paraformaldehyde; other gases were used as supplied from commercial sources. A good linear relationship was observed between the integrated absorption intensity and the amount of gas deposited. In most cases, the band positions and widths were somewhat dependent on temperature, but the integrated intensities were essentially constant. The exceptions were N_2O_3 and $(NO)_2$, for which some of the integrated intensity of some bands increased as much as 30% from 17 K to 77 K. In the case of NO and NO_2, the absorption coefficients were determined by depositing these samples as monomers in an excess of argon matrix gas. Annealing these samples to evaporate the argon component produced bands that have been assigned previously to the dimers[15] and (in the case of mixed NO/NO_2 samples) N_2O_3.[16] The integrated absorption coefficients (in cm/ μmol) measured in this manner are given in Table 1.

Results

UV Laser Photolysis of GAP. Transmission FTIR spectra of thin films of GAP were obtained before and after UV laser photolysis, as illustrated in Figure 1a,b. After photolysis, the intensity of the characteristic azide band at 2100 cm^{-1} is greatly reduced compared with the other bands. New absorption bands

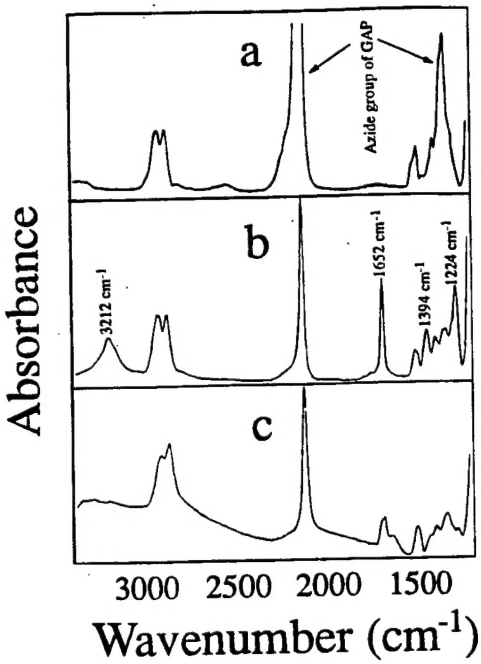

Figure 1. Infrared spectrum of a GAP sample (a) prior to and (b) following 266 nm laser photolysis at 77 K. Spectrum c is the same sample after warming to room temperature for several hours.

appear at 3212, 1652, 1394, and 1224 cm^{-1}. The intensities of the new bands are highly correlated, suggesting that they come from the same products or group of products. It is noteworthy that absorption bands of GAP associated with C−O−C stretching vibrations (1082−1128 cm^{-1}) and C−H stretch vibrations (2750−3000 cm^{-1}) remain almost unchanged after photolysis. This suggests that the backbone of the polymer is rather stable with respect to 266 nm radiation. Photolysis for extended periods (i.e., until all the azide groups are destroyed) revealed a tiny infrared band due to CO, suggesting that only a tiny portion of backbone is broken to release CO.

A control experiment was carried out in which a sample of poly(propylene glycol) polymer was photolyzed for extended periods.

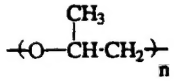

poly (propylene glycol)

This polymer is similar to GAP except that the azide group is replaced by a hydrogen atom. No change in reactant bands was observed, and no products were formed.

When photolyzed samples are warmed to room temperature, additional changes occur over a time scale of several hours. The polymer undergoes a transformation from a transparent viscous liquid to a solid that is highly light scattering. The infrared spectra show that the bands at 3212, 1394, and 1224 cm^{-1} disappear completely, and the band at 1652 cm^{-1} broadens and diminishes in intensity, as shown in Figure 1c. The quantum yield for destruction of the azide group under 266 nm photolysis was measured by recording the integrated absorption intensity, A, of the azide band at 2102 cm^{-1} as a function of cumulative laser fluence, J (photons/cm^2). For optically thin samples, the quantum yield can be found from the relationship

$$\ln(A/A_0) = -\Phi\sigma J \qquad (1)$$

where Φ is the quantum yield and σ is the measured 266 nm absorption coefficient. A plot of $\ln(A/A_0)$ was found to be linear in J, and the resulting value of Φ determined from the slope is 8×10^{-3}.

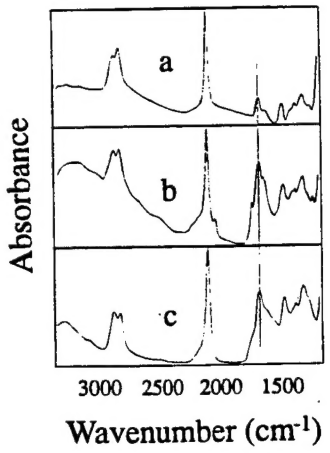

Figure 2. Infrared spectra of GAP showing the similarity of samples that were (a) subjected to 266 nm laser pyrolysis and warmed to room temperature for several hours, (b) subjected to CO_2 laser pyrolysis at 77 K, and (c) a residue of a GAP film that was heated to 170 °C for 30 min.

Pyrolysis of GAP. The spectra of GAP films that were subjected to pulsed CO_2 laser pyrolysis at 2 J/cm^2 are illustrated in Figure 2b. A new broad band around 1660 cm^{-1} and a small band around 2032 cm^{-1} are formed after pyrolysis. We found that varying the laser fluence does not have any significant effect on the shape or position of the new bands, but simply changes the magnitude of the product absorptions.

The spectra of thin film residues formed by heating GAP to 170 °C for several minutes is shown in Figure 2c. The spectrum bears a strong resemblance to the spectrum of GAP subjected to CO_2 laser pyrolysis (Figure 2b) and to the spectrum of GAP subjected to UV photolysis followed by warming to room temperature for several hours (Figure 2a). The gas evolved during the 170 °C pyrolysis period was collected and found to be essentially infrared-inactive, except for a trace of CO.

Pyrolysis and Photolysis of PGN. Infrared spectra of PGN obtained before and after pulsed CO_2 laser pyrolysis at a fluence of about 2 J/cm^2 are shown in Figure 3a,b. Reaction product bands were observed at 1723 and 1498 cm^{-1} (CH_2O), 1862 (mainly NO_2 dimer), 1595 (N_2O_3), and 1302 cm^{-1} (NO_2 dimer and N_2O_3). A shoulder observed at 1744 cm^{-1} exists in the reference spectra of $(NO)_2$ and $(NO_2)_2$. This band persists to relatively high temperatures during the warm-up cycle, suggesting that it is mainly attributable to $(NO_2)_2$. In addition, small bands were observed at 2341 cm^{-1} (CO_2); 2133 cm^{-1} (CO); 2282 and 2276 cm^{-1} (HNCO); 2257 and 2247 cm^{-1} (HOCN); and 2236 cm^{-1} (N_2O). The product band observed at 1731 cm^{-1} belongs to a nonvolatile product because it persists after warming to room temperature. The band observed at 1567 cm^{-1} cannot be definitively assigned, though aliphatic nitro and nitroso compounds typically have strong absorption bands near this position.

Pyrolysis experiments carried out at 17 and 77 K exhibit similar product absorption spectra except for smaller amounts of CO that are observed at the higher temperature, due to the volatility of this product.

Figure 3c shows the gaseous products from heated PGN at 160 °C in an ordinary thermal decomposition experiment. The evolved gas was deposited onto an infrared window at 17 K. In addition to the major products CH_2O, NO, NO_2, and CO_2, (which were observed in the laser pyrolysis experiment), we

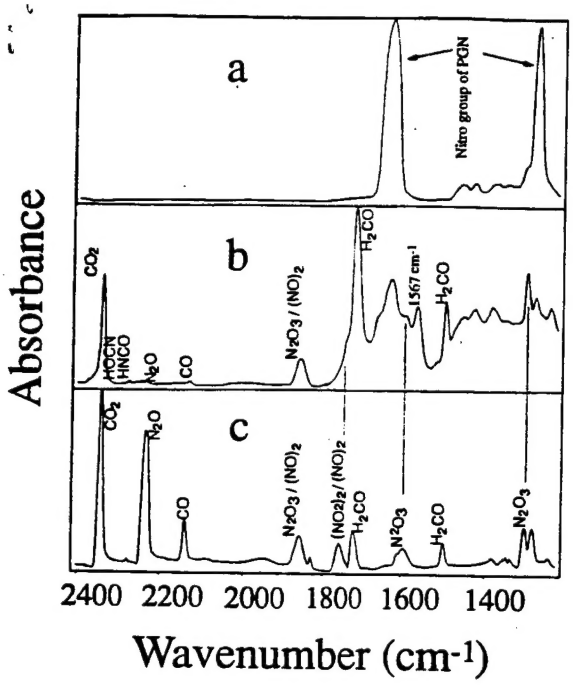

Figure 3. Infrared spectrum of a PGN sample (a) prior to and (b) following CO_2 laser pyrolysis at 17 K. Spectrum c is a film produced by collecting the vapor evolved from a sample of PGN heated to 160 °C and condensing it onto an infrared window at 17 K in vacuum.

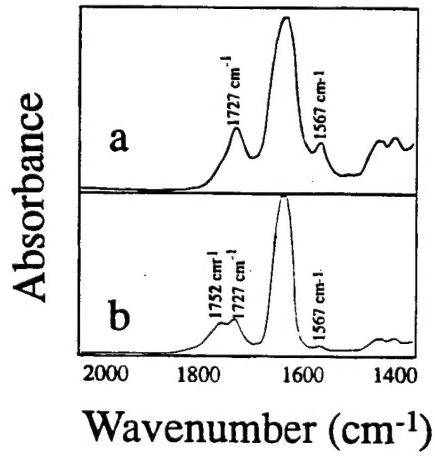

Figure 4. (a) Partial infrared spectrum of a PGN sample that was pyrolyzed with a CO_2 laser and subsequently warmed to room temperature. (b) Residue of a PGN film that subjected to ordinary thermal pyrolysis at 160 °C.

see a significant enhancement in the intensity of bands attributed to CO and N_2O.

Thermal decomposition of PGN at higher temperature produces gaseous products CH_2O, NO_2, NO, N_2O, CO, CO_2, HCN, HONO, CH_4, and H_2O, which were detected both in the gas phase and in the low-temperature condensed phase. Explosive thermal decomposition occurs in samples of PGN, but requires somewhat higher temperatures than GAP.

In addition to the gas phase products, two bands at 1730 and 1567 cm^{-1} were observed after warming laser-pyrolyzed samples to room temperature (Figure 4a). Similar bands were observed in the residue of PGN heated to 160 °C (Figure 4b).

UV laser photolysis of PGN at 266 nm results in the spectra illustrated in Figure 5b. Compared with pyrolysis, the main difference is the much smaller amounts of H_2CO (1499 cm^{-1}) and NO (1862 cm^{-1}) produced in the photolysis experiments. A thermal annealing experiment showed that the 1862 cm^{-1} band belongs to a volatile compound and is therefore more likely

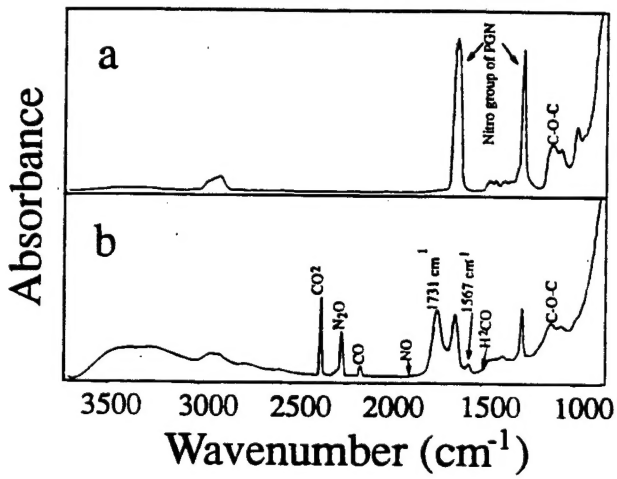

Figure 5. Infrared spectra of a PGN sample (a) prior to and (b) following 266 nm laser photolysis at 77 K.

assigned as NO in this spectrum rather than $(NO_2)_2$. The major products, CO_2, CO, and N_2O, were produced in relative amounts 1.0/1.27/1.57, after correcting for differences in infrared absorption band intensities. An excellent correlation was also found between the decrease in intensity of the PGN nitro group band and the increase of the condensed phase product band at 1731 cm^{-1}. A second condensed phase product band at 1567 cm^{-1} was also observed. A band near 1200 cm^{-1} associated with C−O−C vibrations of the polymer backbone is essentially unchanged during the photolysis period. The C−H stretching bands around 2900 cm^{-1} were decreased after photolysis, and a new broad OH band around 3200−3400 cm^{-1} appeared. During warming to room temperature, the bands at 1730 and 1567 cm^{-1} decreased about 20−40%. The C−O−C band and OH band also decreased after warming up.

The quantum yield for 266 nm laser photolysis was measured, using the technique described above, to be 1×10^{-3}.

UV Laser Photolysis of Nitromethane. To aid the interpretation of some of the experimental results with PGN, we found it necessary to investigate the UV laser photolysis of nitromethane isolated in a 17 K argon matrix at relative concentration of 1/1200. The products were found to be CH_2O, HNO, NO, CO, CO_2, HNCO, nitrosomethanol, and a small amount of N_2O, in agreement with previously published results.[17,18] The most important new result in our experiment is that, upon warming to 40 K, the argon matrix is evaporated and changes in the product band intensities were recorded. The band corresponding to HNO disappears completely, and HNCO is diminished. At the same time, the band due to N_2O is greatly enhanced.

Thermally Activated and Photolytic Oxidation of Formaldehyde. Two experiments were carried out to determine the thermal reaction products of CH_2O with NO and NO_2. Equal amounts of CH_2O and NO or NO_2 were mixed in a sealed glass tube, one end of which was immersed in oil bath at 160 °C. After 30 min, the gaseous contents of the tube were deposited onto an infrared window at 17 K. The principal products of the CH_2O + NO reaction are N_2O and CO, along with smaller amounts of CO_2. The main products of the CH_2O + NO_2 reaction are CO and NO; moderate amounts of CO_2 were also observed, along with a small yield of N_2O.

In a separate series of experiments, we prepared thin films of formaldehyde and NO by vapor deposition of the two gases directly onto a 17 K infrared window in vacuum. UV photolysis at 266 nm forms CO, N_2O, and CO_2. Similar experiments carried out by photolyzing films of formaldehyde and NO_2 at

17 K formed CO, NO, and CO_2. After extended periods of UV photolysis, N_2O also appears as a secondary product.

Discussion

UV Photolysis and Thermal Pyrolysis of GAP. Photolytic decomposition of GAP appears to take place in two distinct steps. The first is elimination of molecular nitrogen and formation of the corresponding imine,

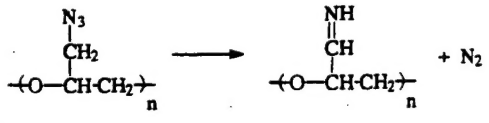

(2)

This reaction is analogous to the mechanism previously studied for simple alkyl azide compounds.[19] By analogy to the published spectra of methylenimine,[5] we may readily assign the 1652 cm^{-1} product band observed in our GAP experiments to the C=N stretching vibration of the imine product. Similarly, the 3212 cm^{-1} band is assigned to the N−H stretching vibration, and the bands at 1394 and 1224 cm^{-1} belong to NH and/or CH deformation modes.

The second stage of reaction occurs after warming to room temperature. The imine bands disappear, and the sample becomes highly light scattering. This behavior is consistent with cross-linking of the imine functional groups to form a higher molecular weight polymer. The cross-linking reaction most likely involves reaction of two imine groups with each other, rather than imine with azide. This is supported by the observation that during the room-temperature reaction there is little change in the intensity of the remaining azide band at 2103 cm^{-1}.

It is important to note that essentially all of the chemistry that occurs in the GAP reactions involves only the azide functional groups. Infrared bands associated with vibrational modes of the polymer backbone are nearly unaffected by the photolysis reaction. Moreover, the unfunctionalized poly(propylene glycol) polymer was completely unaffected by UV laser photolysis at 266 nm.

The pyrolysis experiments (infrared laser and ordinary thermal pyrolysis) give results that are substantially similar to the UV photolysis experiments, except that the intermediate imine bands are not observed. The evolved gas from the thermal pyrolysis experiment is essentially infrared-inactive, consistent with elimination of N_2. Figure 2 demonstrates the similarity of the product spectra obtained in the two pyrolysis experiments and the UV photolysis experiment after warming. The similarity of the broad band near 1660 cm^{-1} in all three experiments is particularly significant.

Thermal Pyrolysis of PGN. Interpretation of the PGN pyrolysis experiments is straightforward. Like GAP, the reaction of PGN is centered at the nitrate ester functional groups. The observed products in these experiments are NO_2 and CH_2O, leading us to conclude that the initial step in the photolytic reaction is

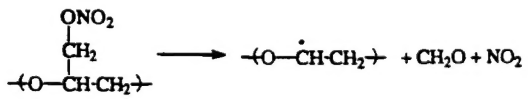

(3)

This is consistent with the conclusions of Oxley *et al.*, who studied the thermal pyrolysis of a series of nitrate ester compounds.[6] According to them, the elimination of NO_2 and CH_2O is not concerted, although we have been unable to cleanly separate the two sequential reaction steps in our experiments. Subsequent reaction of CH_2O with NO_2 forms CO, NO, CO_2, and N_2O, in agreement with the supplementary formaldehyde oxidation experiments that were carried out in this study. It is likely that H_2O is a reaction product in this scheme; however, contamination of all samples by atmospheric water makes it difficult to isolate and quantify this. Other side reactions produce minor amounts of HNCO and possibly HOCN.

We observed a product band at 1731 cm^{-1} that is consistent with formation of a polymeric carbonyl functional group, leading us to speculate that the backbone of the polymer begins to depolymerize according to

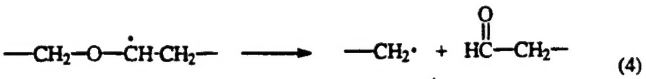

(4)

Chen and Brill had previously reported a similar band, which they attributed to formic acid decomposition product.[7,8] However, the involatile nature of the band in our experiments leads us to favor an assignment as a polymeric aldehyde. Some of the polymeric radicals in (4) may react with NO or NO_2 to form nitro and nitroso functional groups along the polymer backbone, as evidenced by the observed nonvolatile product band at 1567 cm^{-1}, which is consistent with this type of assignment.

In the supplementary formaldehyde oxidation experiments, the amount of CO_2 produced was always less than CO. The thermal pyrolysis experiment on PGN also bears this out, but the pulsed infrared laser pyrolysis experiment produced greatly enhanced amounts of CO_2. It is possible that the higher temperature environment associated with the laser pyrolysis experiment causes the branching ratio for the $NO_2 + CH_2O$ reaction to favor the CO_2 product channel. The other obvious difference between the thermal and laser pyrolysis experiments is the formation of N_2O in the former. This product is presumed to arise from $CH_2O + NO_2$ reactions (as shown by the supplementary formaldehyde oxidation experiments), but the short time scale of the laser pyrolysis experiment (~1 ms) precludes the formation of significant amounts of N_2O because products from thermolysis of at least two different functional groups are required to form it.

UV Laser Photolysis of PGN. The most obvious difference between the pyrolysis and photolysis experiments on PGN is that the former produces large quantities of NO_2, whereas the latter does not. Instead, we observed production of small amounts of NO and a relatively large amount of N_2O. Therefore, it is likely that in this case the photolytic reaction occurs by a different mechanism than the pyrolysis reaction. One mechanism consistent with our observations involves initial elimination of CH_2O and NO (or HNO) with formation of the corresponding polymeric carbonyl compound:

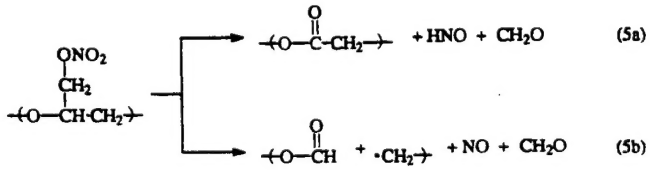

(5a)

(5b)

Again, reaction of the polymeric radicals in (5b) with NO or NO_2 can easily afford the observed product band at 1567 cm^{-1}, which is associated with nonvolatile nitro or nitroso products.

The N_2O, CO, and CO_2 products are presumed to arise from reaction of NO with CH_2O, consistent with our supplementary formaldehyde oxidation experiments. Of these, the N_2O product clearly arises from reactions involving at least two of the nitrate ester functional groups, e.g.

$$2HNO \rightarrow N_2O + H_2O \quad (6)$$

In our PGN experiments we did not detect HNO directly. However, the UV photolysis experiments that we carried out on matrix-isolated nitromethane provide indirect evidence for the participation of this reaction in our study. When isolated in an argon matrix, we observe the formation of HNO as a photolysis product. However, upon warming the argon vaporizes and allows HNO molecules to react with each other, forming N_2O.

Finally, we note that the C−O−C backbone vibrational modes of the PGN polymer are not strongly affected by the UV photolysis reaction. This suggests that depolymerization of the C−O bond in the polymer backbone is evidently not extensive.

Conclusions

UV laser photolysis and thermal pyrolysis of GAP appear to follow the same general mechanism. This begins with elimination of molecular nitrogen from the azide functional groups and rearrangement to a polymeric imine. Subsequent cross-linking of the imine groups results in a higher molecular weight polymer. For PGN, the UV laser photolysis proceeds by elimination of NO and CH_2O, followed by reactions of these species to generate several other reaction products. In contrast, pyrolysis begins with elimination of NO_2 and CH_2O, which is followed by similar side reactions that oxidize the formaldehyde to CO and CO_2. In both compounds, the reactions begin with and are centered around the azide or nitrate ester functional groups. Aside from formation of polymeric carbonyl compounds and small amounts of nonvolatile nitro and nitroso polymers, the backbone of the polymer appears to be largely inert to application of moderate heat or light stimuli.

Acknowledgment. This work was supported by the U.S. Air Force Office of Scientific Research under Grant No. F-049620-94-1-0125. We thank Dr. Rob Hunter (3M Company) and Dr. Robert Wardle (Thiokol Corporation) for generously supplying samples of GAP and PGN, respectively.

References and Notes

(1) Chen, J. K.; Brill, T. B. *Combust. Flame* **1991**, *87*, 157.
(2) Oyumi Y.; Brill, T. B. *Combust. Flame* **1987**, *65*, 127.
(3) Kubota, N.; Sonobe, T. *Propellants Explos. Pyrotech.* **1988**, *13*, 172.
(4) Hass, Y.; Eliahu, Y. B.; Welner, S. *Combust. Flame* **1994**, *96*, 212.
(5) Milligan, D. E. *J. Chem. Phys.* **1961**, *35*, 1491.
(6) Hiskey, M. A.; Brower, K. R.; Oxley, J. C. *J. Phys. Chem.* **1991**, *95*, 3955.
(7) Chen, J. K.; Brill, T. B. *Thermochim. Acta* **1991**, 181, 71.
(8) Chen, J. K.; Brill, T. B. *Combust. Flame* **1991**, 85, 479.
(9) Gelernter, G.; Browning, L. G.; Harris, S. R.; Mason, C. M. *J. Phys. Chem.* **1956**, *60*, 1260.
(10) Leider, H. R.; Seaton, D. L. *Nitrate Ester Decomposition and Degradation of Molecular Weight in Nitrocellulose from Thermal Decomposition of PBX-9404 Below 100C*; Nat. Tech. Info. Serv.: Springfield, VA, 1979.
(11) Botcher, T. R.; Wight, C. A. *J. Phys. Chem.* **1993**, *97*, 9149. Botcher, T. R.; Wight, C. A. *J. Phys. Chem.* **1994**, *98*, 5441.
(12) Odiot, S. In *Chemistry and Physics of Energetic Materials*; Bulusu, S. N., Ed.; Kluwer Academic Publishers: The Nertherlands, 1990; p 79.
(13) Benderskii, A. V.; Wight, C. A. *J. Chem. Phys.* **1994**, *101*, 292.
(14) Rao, C. N. R. *Ultra-violet and Visible Spectroscopy*; The Whitefriars Press Ltd.: London, 1975; p 30.
(15) Fateley, W. G.; Bent, H. A.; Crawford, B., Jr. *J. Chem. Phys.* **1959**, *31*, 204.
(16) Hisatsune, I. C.; Devlin, J. P. *Spectrochim. Acta* **1961**, *17*, 218.
(17) Brown, H. W.; Pimentel, G. C. *J. Chem. Phys.* **1958**, *29*, 883.
(18) Jacox, M. E.; Rook, F. L. *J. Phys. Chem.* **1982**, *86*, 2899.
(19) Wentrup, C. In *Azides and Nitrenes*; Scriven, E. F. V., Ed.; Academic Press. Inc.: New York, 1984; p 395.